

Star forming galaxies in the AKARI Deep Field South: identifications and SEDs

K. Małek¹, A. Pollo^{2,3}, T. T. Takeuchi⁴, P. Bienias⁵, M. Shirahata⁶, S. Matsuura⁶ and M. Kawada⁷

¹ Center for Theoretical Physics of the Polish Academy of Sciences, Al. Lotników 32/46, 02-668 Warsaw, Poland
e-mail: malek@cft.edu.pl

² The Andrzej Sołtan Institute for Nuclear Studies, 69, ul. Hoża, 00-681 Warsaw, Poland

³ The Astronomical Observatory of the Jagiellonian University, ul. Orla 171, 30-244 Kraków, Poland

⁴ Institute for Advanced Research, Nagoya University, Furo-cho, Chikusa-ku, Nagoya 464-8601, Japan

⁵ College of Inter-Faculty Individual Studies in Mathematics and Natural Sciences, University of Warsaw, ul. Żwirki i Wigury 93, 02-089 Warsaw, Poland

⁶ Institute of Space and Astronautical Science, JAXA, 3-1-1 Yoshinodai, Sagami-hara, Kanagawa 229-8510, Japan

⁷ Division of Particle and Astrophysical Science, Nagoya University, Furo-cho, Chikusa-ku, Nagoya 464-8602, Japan

Received ; accepted

ABSTRACT

Aims. We investigate the nature and properties of far-infrared (FIR) sources from the AKARI Deep Field South (ADF-S).

Methods. We performed an extensive search for the counterparts of 1000 ADF-S objects brighter than 0.0301 Jy in the *WIDE-S* (90 μ m) AKARI band in the public databases (NED and SIMBAD). We analyzed the properties of the resulting sample: statistic of the identified objects, quality of position determination of the ADF-S sources, their number counts, redshift distribution and comparison of morphological types, when the corresponding information was available. We also made a crude analysis of the clustering properties of the ADF-S sources and we constructed spectral energy distributions (SEDs) of selected objects with the best photometry, using three different models.

Results. Among 1000 investigated ADF-S sources, 545 were identified at other wavelengths using the public databases. From them, 518 are known galaxies, and 343 of these galaxies were not known previously as infra-red sources. Among the remaining sources there are two quasars and infrared and radio sources of unknown origin. Among six stellar identifications, at least five is probably an effect of contamination. We found redshifts of 48 extragalactic objects and morphological types of 77 galaxies. We present models of SEDs of 47 sources with sufficiently good photometric data.

Conclusions. We conclude that the bright FIR point sources observed in the ADF-S are mostly nearby galaxies. Their properties are very similar to properties of the local population of optically bright galaxies, except an unusually high ratio of peculiar or interacting objects and a smaller percentage of elliptical galaxies. The percentage of lenticular galaxies is the same as in the optically bright population which suggests that galaxies of this type may frequently contain a significant amount of cool dust. It is possible that source confusion plays a significant role in more than 34 % of measurements. The SEDs display a variety of galaxy types, from very actively star forming to very quiescent. Thanks to the AKARI long wavelength bands it was revealed for the first time that these galaxies form a population of objects with very cool dust.

Key words. Surveys – Galaxies: fundamental parameters – Galaxies: evolution – Infrared: galaxies

1. Introduction

Active star formation (SF) is followed by heavy element production from the birth and death of stars. Several of the heavy elements produced by stars end up substantially depleted into dust grains. These dust grains in galaxies tend to absorb ultraviolet (UV) light, emitted by young stars, and re-emit it in the far infrared (FIR). Indeed, there is an extreme category of galaxies which have large amount of dust and are extremely luminous in the FIR and submillimeter (submm) wavelengths. Heavily hidden SF is suggested in these galaxies.

By examining the luminosity functions (LFs) at UV and FIR from GALEX and IRAS/Spitzer, Takeuchi et al. (2005a) proved that the FIR LF shows much stronger evolution than that of UV, though both evolve very strongly. This indicates that the fraction of hidden SF rapidly increases toward higher redshifts up to $z < 1$. There is another important observable closely related to the dust emission from galaxies: the cosmic IR background (CIB). Recently, Takeuchi et al. (2006) constructed the IR spec-

tral energy distribution (SED) of the Local Universe. The energy emitted in the IR is 25–30 % of the total energy budget. In contrast, the IR (from near/mid-IR to millimeter) contribution is roughly (or even more than) a half in the CIB spectrum (e.g., Dole et al., 2006). This also suggests a strong evolution of the IR contribution to the cosmic SED in the Universe.

Thus, understanding the radiative physics of dust is a fundamental task to have an unbiased view of the cosmic SF history. Especially, exploring the evolution of SEDs of galaxies at each epoch is a key to have a unified view of the SF history. First step to this is to know the properties of Local galaxies. Vast amount of new knowledge about the IR universe was provided by IRAS (e.g., Soifer et al., 1987), followed by MSX (e.g., Egan et al., 2003), ISO (e.g., Genzel & Cesarsky, 2000; Verma et al., 2005) and Spitzer (e.g., Soifer et al., 2008).

Recently, after IRAS, a Japanese IR satellite AKARI has performed an all-sky survey (Murakami et al., 2007) and various smaller but deeper surveys at different IR wavelengths. In particular, with the aid of the Far-Infrared Surveyor (FIS:

Kawada et al., 2007), observations in four FIR bands were possible. Among the observed fields, the lowest Galactic cirrus emission density region near the South Ecliptic Pole was selected for observations since it can provide the best FIR extragalactic image of the Universe. This field is referred to as the AKARI Deep Field South (ADF-S). This survey is unique in having continuous wavelength coverage with four photometric bands (65, 90, 140 and 160 μm) mapped over a wide area (~ 12 square degrees). 2268 infrared sources were detected, down to ~ 20 mJy at 90 μm , and infrared colors for about 400 of these were measured.

By the advent of AKARI surveys, a new generation of large database of the Local Universe will be available. In this paper, we present first result of our cross identification (cross-ID) of the sources in the ADF-S. After showing the process of identification of the ADF-S objects, we discuss their statistical properties. Further, we show the UV-optical-FIR SEDs of selected nearby star-forming galaxies from our sample with the best photometric data. We have made a analysis of these SEDs by fitting a few simple model of dust emission from galaxies.

The paper is organized as follows: in Section 2, we present the data. Section 3 is devoted to the basic analysis of the properties of identified sources, their distribution on the sky, and the quality of the catalog and possible biases, e.g. related to the source confusion. Then we discuss the statistical properties of the obtained sample, e.g., the number counts, redshift distribution, galaxy morphologies, and other properties. In Section 4 we present SEDs of the identified galaxies and we attempt to model the dust emission from them. We present our conclusions in Section 5.

2. The data

We cross-identified the ADF-S point source catalog (based on 90 μm) with publicly available databases, mainly the SIMBAD¹ and NED². We performed this search in two stages: first for 500 ADF-S sources brighter than 0.0482 μJy in the *WIDE-S* AKARI band (90 μm), which corresponds roughly to $\sim 10\sigma$ detection, and then for the next 500 ADF-S sources, brighter than 0.0301 μJy in the *WIDE-S* band, which corresponds approximately to $\sim 6\sigma$ detection. In the following sections, we will refer to these two data sets as 10σ and 6σ catalogs. We will present the properties of sources in these catalogs.

The search for counterparts was performed in the radius of 40'' around each source. The ADF-S images were obtained by the slow-scan mode of FIS. The synthesized point spread functions (PSFs) of the slow-scanned image were presented and examined extensively in Shirahata et al. (2009). They showed that the PSF at each band is well represented by a “double-Gaussian profile”, i.e., a superposition of two 2-dimensional Gaussian profiles with different standard deviations. The standard deviations of the narrower component are $32'' \pm 1''$ (for the 65 μm band), $30'' \pm 1''$ (the 90 μm band), $41'' \pm 1''$ (the 140 μm band), and $38'' \pm 1''$ (the 160 μm band). They have also shown that approximately 80 % of the flux power is included in this component. Hence, practically this size can be regarded as a reasonable counterpart search radius. In the case of ADF-S, nearby galaxies have more extended profile than a simple point source, and the reduction method and scan speed are slightly different from the early PSF analysis. In addition, we have used all the four

FIS bands. Hence, we have chosen the largest size 40'' as the tolerance radius of the counterpart search.

For sources from the 10σ catalog in the search radii we found in total 500 counterparts, corresponding to 330 ADF-S sources. Among them there are two cases of two ADF-S sources corresponding to the same counterpart (one star and one galaxy). For 170 sources (34 %) no counterparts were found. 208 sources (42 %) have one possible counterpart, 114 sources (23 %) have two or three counterparts and for 8 sources (1.6 %) more than 3 possible counterparts were found.

Extending the identification process to the 6σ level, we found 284 more counterparts, corresponding to 215 sources fainter than 0.0482 μJy and brighter than 0.0329 μJy in the *WIDE-S* band. Among them were 49 cases (10 % of this fainter part of the sample) of a double and 10 cases (2 %) of a triple counterpart. Two sources correspond to the same counterpart (Seyfert-1 galaxy located at $z \sim 0.24$). One of the sources corresponds to the extragalactic X-ray source which is related to a starburst galaxy NGC 1705, identified as the fourth brightest source in the 10σ sample. For 156 sources (31 %), we found just one counterpart. No counterparts were found for 285 sources (57 %). Thus, the probability of finding a counterpart decreases with the 90 μm brightness of sources by a factor of 1.5. However, in the same time the probability of a source having multiple counterparts decreases much faster, by a factor of 2. There are two possible reasons for this behavior: 1) in ADF-S data, a source confusion would give a more significant contribution to the flux of the brighter sources. This is usually not the case (e.g., Takeuchi & Ishii, 2004), but because of the special way of image construction in the ADF-S data, the confusion effect might play some role, 2) interaction between physically close galaxies (and, consequently, on the sky) may increase their intrinsic IR luminosity significantly. Actual situation would be a mixture of these two effects.

For the purpose of this work we assume, unless specified otherwise, that the most nearby counterpart of an ADF-S source are real ones. However, as stated above, we are aware that the source confusion plays an important role at least in a part of measurements of the multiply identified sources. We will try to address this issue in Section 3.7.

3. Basic Analysis

3.1. Accuracy of the position determination of the ADF-S sources

As shown in Figure 1, the angular separation between the ADF-S source and its counterpart is smaller than 20'' in most cases. It suggests that the actual resolution of the ADF-S map roughly corresponds to the pixel size of the FIS detector. It is plausible that the more distant identifications are caused by the contamination. However, since they are very few, their presence should not affect the quality of our sample and we decided to keep our original criterion.

Positional scatter map, shown in Figure 2, displays a small but systematic bias of $\sim 4''$ in declination of the ADF-S positions with respect to counterparts. Dependence of a positional deviation in the right ascension α and declination δ as a function of α and δ is presented in the four panels of Figure 3. We can observe that the bias of the position determination depends on the source position, being the strongest in the south-west part of the field. However, it should be noted that in all cases the bias is much smaller than the uncertainty of the determined position resulting from the AKARI FIS detector resolution.

¹ URL: <http://simbad.u-strasbg.fr/simbad/>.

² URL: <http://nedwww.ipac.caltech.edu/>.

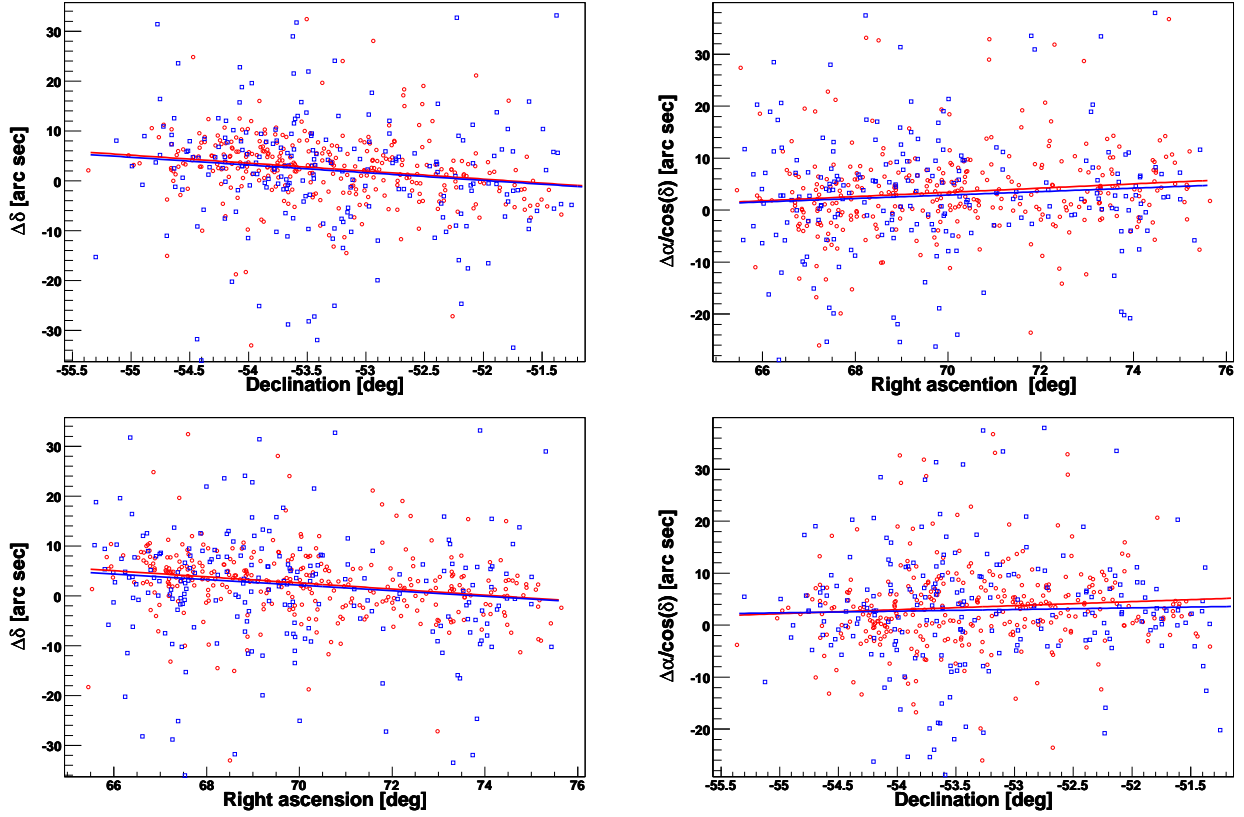


Fig. 3. Dependence of the deviation of the position of counterparts of the ADF-S sources in right ascension and declination, as a function of right ascension and declination. As in Figure 2, open circles correspond to sources from the 10σ catalog and open squares - to sources from the faint part of the 6σ catalog. The solid lines correspond to the best *rms* fits for the bright and faint samples.

Table 1. Best *rms* fit of the positional deviation

Deviation	10 σ catalog	6 σ catalog
	slope	slope
$\Delta\alpha/\cos(\delta)$ vs α	$+0.4\pm 0.2$	$+0.3\pm 0.2$
$\Delta\delta$ vs δ	-1.6 ± 0.5	-1.6 ± 0.5
$\Delta\delta$ vs α	-0.6 ± 0.2	-0.6 ± 0.2
$\Delta\alpha/\cos(\delta)$ vs δ	$+0.8\pm 0.5$	$+0.3\pm 0.5$
	amplitude	amplitude
$\Delta\alpha/\cos(\delta)$ vs α	-25 ± 12	-20 ± 12
$\Delta\delta$ vs δ	-83 ± 24	-80 ± 24
$\Delta\delta$ vs α	$+45\pm 10$	$+41\pm 11$
$\Delta\alpha/\cos(\delta)$ vs δ	$+45\pm 28$	$+20\pm 26$

The parameters of the the best *rms* fits to the data in Figure 3 are listed in Table 1. The results are presented both for the 330 identified sources from the 10σ catalog and for all 545 identified sources from the full 6σ sample. We can observe that including the fainter sources into the sample increases the observed scatter, however, at the same time it reduces the bias in the determination of α and its dependence on the source position in the ADF-S. Thus, we should be aware that the positions of brightest ADF-S sources are the most biased, even if the bias itself remains small. This bias may result from the complex method of source extraction from the slow-scan data in the ADF-S (see Shirahata et al., 2010, for details).

3.2. Classification of objects identified in the ADF-S

In the 10σ catalog, among 330 identified objects, 314 are known galaxies (one appearing twice). 173 (55 %) of these galaxies were previously observed in the infrared (either by IRAS or 2MASS) but 141 (45 %) of them were not known previously as infrared sources. Remaining 16 objects include radio and infrared sources of unknown nature, five stars and one quasar at $z = 1.053$. However, the stars in this sample belong to a sparse group of objects with the distance of a counterpart from the ADF-S object close to $40''$. A careful examination has revealed that they are most probably falsely identified because of the contamination (M. Fukagawa, private communication).

In the fainter half of the 6σ catalog, i.e. fainter than 10σ , among 215 identified sources, 205 are known galaxies (one appearing twice). However, only 32 (16 %) of them were previously known as infrared sources. The remaining 173 galaxies are observed in infrared for the first time. Among the remaining objects there are 7 radio sources of an unknown nature, one quasar at $z \sim 1.23$, one X-ray source related to the starburst galaxy NGC 1705, which is the fourth brightest source in our 10σ data set, and one double stellar system of $B \sim 6$. Summary of the properties of identified sources is given in Table 2.

The data related to the nearest counterparts of the ADF-S sources are summarized in the tables which are available online. The names of counterparts (in case of different naming conventions, we use the primary name given by the NED, when available; otherwise the primary name given by the SIMBAD), the positions of the ADF-S sources and corresponding nearest coun-

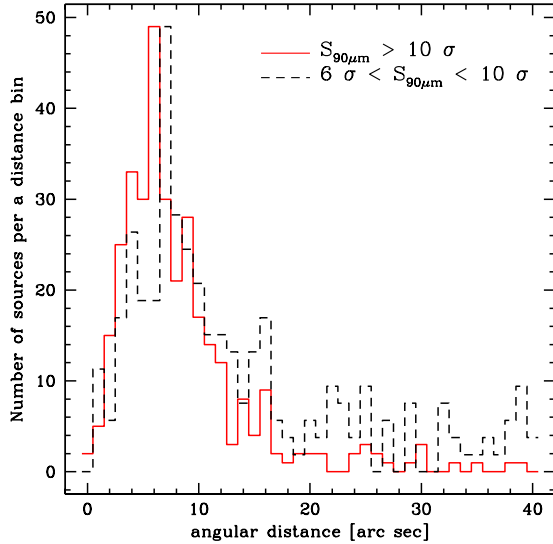


Fig. 1. The distribution of the angular deviations of the nearest counterparts from the ADF-S sources. A solid line corresponds to the 10σ catalog, while a dashed line corresponds to the faint part of the 6σ sample. In both cases most of the identified sources have counterparts closer than $20''$. The precision of the position determination is decreasing with the source flux density - for the 10σ sample the median value of angular distance of the source from a counterpart is 6.9 arc sec (6.45 below $20''$), while for the faint part of the 6σ sample the median value of angular distance of the source from a counterpart is 9.7 arc sec (8.2 below $20''$). The identifications at angular distance $> 20''$ might be an effect of contamination.

Table 2. Classification of identified ADF-S sources

Catalogs:	10σ	6σ
Galaxies	314	518
infrared galaxies	144	176
radio-loud galaxies	12	13
galaxies in a cluster of galaxies	33	40
galaxies in a pair of galaxies	2	2
interacting galaxies	2	2
low surface brightness galaxies	1	1
Seyfert-1 galaxies	1	2
starburst galaxies	1	1
Stars	5	6
IR sources	3	3
Radio sources	6	13
Quasars	1	2
X-ray sources	-	1

terparts, the angular distances of counterparts from the ADF-S sources, as well as their redshifts, when available, are given in the online Tables 1 and 2. The exemplary part of this table, containing data for the 10 brightest ADF-S sources, is shown in the text as Table 7. Flux densities of ADF-S sources with the identified counterparts, in four FIR bands, are given in online Tables 3 and 4. Again, an exemplary part containing data for the 10 brightest ADF-S sources, is shown in the text as Table 8. The flux densities of counterparts in all the other wavebands, always in the units of Janskys, are given in online Tables 5, 6, 7, 8, 9,

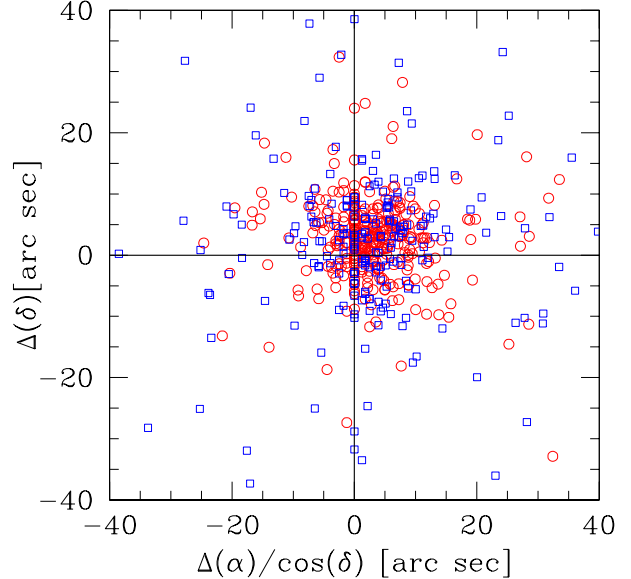


Fig. 2. Scatter plot of the deviation of counterparts from the ADF-S sources in right ascension and declination. Open circles denote sources from the 10σ catalog, open squares - remaining objects from the faint part of the 6σ catalog. We can observe a small but systematic bias, similar for brighter and fainter part of the sample, even if the scatter for the fainter objects is larger.

and 10. An example of such a table, showing a part of the data for the 10 brightest ADF-S sources, is shown in the text as Table 9.

As shown in Figure 4, the sources with multiple counterparts appear mainly in a particular part of the ADF-S, where the nearby cluster of galaxies Abell S0463 is located. We can also observe that in the region corresponding to this cluster there are very few unidentified sources. This facts can be partially related to the higher local density of galaxies in this part of the field, which increases the risk of the chance coincidence of the angular position of the ADF-S source with one of the cluster galaxies. On the other hand, however, this cluster has been intensely observed in the past, and the optically bright galaxies in this area are sampled much better and deeper than in the rest of the ADF-S. Then, if we assume that most of the identifications in the cluster area correct, we can deduce that the unidentified objects in the other part of the field are similar nearby galaxies, not observed before because of their relatively low surface brightness.

3.3. Number counts

A similar conclusion that the bright ADF-S sources are mostly nearby galaxies can be deduced by the analysis of number counts of our sample, which is presented in Figure 5 (for a more detailed analysis of the number counts of the ADF-S galaxies, see Shirahata et al., 2010). In a homogeneous Euclidean Universe it is expected that the cumulative number counts of sources follow a power law $N(> S) \propto S^{-3/2}$ (for cosmological discussions, see e.g., Peebles, 1993). This relation does not depend on the luminosity function of the sources. Indeed, the number counts of nearby galaxies usually can be well fitted by the power law with a slope -1.5 . This relation deviates from the Euclidean slope when the cosmological and evolutionary effects become important (e.g., Yoshii & Takahara, 1988; Metcalfe et al., 1996). Thus,

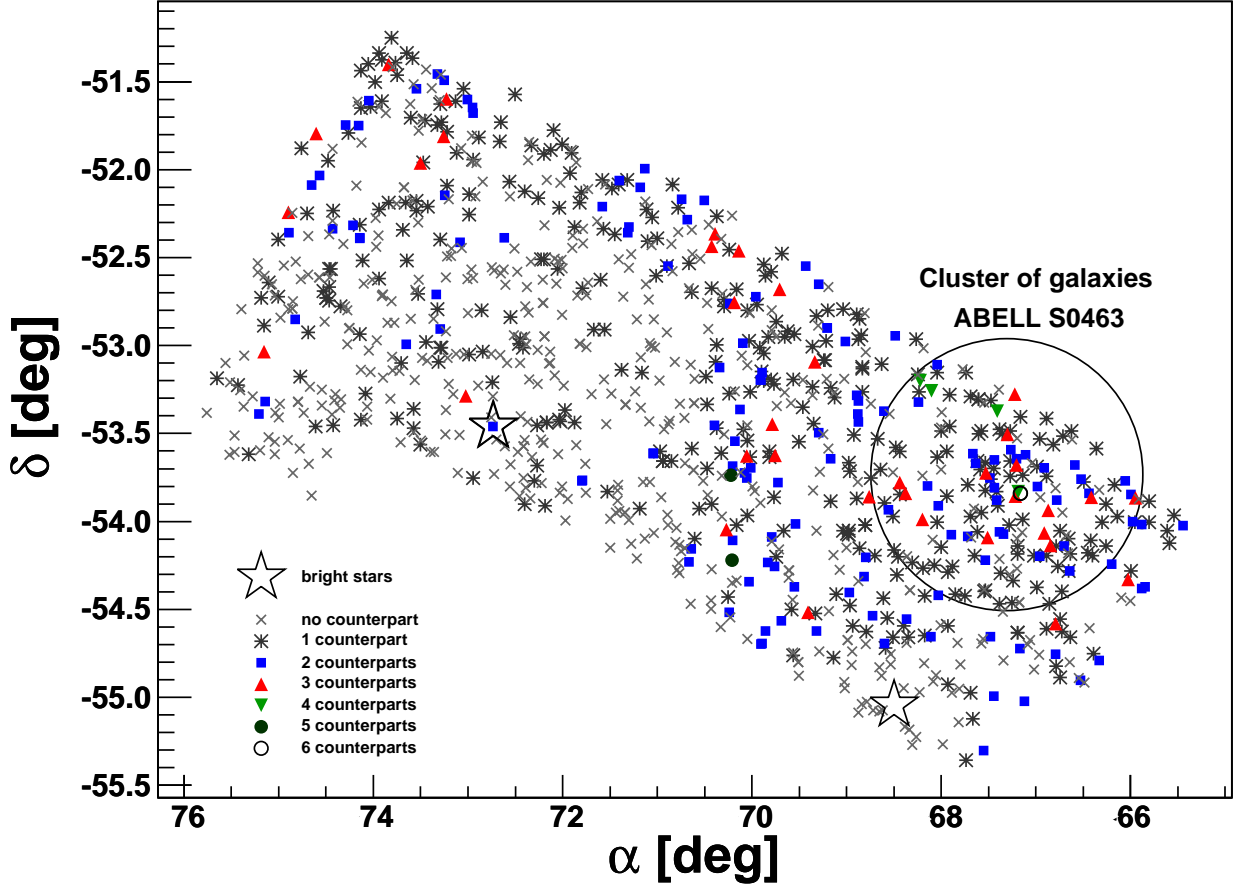


Fig. 4. The map of the ADF-S with the positions of the identified and unidentified objects marked. Sources for which no identification was found (455 sources) are marked as x-s. Sources with one counterpart (362) as shown as small stars, sources with two counterparts (139) are marked as full squares, those with three counterparts (36) triangles, with four counterparts (4) – as upside-down triangles, with five counterparts (2) as full circles and with six counterparts (2) as open circles. The positions of two optically bright stars (around 3 and 6 mag) present in the ADF-S are indicated by big empty stars. One of these stars is the double system and an X-ray source; we have also identified it as one of the ADF-S sources. The position of the cluster of galaxies Abell S0463 at $z \sim 0.04$ is indicated by a big empty circle.

the deviation of the measured number counts of the sample from the Euclidean slope at the bright flux densities may be a simple test of the completeness of the sample at a first approximation.

Table 3. Slope of number counts of ADF-S sources

Objects	10 σ sample	6 σ sample
	$S_{90\mu\text{m}} > 0.0482 \text{ Jy}$	$S_{90\mu\text{m}} > 0.0301 \text{ Jy}$
All	-1.63 ± 0.03	-1.58 ± 0.02
Identified	-1.45 ± 0.03	-1.34 ± 0.02
Not identified	-3.15 ± 0.09	-2.55 ± 0.04
Known z	-0.84 ± 0.05	-0.77 ± 0.04

As shown in Figure 5, the number counts for all the FIR-bright ADF-S sample, from the 90 μm WIDE-S measurement, are quite well fitted to the Euclidean number counts, being only slightly steeper. It implies that these objects are mainly nearby galaxies. The number counts of identified sources are less steep, while the number counts of unidentified sources are steeper than Euclidean. This, together with the above discussion, implies that the unidentified sources are less luminous (and, therefore, more difficult to observe also optically) nearby population of galaxies.

As expected, galaxies with known redshifts form the brightest sample with the flattest number counts.

For the twice larger 6 σ sample the situation changes only slightly. The comparison of slopes of the best *rms* fits to the observed number counts for both samples are given in Table 3.

In total, we conclude that the bright part of the FIR-selected sample of celestial objects in the ADF-S consists mainly of nearby galaxies. The average properties of these galaxies are examined in the following.

3.4. Redshift distribution

The redshift information is available for 48 galaxies from the full 6 σ sample. The only two high redshift sources are quasars: VV2006 J044011.9-524818, located at $z = 1.053$ and HE 0435 – 5304, located at $z = 1.232$, and two more galaxies are located at $z \sim 0.25$. All the other sources are nearby galaxies at $z < 0.1$. The redshift distribution of these galaxies, shown in Figure 6, demonstrates that a large part of them belongs to a cluster Abell S0463 at $z \sim 0.04$.

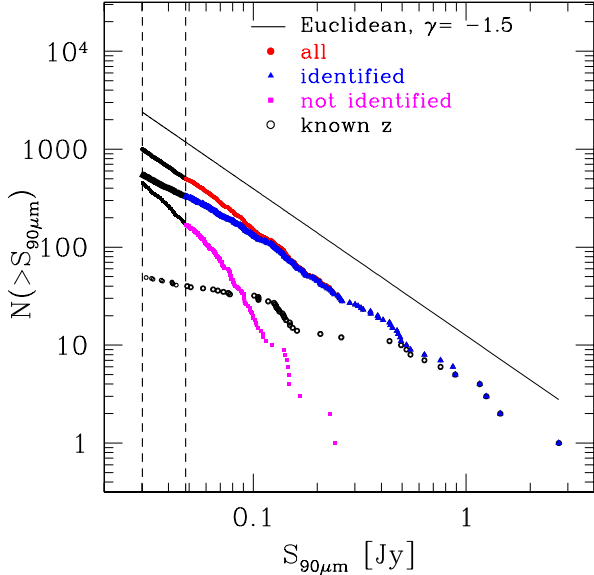


Fig. 5. Integral number counts of objects in the the 10σ and 6σ ADF-S samples in $90\ \mu\text{m}$. Filled circles correspond to all the 6 and 10σ datasets, triangles - to the identified objects, squares - to not identified objects and open circles - to objects with known z . The dashed vertical lines mark the limiting luminosities of 10σ and 6σ catalogs. For comparison, the ideal Euclidean case, with an arbitrary amplitude, has been shown as a solid line.

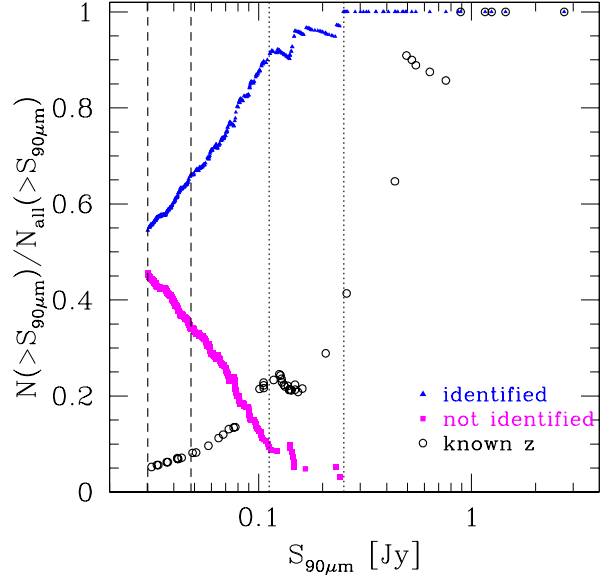


Fig. 7. Ratios of identified and unidentified sources, and of sources with a known redshift, with respect to the total number of sources in the subsamples of a different $90\ \mu\text{m}$ limiting luminosity. Similarly to Figure 5, triangles correspond to the identified objects, squares - to not identified objects and open circles - to objects with known z . The dashed vertical lines mark the limiting luminosities of 10σ and 6σ catalogs. The dotted vertical lines mark the limits of 100 % and 90 % completeness of the catalog of counterparts.

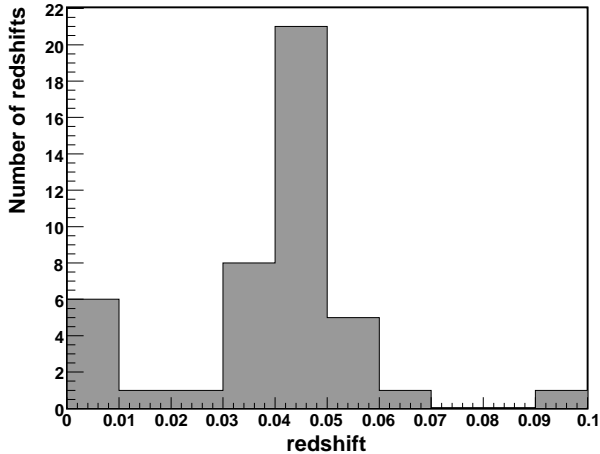


Fig. 6. The redshift histogram of 44 counterparts of the ADF-S objects with known redshifts in 0.01 bins. Four objects with redshifts higher than 0.2 are not shown here. These are: one galaxy at $z = 0.2591$, one Seyfert-1 galaxy at $z = 0.243$ and two quasars: HE 0435 – 5304, located at $z = 1.232$ and VV2006 J044011.9-524818, located at $z = 1.053$.

3.5. Completeness of identifications

In Figure 7 we present the ratio of identified and not identified sources, as well as that of objects with measured redshifts, with respect to the total number of sources in subsamples with different limiting flux density at $90\ \mu\text{m}$. It shows that the sample of identified sources is 100 % complete until $S_{90} = 0.25\ \text{Jy}$, which corresponds to first 32 sources and remains more than 90 % complete until $S_{90} = 0.105\ \text{Jy}$, which corresponds to the first 140

sources. For sources fainter than $0.105\ \text{Jy}$, the completeness of the catalog starts to fall down rapidly to 66 % for the 10σ and 55 % for the complete 6σ sample.

This incompleteness has to be taken into account if we try to apply the conclusions from the analysis of the identified sample to to whole FIR-bright ADF-S dataset.

3.6. Galaxy morphologies and environment

Among the identified galaxies, 67 in the 10σ sample and 10 in the fainter part of the 6σ sample have determined morphologies. Most of them (but not all) belong to the cluster Abell S0463 and were identified by Dressler (1980a). The redshift of the cluster is $z \sim 0.0394$ (Abell et al., 1989). It is a regular (type I-II in the Bautz-Morgan classification), moderately rich (population 84), lenticular-rich galaxy cluster and it was used as a typical regular cluster in a sample investigated by Dressler (1980b). We can assume, then, that our morphological sample can be - in a large part - representative for the nearby bright galaxy population. However, the presence of a rich cluster may introduce some bias for towards dense environments. In Table 4 we present the statistics of the galaxy types in our sample compared to frequencies of different types usually found in an optically bright galaxy population in a nearby Universe (de Vaucouleurs, 1963). The first, not unexpected but striking observation is a high percentage of peculiar galaxies in our sample. The high FIR luminosity of dust in these objects reflects on-going star forming processes induced in them by interactions with other galaxies. We observe slightly more spiral galaxies than expected in an optically-selected sample but - given the number statistics - this over-representation of

spirals is not significant. This is compensated by a significantly (even given a small number statistics) lower amount of elliptical galaxies in the sample. Moreover, among five found elliptical galaxies found one belongs to a pair of interacting galaxies, and one is a Seyfert-1 active galaxy. These particularities probably explain the unusual FIR luminosity of these two galaxies and make a ratio of seemingly normal elliptical galaxies in our sample even lower.

The amount of lenticular (S0) galaxies in our sample turned out to be practically identical among normal optically bright galaxies. The issue of dust in lenticular galaxies has been already discussed in the literature for years. Lanes of dust and gas were found in many objects of this type (e.g. Danks et al., 1979; Sil'chenko & Afanasiev, 2004). The IRAS observations have revealed that $\sim 68\%$ lenticular galaxies, compared to $\sim 45\%$ ellipticals, contain cool dust (Knapp et al., 1989) and remain visible in the infrared. Our results are consistent with the conclusion of Roberts & Haynes (1994) that, taking the FIR detection as a criterion, the most prominent distinction can be made between ellipticals and spirals, with lenticulars remaining an intermediate (and slightly elusive) type. The Spitzer detailed observations of three lenticular galaxies has revealed that even if their bulge-to-disk ratios support their classification as lenticulars, they contain warm dust forming a structure similar to spiral arms (Pahre et al., 2004). The ratio of lenticular galaxies in the FIR selected sample being the same as in the optically selected sample of bright galaxies may be a further evidence that the presence of warm dust in lenticular galaxies may be their common feature.

Although lenticulars were originally introduced as an intermediate transition class between elliptical and spiral galaxies (Hubble, 1936), recently there is a mounting evidence that they are probably a much more complex class of objects. It has been suggested (van den Bergh, 1994) that lenticulars can be divided into two subpopulations, with different formation histories. Some faint lenticulars could indeed form via secular formation processes at early epochs or by slow stripping of gas from spirals in the cluster environment (Abadi, Moore & Bower, 1999). The luminous ones could be rather an effect of mergers of spiral galaxies (Bekki, 1998). Most probably also other processes, like gas starvation, or gas ejection by active nuclei, should be taken into account to describe in a satisfactory way the evolution of these class of galaxies (van den Bergh, 2009). This more complex scenarios seem to be supported by recent observations of lenticulars e.g. in the near infrared (Barway et al., 2009). Detection of a significant population of lenticular galaxies in FIR proves that presence of substantial amounts of cold dust is a quite normal feature for this class of galaxies and may be a further evidence for their complex formation process.

3.7. Correlation function

A careful analysis of the correlation function and clustering properties of galaxies in the ADF-S data will be given in Kawada et al. (2010). Here we present a simple analysis of clustering of galaxies from our sample, aiming at examining the quality of the data and possible biases.

The correlation function is the simplest statistical measurement of clustering, as a function of scale (angular or spatial). It corresponds to the second moment of the galaxy distribution. To compute the angular correlation function ω of the ADF-S galaxies as a function of the angular scale θ , we adopted the

Landy-Szalay estimator (Landy & Szalay, 1993), that expresses $\omega(\theta)$ as:

$$\omega(\theta) = \frac{N_R(N_R - 1)}{N_G(N_G - 1)} \frac{GG(\theta)}{RR(\theta)} - \frac{N_R - 1}{N_G} \frac{GR(\theta)}{RR(\theta)} + 1. \quad (1)$$

In this expression N_G and N_R are the mean densities (or, equivalently, the total numbers) of objects, respectively, in the galaxy sample and in a catalog of random points. The random points are distributed within the same survey area and with the same angular selection biases as galaxies in the ADF-S catalog. $GG(\theta)$ is the number of independent galaxy-galaxy pairs with separation between θ and $\theta + d\theta$; $RR(\theta)$ is the number of independent random-random pairs within the same interval of separations and $GR(\theta)$ represents the number of galaxy-random pairs.

In the nearby Universe, the angular correlation function of galaxies usually can be fitted by a power law $\omega(\theta) = A_\omega \theta^{1-\gamma}$, where an amplitude A_ω is a measure of a clustering strength and γ informs about its scale dependence. In practice, because of the finite size of the survey, the measured $\omega(\theta)$ is a biased estimator of the real correlation function and becomes underestimated on the large scale. The correction factor which needs to be applied is related to as integral constrained IC, (Peebles & Groth, 1976),

$$IC = \frac{1}{\Omega^2} \int \int \omega(\theta) d\Omega_1 d\Omega_2, \quad (2)$$

where Ω is the area of the observed field. Then, the measured correlation function can be written as:

$$\omega(\theta) = A_\omega (\theta^{1-\gamma} - IC). \quad (3)$$

Correlation functions measured for the 10σ and 6σ ADF-S samples are shown in Figure 9. We plot there the best fitted power law with the IC applied. In this case we do not use the covariance matrix to correct for the correlation between the bins, since the precise measurement of the clustering parameters was not our goal. Also, for the same reason, the error bars are simple Poissonian errors. Thus, both the fits and the errors in our calculation are no more than indicative. However, they give a sufficient information to compare the properties of different subsets of our data. The clustering amplitude for the full 10σ ADF-S $90 \mu\text{m}$ sample is equal to 1.1×10^{-3} with the slope $\gamma = 2$, which is not very different from what was found for other infrared galaxy surveys, for example SWIRE (Oliver et al., 2004; de la Torre et al., 2007). In case of the 6σ catalog we observe a lower clustering amplitude of the whole sample, which may be attributed to the fact that we are dealing with fainter and hence less massive sources. Computing the correlation function only for identified sources, in both cases we have a good clustering signal. The correlation function becomes less steep, and the clustering amplitude much higher. This confirms that the identified sources on the sky belong to the brighter local population of galaxies which resides in the denser environments.

In case of the 6σ sample, the clustering amplitude of identified sources is even higher than for the brighter 10σ sample. This increase of the clustering amplitude probably reflects the fact that the identification process, more in case of the fainter sources than in case of brighter ones, was biased because of the presence of the cluster of galaxies Abell S0463 in the ADF-S. The objects from the region occupied by this cluster were observed in the past more intensely and, as a result, they are much better sampled in the public databases. Thus, we should be aware that all the conclusions drawn from the catalog of counterparts of 6σ sources are biased towards the dense environment, comparing to the 10σ catalog. Also, the high clustering amplitude of

Table 4. 77 ADF-S galaxies with known morphological types

	10 σ catalog		6 σ catalog		usual frequency among bright galaxies ^a
	number	frequency	number	frequency	
spiral	45	67 % \pm 10 %	50	65 % \pm 9 %	61 %
lenticular	15	22.5 % \pm 6 %	17	22 % \pm 5 %	22 %
elliptical	4	6 % \pm 3 %	5	6.5 % \pm 3 %	13 %
irregular	1	1.5 % \pm 1.5 %	3	4 % \pm 2 %	3.5 %
compact	2	3 % \pm 2 %	2	2.5 % \pm 2 %	–
peculiar	8	12 % \pm 4 %	8	10 % \pm 4 %	1 %

^a as in de Vaucouleurs (1963)

the counterparts of the 10 σ sources should be probably partially attributed to this bias, even if the effect is clearly smaller.

Deriving real-space clustering parameters requires more detailed estimation of the redshift distribution of our sources, as well as the proper treatment of the possible biases, and will be a subject of future studies.

What is visible for $\omega(\theta)$ is a lack of pairs on scales smaller than ~ 0.2 deg. It is a common feature of measurements in IR data, and is caused mainly by source confusion. The scale where the deficit of pairs occurs in case of a sample of nearest counterparts remains, expectantly, the same as in case of the full dataset. This observation assures us that it is really caused only by a source confusion, and not by some incompleteness in the point source identification process, for instance.

To examine the possible impact of the source confusion on our data, we made an experiment, assuming that all the counterparts found in the 40'' range, not only the nearest ones, can contribute to the FIR flux and, therefore, to the clustering signal. As expected, the clustering amplitude of a sample constructed in such a way is even higher. The deficit of pairs on the small scales decreases significantly but still remains. This result may suggest that the amount of sources missing because of the source confusion in our sample is even larger than the amount of the found secondary counterparts, i.e., 34 % of the sample.

It requires more careful examination of the data to identify what percentage of secondary counterparts actually contributes to the IR flux of ADF-S sources. In the same time, as mentioned above, even the assumption that all the found secondary counterparts could contribute to the clustering signal does not assure a sufficiently large number of close galaxy pairs in our data to obtain a power-law shape of the correlation function. Then, it is very possible that also some other unresolved (and not identified) extragalactic IR sources contribute to the flux of the identified sources. Additionally, since many IR-bright objects found in our sample are peculiar or interacting, we may suspect that even in a greater amount of cases we do not know nor see interacting partners which actually exist and might contribute to the IR flux. The conclusion is that the small-scale environment of the galaxies observed in the infrared should be studied in future even more carefully.

4. Spectral Energy Distributions

As mentioned in Introduction, SEDs give first important clue to the physics of radiation of the sources. The deep image at the AKARI filter bands gives us for the first time the opportunity to analyze SEDs and update the models of their interstellar dust emission. Online Figures 1 – 16 present SEDs of 518 identified infrared ADF-S sources. In the text we show only one exam-

ple of such SED, for the brightest ADF-S source in 90 μ m, in Figure 10.

4.1. SED models

From the 10 σ sample we have selected 47 galaxies with the best available photometry to fit the models of their SEDs. The results are presented in Figures 14–19. The main selection criterion were at least three data points in the infrared range of the spectrum, in order to be able to model dust properties sensibly. In the selected sample 23 galaxies have their morphologies determined. There is one elliptical galaxy, two compact galaxies (one of them being a starburst blue compact dwarf), five lenticular galaxies and 15 spiralgalaxies.

To fit the SEDs of these galaxies we use three methods. First we applied a modified blackbody to the dust emission part, and a blackbody to the stellar emission part in the galaxy SEDs. The results are presented in Section 4.1.1. Since the galaxies in our sample are often evolved, a single blackbody often gives a poor fit to the observed SEDs for the stellar emission part. In a future work, we plan to use a more sophisticated stellar population synthesis model with realistic star formation history to model their stellar component.

It is widely known that some dust components in galaxies cannot establish an equilibrium with ambient radiation field. These components produce strong mid-IR (MIR) emission which extends in a wide range of wavelengths and cannot be well fitted by the modified blackbody (e.g., Purcell, 1976; Draine & Anderson, 1985; Li & Draine, 2001; Draine & Li, 2001; Takeuchi et al., 2003, 2005c). In order to deal with this MIR emission, we should use more sophisticated models for the fit. Then, in addition to the modified blackbody model, we used models of Dale & Helou (2002) and Li & Draine (2001). These more refined models in most cases succeeded in reproducing the MIR part of the dust emission. The results are presented Sections 4.1.2 and 4.1.3.

To fit SEDs of galaxies we tried to use all available measurements from the ADF-S catalog (listed in the online Tables 3 and 4) and data from public databases (listed in the online Tables 5, 6, 7 and 8), excluding only several most dubious measurements, as discussed below.

To fit Dale & Helou (2002) and Li & Draine (2001) models we used all four bands from the ADF-S measurements, when available, i.e. N60 (65 μ m), WIDE-S (90 μ m), WIDE-L (140 μ m) and N160 (160 μ m), four IRAS bands (12 μ m, 25 μ m, 60 μ m and 100 μ m)³, in one case of a galaxy NGC 1705 seven Spitzer bands (3.6 μ m, 4.5 μ m, 5.8 μ m, 8 μ m, 24 μ m, 70 μ m and 160 μ m),

³ Note that in some cases IRAS provides only the upper limits on the IR flux.

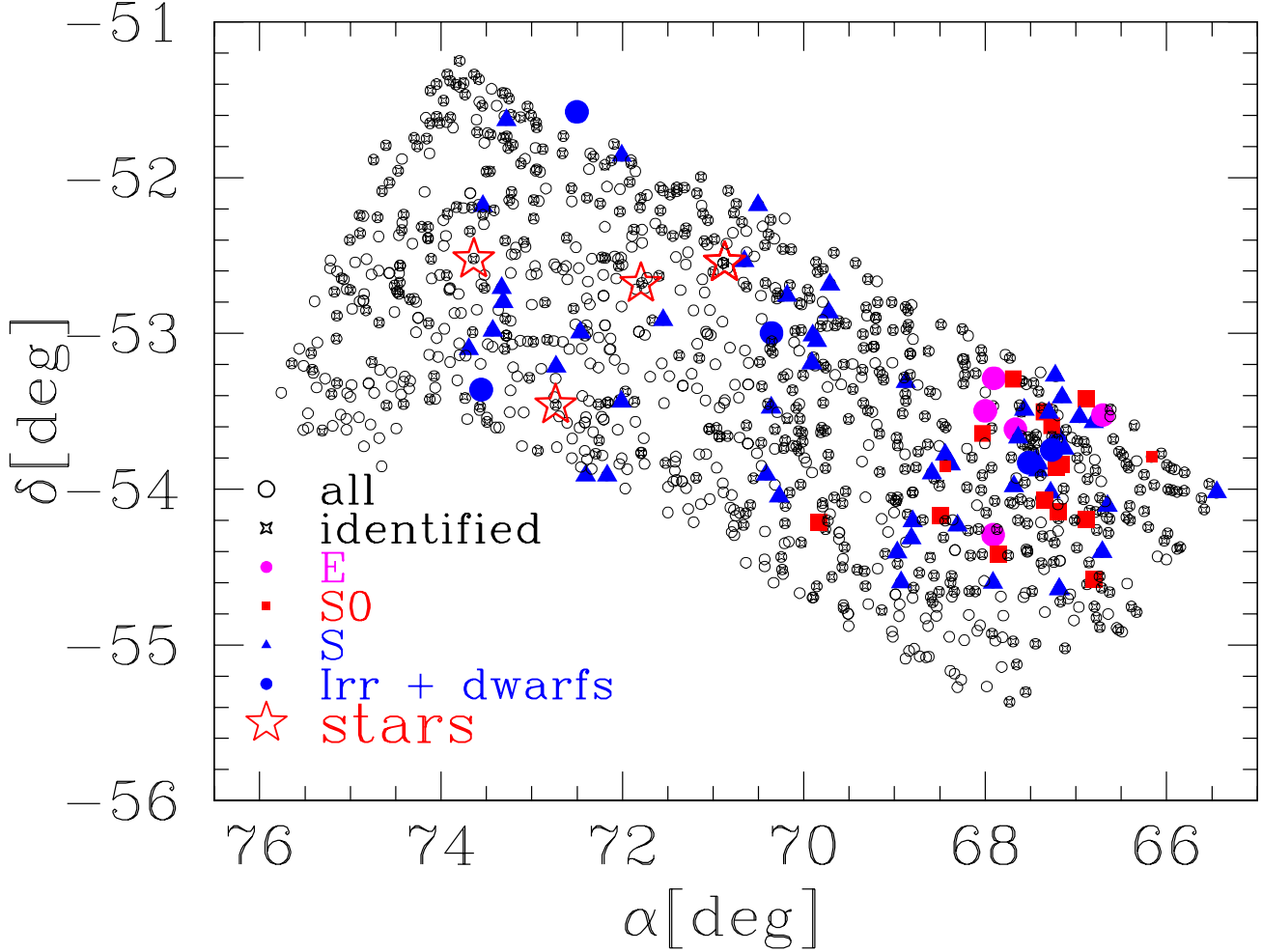


Fig. 8. Positions of galaxies with known morphological types in the ADF-S. In this plot, positions of all the ADF-S sources are marked by open circles. Identified sources are shown as small stars. The elliptical galaxies are shown as full circles, lenticular galaxies - as full squares, spiral galaxies - as full triangles and irregular or dwarf galaxies - as full circles. Positions of identified stars are shown as big empty stars; however, at least three of these identifications are most probably the effect of contamination. We can observe that all the elliptical and lenticular galaxies are located in the region of the galaxy cluster Abell S0463 at $z \sim 0.04$. Their morphologies were mostly determined by Dressler (1980a). The spiral and irregular galaxies, however, are distributed in all the field.

and in one case of a galaxy ESO 157-49 one ISOPHOT band ($170 \mu\text{m}$). We included the uncertainties of all these data points in the fitting process. Data from the ADF-S were not treated in any preferential way.

To find the best fitting models we used a χ^2 test; the details of this procedure in case of simple blackbody and dust models are explained in the corresponding sections below.

Among considered 47 galaxies, there are 15 objects with known redshifts. SEDs of these 15 galaxies are fitted and presented in the rest frame. SEDs of the remaining objects are fitted and presented in the observed frame.

The parameters resulting from all the three methods are summarized in Table 5. As the complementary information, we summarize morphological and environmental properties of galaxies used for the fitting in Table 6.

4.1.1. Modified blackbody model

As the simplest approach, we modeled the stellar component of galaxies $\nu = 5 \times 10^{13} - 10^{15}$ Hz, i.e. $\lambda = 0.3 - 6 \mu\text{m}$) with the blackbody spectrum

$$B_\nu(T) = \frac{2h\nu^2}{c^2} \frac{1}{e^{\frac{h\nu}{kT}} - 1} \quad (4)$$

and their dust emission ($\nu = 10^{12} - 10^{13}$ Hz, i.e. $\lambda = 30 - 300 \mu\text{m}$) with a modified blackbody

$$B'_\nu(T) = \nu^\gamma B_\nu(T) \quad (5)$$

Since we treat these models as indicative only, we looked for the best fitting parameters of the blackbody spectra by a χ^2 minimization, without taking errors into account. Since the blackbody spectra provide rather a poor fit to the data, we found that using the error information does not improve the fitting, and in some cases even makes the blackbody models more difficult to fit.

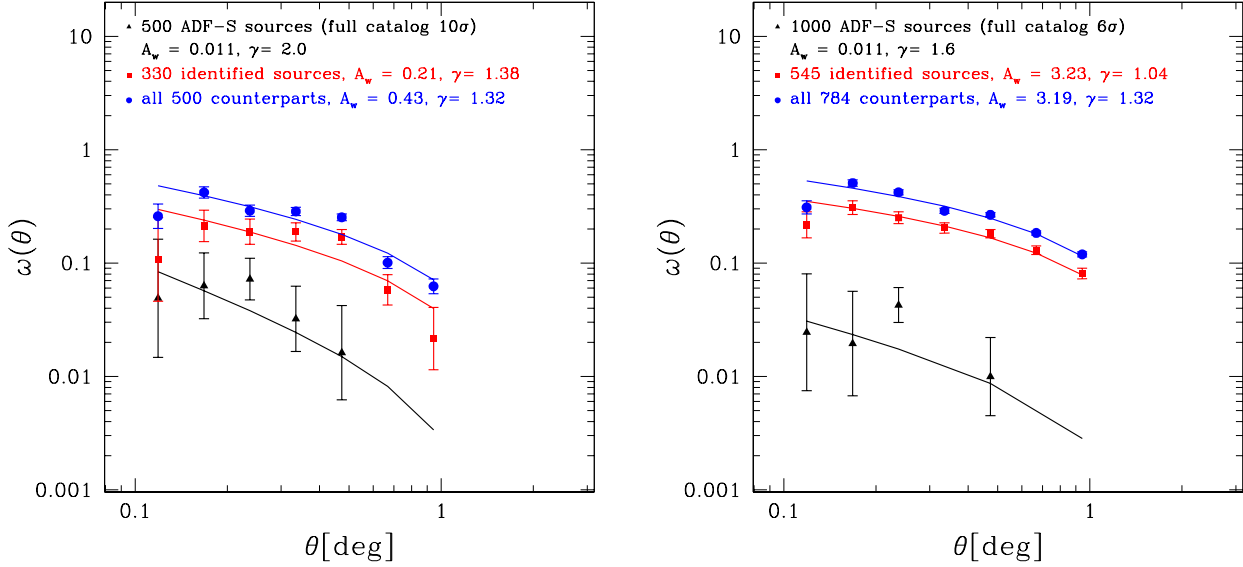


Fig. 9. Correlation function of the 10σ (left panel) and 6σ (right panel) ADF-S samples. Triangles correspond to the full 10σ and 6σ dataset of ADF-S sources, squares to the samples of the most nearby counterparts of identified sources, and circles to samples constructed from all the counterparts of the identified ADF-S sources at the angular distance smaller than $40''$ from the ADF-S source. The corresponding best-fitting power-law with an integral constraint $\omega(\theta) = A\theta^{-\gamma} - IC$ is shown in each case. We can observe a lower clustering of the full sample and a higher clustering of the identified sample, comparing to the 10σ catalog. Correlation function of all the counterparts found shows in both cases a deficit of pairs on small scales which suggests that the level of source confusion is higher than the ratio of secondary counterparts, i.e. 34% of the sample.

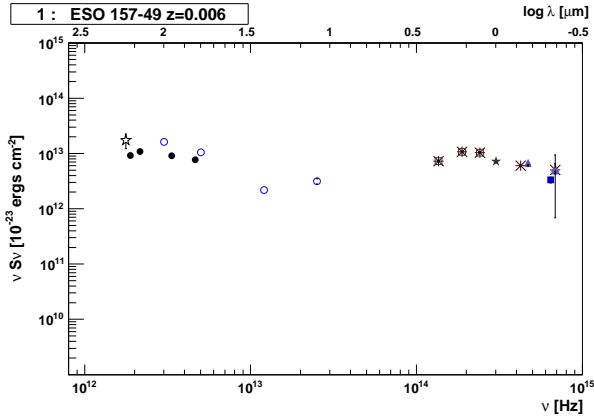


Fig. 10. An example of an SED: here we show the data points for the brightest ADF-S source, plotted using all the information listed in online Tables 3-10. The data points from AKARI Deep Field South (full circles), 2MASS (open squares), SIMBAD database (eight pointed stars), IRAS (open circles), ESO/Uppsala (full triangles), APM (full squares), RC3 (open triangles), ISOPHOT (five pointed stars) are shown. SEDs of all the identified ADF-S sources are included in the online material. Since the redshift of this object is known, the SED is presented in the rest frame.

We found the best fitting parameters looking for a minimal

$$\chi^2 = \sum_{i=1}^n \frac{(\nu S_{\nu,i} - B'_\nu(T)_i)^2}{B'_\nu(T)_i}, \quad (6)$$

where n is a number of data points, $\nu S_{\nu,i}$ is a measured flux and $B'_\nu(T)_i$ is a corresponding theoretical value given by a modified blackbody model.

If the absolute difference between data and the best fit was larger than 2σ , we performed the fitting process again, but without taking into account the point for which the relative difference was the highest, providing that there were still at least three data points left. The result of the rejection of the least fitting point in case of the poor fit can be seen e.g. in Figure 14 in case of a galaxy number 8: the data point in the B filter (the last point in the optical range) had to be removed to provide a reasonable fit. Perhaps not accidentally, the data points which are most often rejected from the fitting procedure are measurements in the optical B filter. In fact, usually they are the measurements of the poorest or most dubious quality. For instance, in case of 4 galaxies (sources 7, 8 in Figure 14, source 9 in Figure 15 and source 45 in Figure 18), these measurements, acquired from the SIMBAD database, originally come from the Dressler's catalog of galaxies in clusters (Dressler, 1980b). In the original paper, they are described as the "estimated total apparent visual magnitude" and their accuracy is about one magnitude. Then, they are obviously not suitable for the SED fitting. Other often rejected points, also in the B band (e.g. galaxy number 6 in Figure 14), come from the APM survey (Maddox et al., 1990), whose photometry is known to suffer a systematic bias (e.g., Metcalfe et al., 1995; Bertin & Dennefeld, 1997).

Having in mind all that was said about the small reliability of the stellar blackbody spectra, we should note that the "temperature" of stellar component works only as a symbolic index of the hardness of the SEDs, and does not have an absolute sense of the temperature of their stellar population. The temperature is

used here only for an internal comparison of the analyzed ADF-S sources.

We did not take into account dust attenuation in the fitting in this analysis. For this kind of analysis, we need to use a more sophisticated stellar spectral synthesis model to extract the information on the dust attenuation assuming a certain dust attenuation curve (e.g., Mathis, 1990; Calzetti et al., 1994, 2000). However, in addition to the adopted rough approximation of stellar spectra by blackbody, almost all our SEDs lack UV–optical photometry which hampers a precise determination of extinction. If we had a FIR/UV flux ratio, we would be able to estimate a correlation between FIR/UV flux ratio and luminosity from newly forming stars (Buat et al., 2005, 2007). Unfortunately, the UV photometry or distance of a source is only available for a small number of sources in our sample. Hence, we only discuss a possible effect of dust attenuation qualitatively.

As stated before, dust scatters and absorbs UV–optical light from stars and re-emits the energy at IR. Since usual attenuation curves of galaxies have a steep rise toward UV, dust attenuation causes reddening of galaxy stellar spectra. Then, this causes a significant underestimation of stellar temperature by blackbody fitting.

The best fitted values of temperature of stars and dust in the modeled galaxies are listed in the second and third column of Table 5. The histograms of these two temperatures for all 47 modeled galaxies are presented in Figure 11. According to this measurement, the both the median and mean temperature of dust is around 32 ± 4 K. The median temperature of the stellar component is 2240 ± 360 K, while its mean is 2830 ± 410 K. In the latter case, the discrepancy between mean and median values is related to the fact that the temperature distribution is far from Gaussian.

The obtained values of stellar temperatures are generally significantly too low for stars emitting UV. As we mentioned above, the estimated low temperature of our sample would be partially due to the dust attenuation. Here we use it only to make an internal comparison of our sample.

The highest stellar temperature we have fitted for a starburst blue compact dwarf NGC 1705. The dust temperature of this galaxy is also significantly higher than average. However, as it can be seen from the fourth panel in Figure 14, a simple blackbody gives a very poor fit to its stellar population.

The elliptical galaxy ESO 157-IGA040 is significantly warmer than the median stellar temperature, with $T_* = 3060$ K, and its dust temperature is also relatively high, at $T_{dust} \approx 38$ K. In its case, as seen from the second panel of Figure 14, blackbody models seem to work quite well. A particular activity of this elliptical galaxy should be probably related to the fact that it is a member of a pair of interacting galaxies.

Even if 15 spiral and five lenticular galaxies make a rather poor statistical sample, we attempted some simple comparison between these two groups.

Rather surprisingly, spiral and lenticular galaxies in our sample seem to have very similar properties, and spirals typically have even lower dust and stellar temperatures than lenticulars. The mean dust temperature of spirals ($\sim 30 \pm 5$ K) is 5 K lower than that of lenticulars ($\sim 35 \pm 17$ K), while the average temperature of a stellar component in spirals is 880 ± 200 K lower than in case of lenticulars. The difference in the dust temperatures is mainly due to the fact that the two outliers with the highest dust temperatures are lenticulars and a galaxy with the lowest fitted dust temperature is a spiral. However, the black bodies of these objects seem to be fitted reasonably well. Consequently, looking at the median values, the difference is less pronounced: the me-

dian dust temperature is 29 ± 4 K for lenticulars and 28 ± 4 K for spirals. Also the difference median between stellar temperatures for spirals and lenticulars is still significant (570 ± 130 K) but smaller.

Of course, given a small number statistics, this difference between spiral and lenticular galaxies is not very significant in a statistical sense. It might be interpreted as lenticulars detected in FIR being particularly active in star formation, at least at the same level as, average spirals. However, it is more plausible that the simplest models are not particularly accurate in reproducing the dust and stellar emission in this type of galaxies.

4.1.2. Dale and Helou model

As mentioned above, modified blackbody gives a poor fit the MIR part of dust spectrum. To fit the dust emission of our galaxies in a whole range of wavelengths between 3 and $1100 \mu\text{m}$, we applied a model proposed by Dale & Helou (2002). It was developed to model a wide range of interstellar environments in normal star-forming galaxies for different heating intensity levels. In this model the local SED of dust is given by a power-law distribution:

$$dM_d(U) \propto U^{-\alpha_{\text{SED}}} dU, \quad (7)$$

where $M_d(U)$ is the mass of dust heated by a radiation field U ; α_{SED} is a parameter that represents relative contributions of active and quiescent regions from different galaxies. Values of $\alpha_{\text{SED}} \leq 1$ represent actively star-forming galaxies. The lower value of α_{SED} , the more actively star forming is a galaxy. More quiescent cooler galaxies have $1 < \alpha_{\text{SED}} < 2.6$. The case of $\alpha_{\text{SED}} = 2.6$ corresponds to the most quiescent dust model. Values of α_{SED} between 2.6 and 4 are fitted for galaxies where the FIR emission peak appears at even longer wavelengths than in case of most quiescent well examined galaxies (Dale et al., 2005). This region is still not very well examined, but it appears to correspond to the coolest and most quiescent galaxies.

If enough data are available, it is possible to calculate the expected value of α_{SED} e.g., from IRAS $f_v(60\mu\text{m})$ and $f_v(100\mu\text{m})$ measurements (Moshir et al. (1990); this method was presented e.g. in Dale & Helou, 2001). However, in our case, a relatively small amount of data and the fact that we are exploring a rather poorly known regime of FIR have prompted us to use a minimal χ^2 -fitting. We took into account uncertainties of photometric measurements. To compare our data points to the models effectively, the modeled spectra have been convolved with the AKARI, IRAS, and Spitzer photometric bands. Using a grid of models with all the parameters available, we looked for the best fitting model with a minimal χ^2 defined as:

$$\chi^2 = \sum_{i=1}^n \frac{((\nu S_{\nu,i} + K) - F_{\nu,i})^2}{\sigma_{\nu,i}^2}, \quad (8)$$

where n is a number of points, K - a normalization constant, used as a free parameter, $\nu S_{\nu,i}$ is a measured flux, $F_{\nu,i}$ is a corresponding theoretical value of flux from the dust model, $\sigma_{\nu,i}$ is a corresponding measurement error.

The resulting α_{SED} for all modeled galaxies are listed in column 4 of Table 5.

Histogram of α_{SED} , presented in Figure 12, shows that the distribution of α_{SED} is quite discontinuous. Most of the analyzed sources have extreme values of α_{SED} : less than 0.9 (19 sources) or more than 3.5 (17 sources). We have found seven galaxies with values of α_{SED} between 1.7 and 2.1 and five with values

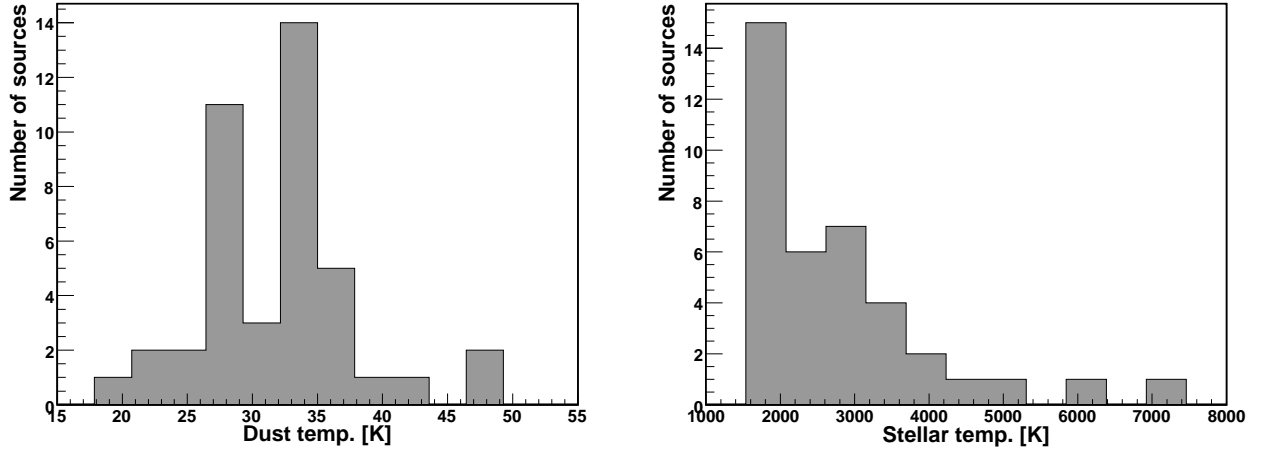


Fig. 11. Histograms of temperatures of dust and stellar components of galaxies in the best fit modified blackbody models.

α_{SED} between 0.9 and 1.7. No galaxies were fitted by models with α_{SED} between 2.2 and 3.5.

Among galaxies with known morphological types, 80 % of lenticular galaxies were fitted as the warmest, actively star forming galaxies with $\alpha_{\text{SED}} < 1$ and only one of them, 2MASX J04292360 – 5330114, was placed in a different regime, as the most quiescent galaxy with $\alpha_{\text{SED}} = 4$. No lenticular galaxy was found to be in the $\alpha_{\text{SED}} = 1 - 2.6$ regime.

The elliptical and 4 of the spiral galaxies were classified as cool and quiescent. One of the compact galaxies, the starburst blue compact dwarf NGC 1705, similarly to 60 % of spiral galaxies, is classified as warm and actively star forming. ESO 157-51, a second compact galaxy, and the remaining 40 % of spiral galaxies were placed in poorly examined and, in all probability, the most quiescent regime with $\alpha_{\text{SED}} > 3$. This suggests that the peak of their dust emission is located at yet longer wavelengths.

We have compared our conclusions with the results of Dale et al. (2005), who constructed SEDs for 71 nearby galaxies from the SINGS sample (Kennicutt et al., 2003) in the range of λ from 1 μm to 850 μm . Among them there are five elliptical galaxies with α_{SED} between 1.32 and 2.14 and one with $\alpha_{\text{SED}} = 4$. This range of α_{SED} indicates that all elliptical galaxies in the SINGS sample are cold and quiescent. The only elliptical galaxy in our sample seems to belong to the same type. This is expected, however, not consistent with the results of the simple blackbody fitting, which may point out the insufficiency of the latter.

In the sample used by Dale et al. (2005) there were also two lenticular galaxies, one of them warm and active in star formation ($\alpha_{\text{SED}} = 0.6$) and one cold ($\alpha_{\text{SED}} = 2.67$). In this case, because of a poor number statistics, it is difficult to make any comparison, but our modeling confirms that lenticulars can be very warm as well as extremely quiescent.

The only discrepancy concerns spiral galaxies. In the data used by Dale et al. (2005), 54 spiral galaxies were included, and none of them was classified as actively star forming: 54 % of them were cold and quiescent with α_{SED} between 1.68 and 2.6 and the remaining 45 % were described as even more quiescent with $\alpha_{\text{SED}} > 2.6$. In our case a half of spiral galaxies is very warm and active in star formation, there are no quiescent ones with α_{SED} between 1.68 and 2.6 but the other half are spiral galaxies with $\alpha_{\text{SED}} = 4$, i.e., extremely quiescent. This finding is consistent with the fact that our sample is based on a genuine FIR (90 μm) selection. On one hand, this sample is sensitive to

pick up dusty IR galaxies, but on the other hand, it can also select galaxies which are quiescent because of the long wavelength comparing with IRAS-based studies (usually based on 60 μm selected).

4.1.3. Li & Draine model

As yet another more refined model of the infrared emission from dust grains heated by starlight in galaxies we have chosen the model proposed by Draine & Li (2007), which is an improved version of Li & Draine (2001). This model assumes that the dust heated by starlight consists of a mixture of amorphous silicate and carbonaceous grains. Each molecules have a wide size distribution ranging from molecules containing tens of atom to large grains $\geq 1 \mu\text{m}$ in diameter (Draine & Li, 2007). In this paper authors have calculated the emission spectrum for dust heated by the stellar light and parametrized this model using three parameters: the fraction of the total dust mass that is contributed by the polycyclic aromatic hydrocarbon (PAH) particles (q_{PAH}), lower (U_{min}) and higher (U_{max}) cutoff of the starlight intensity distribution and the fraction of a dust heated by the starlight (γ).

As before, the modeled spectra have been first convolved with the AKARI, IRAS, and Spitzer photometric bands. We have fitted Draine & Li (2007) using a χ^2 test including - as in case of the Dale & Helou model - the information about the photometric errors.

Draine & Li (2007) calculate the parameters directly from Spitzer data which was impossible in our case, but may be a part of a future project. The resulting values of q_{PAH} are listed in column 7 of Table 5. The histogram of q_{PAH} , shown in Figure 13, is very discrete, with peaks around three specific values: $q_{\text{PAH}} = 0.75, 2.37$ and 4.58, which correspond to the Large Magellanic Cloud models.

Spectra presented by Draine & Li (2007) correspond to 11 dust models with q_{PAH} ranging from 0.1 % to 4.58 %. The lowest value of q_{PAH} corresponds to the Small Magellanic Cloud (SMC) model; $q_{\text{PAH}} = 0.75 \%$, 1.49 % and 2.37 % correspond to the Large Magellanic Cloud (LMC) and the remaining 7 models are related to the Milky Way (MW)-like galaxies. 81 % from 47 modeled ADF-S sources were identified as LMC-like galaxies and 9 % corresponded to MW-type galaxies. No SMC-like galaxy was found. In all the sample, the median $q_{\text{PAH}} = 2.37 \%$.

All five lenticular galaxies, as well as both compact dwarfs in our sample are best fitted by LMC-like models with values

of $q_{\text{PAH}} \leq 2.37$. Also the majority (87.5 %) of spiral galaxies is best fitted by LMC-like models, while for the rest MW-like models are applied. Maximal q_{PAH} for spiral galaxies is 3.9 %. Then, spiral galaxies tend to be bigger and richer in PAH, but the difference with lenticulars is not statistically significant. The elliptical galaxy has the highest $q_{\text{PAH}} = 4.55$ % among modeled galaxies and is classified as MW-like galaxy. The discrepant conclusions about this particular galaxy probably reflect its more complex structure and processes, related to its interactions with another galaxy.

5. Conclusions

1. In this paper, we presented the catalog of counterparts of the ADF-S 90 μm sources, detected at the $> 6\sigma$ level. We found counterparts for 545 among 1000 sources from the analyzed catalog. We discussed the properties of these sources and tried to derive conclusions about the average properties of the sample.
2. The point source ADF-S catalog itself appeared to be quite reliable in the position determination, with most of the counterparts located at the angular distance significantly lower than the nominal resolution of the FIS detector. A small number of counterparts detected at higher angular distances can be possibly an effect of contamination. In the position determination we observe a small (of an order of $4''$, but systematic bias, which depends on the location in the ADF-S. This small systematics should be taken into account in the future works on these data.
3. We conclude that FIR sources detected in the ADF-S are mostly nearby galaxies. This conclusion is supported, first of all, by source number counts in the FIR, but also a large number of bright optical counterparts and the redshift distribution of counterparts. It should be noted, however, that the completeness of the identified sample, close to 100% for sources brighter than 0.1 Jy, falls down rather rapidly for fainter sources, to 55 % for the whole 10σ catalog.
4. The population of identified galaxies appears surprisingly "normal", similar to one expected for local optically bright galaxies. The main differences are:
 - a) a significantly lower percentage of elliptical galaxies, which can be explained by the fact they are less dusty than other galaxies,
 - b) much higher percentage of peculiar galaxies, which can be attributed to strong star-forming activity of these objects, related to intergalactic interactions, and hence stronger radiation of cold dust in them).
 - c) We detected also a fraction of lenticular galaxies (all from the cluster of galaxies Abell S0463) which is practically the same as expected in the optically bright galaxy population. It suggests that these galaxies contain a significant amount of cold dust and supports more complex models of their formation than a simple secular evolution.
5. The estimated source confusion is on the level higher than 34 % of the number of identified sources. It suggests that to remove the effect of the source confusion from the IR flux measurements and for a proper estimation of local environment of the FIR-bright galaxies dedicated observations of their closest neighborhood will be required.
6. The SEDs of the identified sources display a variety of properties. In the first approach, the examined galaxies seem to be either extremely quiescent or very active in star formation. The lenticular galaxies usually belong to the actively star forming group. The analysis suggests that to explain well

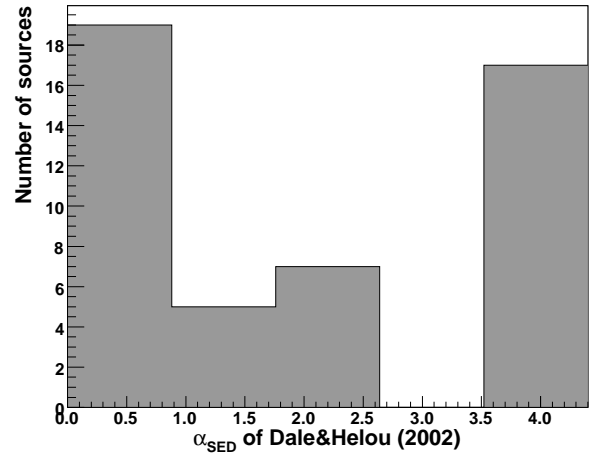


Fig. 12. The histogram of the parameter α of the model by Dale & Helou (2002).

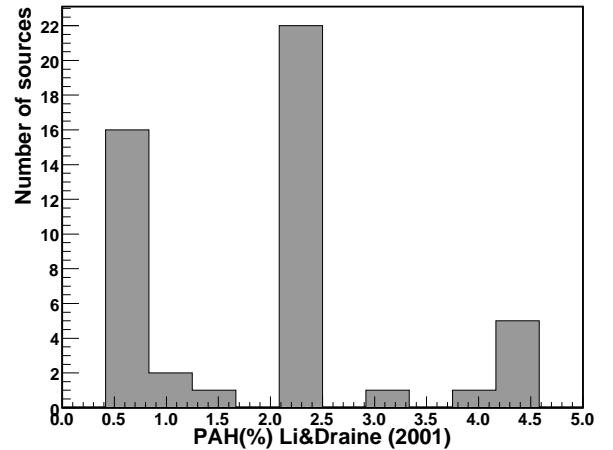


Fig. 13. The histogram of the amount of polycyclic aromatic hydrocarbons (PAH) in the dust of the analyzed galaxies, according to the model by Li & Draine (2001).

the FIR properties of otherwise "normal" galaxies from our sample new updated models should be developed.

Acknowledgements. We thank the anonymous referee for her/his very careful reading of the manuscript and giving useful comments which significantly improved the clarity of this paper. This work is based on observations with AKARI, a JAXA project with the participation of ESA. This research has made use of the NASA/IPAC Extragalactic Database (NED) which is operated by the Jet Propulsion Laboratory, California Institute of Technology, under contract with the National Aeronautics and Space Administration, and the SIMBAD database, operated at CDS, Strasbourg, France We thank Misato Fukagawa for sending the information about Vega-like star candidates. This work has been supported in part by the Polish Astroparticle Physics Network. AP was financed by the research grant of the Polish Ministry of Science PBZ/MNiSW/07/2006/34A. TTT has been supported by Program for Improvement of Research Environment for Young Researchers from Special Coordination Funds for Promoting Science and Technology, and the Grant-in-Aid for the Scientific Research Fund (20740105) commissioned by the Ministry of Education, Culture, Sports, Science and Technology (MEXT) of Japan. TTT has been partially supported from the Grand-in-Aid for the Global COE Program "Quest for Fundamental Principles in the Universe: from Particles to the Solar System and the Cosmos" from the MEXT.

References

Abell, G. O., Corwin, H.G. Jr. & Olowin, R.P. 1989, ApJS, 70, 1

- Abadi, M. G., Moore, B. & Bower, R. G. 1999, *MNRAS*, 308, 947
- Barway, S., Wadadekar, Y., Kembhavi, A. K. & Mayya, Y. D. 2009, *MNRAS*, 394, 1991
- Bekki, K. 1998, *ApJ*, 502, L133
- Bertin, E. & Dennefeld, M. 1997, *MNRAS*, 317, 43
- Buat, V., Iglesias-Páramo, J. & Seibert, M. 2005, *ApJ*, 619, L51
- Buat, V., et al. 2007, *ApJS*, 173, 404
- Calzetti, D., Kinney, A. L. & Storchi-Bergmann, T. 1994, *ApJ*, 429, 582
- Calzetti, D., Armus, L. & Bohlin, R. C. 2000, *ApJ*, 533, 682
- Cannon, J. M., Smith, J.-D. T., Walter, F. et al. 2006, *ApJ*, 647, 293
- da Costa, L. N., Pellegrini, P.S., Davis, M. et al. *ApJS*, 1991, 75, 935
- Dale, D. A. & Helou, G. 2001, *ApJ*, 549, 215
- Dale, D. A. & Helou, G. 2002, *ApJ*, 576, 159
- Dale, D.A., Bendo, G. J., Engelbracht, C. W. et al. 2005, *ApJ*, 633, 857
- Dale, D. A., Gil de Paz, A., Gordon, K. D. et al. 2007, *ApJ*, 655, 863
- Danks, A.C., Laustsen, S., van Woerden, H. 1979, *A&A* 73, 247
- de la Torre, S. and Le Fèvre, O. and Arnouts, S. 2007, *A&A*, 475, 443
- de Souza, R. E., de Mello, D. F. & Dos Anjos, S. 1997, *A&AS*, 125, 329
- de Vaucouleurs, G. 1963, *ApJ Suppl.* 8, 31
- de Vaucouleurs, G., de Vaucouleurs, A., Corwin, Jr. H. G. et al. 1991, Springer-Verlag, Berlin – Heidelberg – New York
- Dole, H., Lagache, G., Puget, J.-L. et al. 2006, *A&A*, 451, 417
- Draine, B. T., & Anderson, N. 1985, *ApJ*, 292, 494
- Draine, B. T., & Li, A. 2001, *ApJ*, 551, 807
- Draine, B.T., & Li, A. 2007, *ApJ*, 657, 810
- Dressler, A. 1980a, *ApJS*, 42, 565
- Dressler, A. 1980b, *ApJ*, 236, 351
- Dressler, A., Shectman, S. A. 1988, *AJ*, 95, 284
- Doyle, M. T., Drinkwater, M. J. & Rohde, D. J. 2005, *MNRAS*, 361, 34
- Egan, M. P., Price, S. D., Kraemer, K. E. et al. 2003, *VizieR Online Data Catalog*, 5114
- Ellis, R. S., Gray, P. M., Carter, D. & Godwin, J. 1984, *MNRAS*, 206, 285
- Fairall, A.P. 1984, *MNRAS*, 210, 69
- Fox, A. J., Savage, B. D. & Wakker, B. P. 2006, *ApJS*, 165, 229
- Genzel, R., & Cesarsky, C. J. 2000, *ARA&A*, 38, 761
- Gil de Paz, A., Madore, B. F., & Pevunova, O. 2003, *ApJS*, 147, 29
- Hubble, E. P. 1936, *The Realm of the Nebulae*, New Haven: Yale University Press
- Karl, B. et al. 1995, *ApJS*, 100, 69
- Kawada, M., Baba, H., Barthel, P. D. et al. 2007, *PASJ* 59, S389
- Kawada, M. et al., 2010, in preparation
- Kennicutt, R. C., Armus, L., Bendo, G. et al. 2003, *PASP* 115, 928
- Kinney, A. L., Bohlin, R. C., Calzetti, D., Panagia, N. & Wyse, R. F. G. 1993, *ApJS*, 86, 5
- Knapp, G.R., Guhathakurta, P., Kim, D.-W., Jura, M. A. 1989, *ApJS*, 70, 329
- Landy, S.D. & Szalay, A.S. 1993, *ApJ*, 412, 64
- Lauberts, A. & Valentijn, E. A. 1989, *The surface photometry catalogue of the ESO-Uppsala galaxies*, Garching: European Southern Observatory
- Lawrence, A., Rowan-Robinson, M., Ellis, R. S. et al., 2001, *MNRAS*, 326, 1333
- Li, A., & Draine, B. T. 2001, *ApJ*, 554, 778
- Loveday, J., Peterson, B. A., Maddox, S. J. & Efstathiou, G. 1996, *ApJS*, 107, 201
- Maddox, S. J., Efstathiou, G., Sutherland, W. J. & Loveday, J. 1990, 1990, *MNRAS*, 243, 692
- Mathis, J. S. 1990, *ARA&A*, 28, 37
- Mauch, T., Murphy, T., Buttery, H. J., et al. 2003, *MNRAS*, 342, 1117
- Mathewson, D. S. & Ford, V. L. 1996, *ApJS*, 107, 97
- Mathewson, D. S., Ford, V. L. & Buchhorn, M. 1992, *ApJS*, 81, 413
- Metcalfe, N., Fong, R. & Shanks, T. 1995, *MNRAS*, 274, 769
- Metcalfe, N., Shanks, T., Campos, A., Fong, R. & Gardner, J.P. 1996, *Nature*, 383, 236
- Moshir, M., Kopan, G. & Conrow, T. 1990, *Bulletin of the American Astronomical Society*, 22, 1325
- Murakami, H., Baba, H., Barthel, P. et al. 2007, *PASJ* 59, S369
- di Nella, H., Paturel, G., Walsh, A. J. et al. 1996, *A&AS*, 118, 311
- Oliver, S., Waddington, I., & Gonzalez-Solares, E. 2004, *ApJS*, 154, 30
- Pahre, M. A., Ashby, M. L. N., Fazio, G. G. & Willner, S. P. 2004, *ApJS*, 154, 229
- Paturel, G., Dubois, P., Petit, C. & Woelfel, F. 2002, *LEDA*, 0
- Peebles, P. J. E., & Groth, E. J. 1976, *A&A*, 53, 131
- Peebles, P. J. E. 1993, *Principles of Physical Cosmology*, Princeton University Press, Princeton
- Purcell, E. M. 1976, *ApJ*, 206, 685
- Rifatto, A., Longo, G. & Capaccioli, M. 1995, *A&AS*, 114, 527
- Roberts, M. S., & Haynes, M. P. 1994, *ARA&A*, 32, 115
- Sandage, A. 1975, *ApJ*, 202, 563,
- Shirahata, M., et al. 2009, *PASJ*, 61, 737
- Shirahata, M., Matsuura, S., Kawada, M., et al. 2010, in preparation
- Sil'chenko, O. K. & Afanasiev, V. L. 2004, *AJ*, 127, 2641
- Skrutskie M. F., Cutri, R. M. & Stiening, R. 2003, *The 2MASS Extended sources (IPAC/UMass, 2003-2006)*, *VizieR Online Data Catalog*
- Soifer, B. T., Houck, J. R., & Neugebauer, G. 1987, *ARA&A*, 25, 187
- Soifer, B. T., Helou, G., & Werner, M. 2008, *ARA&A*, 46, 201
- Takeuchi, T. T., Hirashita, H., Ishii, T. T., Hunt, L. K., & Ferrara, A. 2003, *MNRAS*, 343, 839
- Takeuchi, T. T., & Ishii, T. T. 2004, *ApJ*, 604, 40
- Takeuchi, T. T., Buat, V., & Burgarella, D. 2005a, *A&A*, 440, L17
- Takeuchi, T. T., Buat, V., Iglesias-Páramo, J., Boselli, A., & Burgarella, D. 2005b, *A&A*, 432, 423
- Takeuchi, T. T., Ishii, T. T., Nozawa, T., Kozasa, T., & Hirashita, H. 2005c, *MNRAS*, 362, 592
- Takeuchi, T. T., Ishii, T. T., Dole, H., Dennefeld, M., Lagache, G., & Puget, J.-L. 2006, *A&A*, 448, 525
- Thomas, H.-C., Beuermann, K., Reinsch, K. et al. 1998, *A&A*, 335, 467
- van den Bergh, S. 1994, *AJ*, 107, 153
- van den Bergh, S. 2009, *ApJ*, 702, 1502
- Verma, A., Charmandaris, V., Klaas, U., Lutz, D., & Haas, M. 2005, *Space Science Reviews*, 119, 355
- Wenger, M., Ochsenbein, F., Egret, D. et al. 2000, *A&AS*, 143, 9
- Wisotzki, L., Christlieb, N., Bade, N. et al. 2000, *A&A*, 358, 77
- Yoshii, Y., & Takahara, F. 1988, *ApJ*, 326, 1

Table 5. Parameters of the fitted models of SEDs of 47 ADF-S galaxies with the best photometric data. The table contains ADF-S identification numbers (first column), indicative temperatures of dust and stellar component resulting from the best fitted modified blackbody models, the parameter α of the Dale & Helou (2001) model, three parameters and the name of the best fitted Li & Draine (2001) model.

ID (ADF-S)	Modified blackbody		Dale & Helou	Li & Draine			name
	Dust temp. [K]	Stellar temp. [K]	α	Umin	Umax	PAH (%)	
1	26.9 ± 0.2	2800 ± 40	2.4375	4.00	4.00	2.37	LMC2
2	37.8 ± 0.3	3060 ± 30	2.1250	0.10	100	4.58	MW3.1
3	22.9 ± 0.2	2950 ± 30	2.1250	0.50	0.50	2.37	LMC2
4	36.3 ± 0.1	7000 ± 120	1.0000	1.20	100	2.37	LMC2
5	33.6 ± 0.3	3260 ± 50	1.3125	0.10	100	2.37	LMC2
6	32.6 ± 0.3	2110 ± 70	1.3125	5.00	5.00	2.37	LMC2
7	47.8 ± 0.4	5110 ± 50	0.0625	8.00	1e4	2.37	LMC2
8	36.8 ± 0.4	2020 ± 70	0.0625	0.10	1e4	1.12	MW3.1
9	-	3890 ± 50	1.1875	0.80	1e4	3.90	MW3.1
10	27.8 ± 0.2	3230 ± 30	4.0000	2.00	2.00	2.37	LMC2
11	28.9 ± 0.3	3030 ± 40	4.0000	2.00	2.00	2.37	LMC2
12	36.0 ± 0.6	2070 ± 120	4.0000	5.00	1e4	2.37	LMC2
13	33.2 ± 0.4	-	4.0000	0.10	100	0.75	LMC2
14	32.4 ± 0.4	-	0.0625	8.00	100	2.37	LMC2
15	32.1 ± 0.2	1980 ± 10	0.0625	0.10	100	0.75	LMC2
16	28.2 ± 0.7	-	0.0625	0.10	100	4.58	MW3.1
17	33.2 ± 0.6	5890 ± 60	0.0625	0.10	1e4	0.75	LMC2
18	28.8 ± 0.2	2260 ± 70	0.0625	4.00	4.00	2.37	LMC2
19	33.8 ± 0.1	2050 ± 10	0.0625	15.0	15.0	0.75	LMC2
20	33.0 ± 0.5	1980 ± 70	0.0625	0.10	1e4	0.75	LMC2
21	29.4 ± 0.2	2210 ± 10	0.0625	4.00	4.00	2.37	LMC2
22	38.0 ± 0.1	2060 ± 40	4.0000	0.10	100	0.75	LMC2
23	28.1 ± 0.3	2340 ± 70	4.0000	0.10	100	2.37	LMC2
24	33.4 ± 0.6	2140 ± 10	4.0000	0.10	1e6	0.75	LMC2
26	43.5 ± 0.1	-	0.0625	4.00	1e4	0.75	LMC2
27	35.7 ± 0.3	-	0.0625	0.80	100	2.37	LMC2
29	27.5 ± 0.8	2950 ± 20	0.0625	0.10	100	0.75	LMC2
30	32.7 ± 0.7	1900 ± 10	0.0625	0.10	1e6	4.58	MW3.1
31	32.8 ± 0.3	1970 ± 120	0.0625	8.00	8.00	2.37	LMC2
39	47.4 ± 0.4	3500 ± 60	0.0625	0.20	1e6	0.47	MW3.1
41	32.5 ± 0.1	1950 ± 10	0.0625	12.0	12.0	0.75	LMC2
42	-	2210 ± 30	0.0625	0.10	1e5	0.75	LMC2
43	33.3 ± 0.7	1970 ± 10	0.0625	0.10	1e6	0.75	LMC2
45	28.5 ± 0.1	4160 ± 80	3.8750	0.10	100	0.75	LMC2
46	-	1650 ± 20	3.8750	0.10	1e6	4.58	MW3.1
48	24.3 ± 0.1	2010 ± 10	3.8750	1.20	1.20	2.37	LMC2
49	26.6 ± 0.1	-	3.8750	0.10	100	0.75	LMC2
50	33.6 ± 0.1	3380 ± 60	3.8750	0.10	1e6	1.49	LMC2
51	29.7 ± 0.2	3120 ± 30	2.2500	0.10	100	0.75	LMC2
52	-	2000 ± 30	2.2500	2.00	1e6	2.37	LMC2
56	34.8 ± 0.1	-	2.2500	0.10	1e6	4.58	MW3.1
64	23.1 ± 0.1	1940 ± 10	2.2500	0.70	0.70	2.37	LMC2
65	28.0 ± 0.1	4600 ± 110	4.0000	1.50	1.50	2.37	LMC2
69	26.4 ± 0.1	1770 ± 80	4.0000	2.00	2.00	2.37	LMC2
73	-	-	4.0000	1.50	1e6	2.37	LMC2
82	27.8 ± 0.1	-	4.0000	2.00	2.00	3.19	MW3.1
103	20.2 ± 0.1	2910 ± 50	4.0000	0.10	0.10	2.37	LMC2

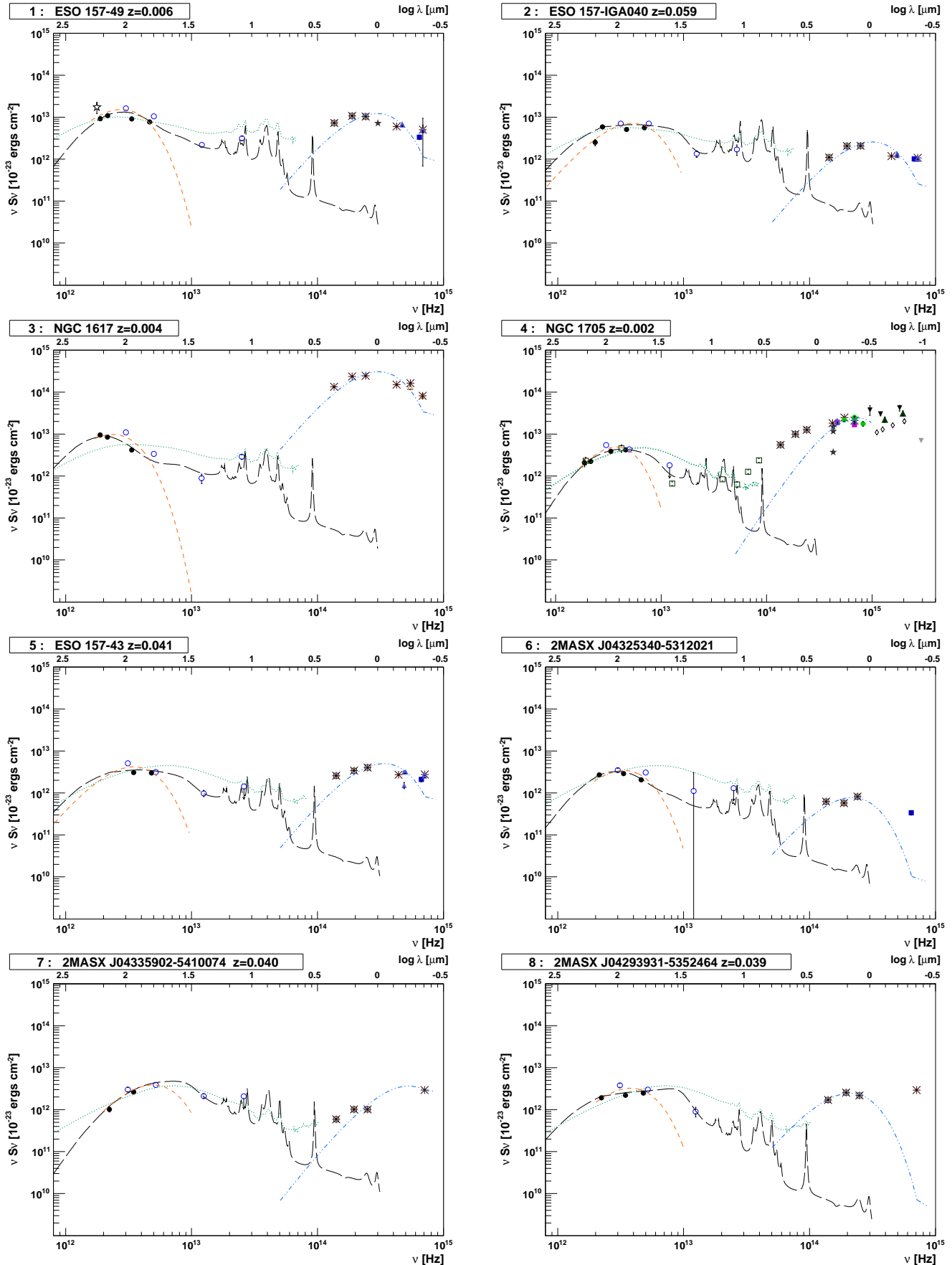


Fig. 14. The SEDs of ADF-S galaxies with the best photometry and available data from other catalogs. The data points from AKARI Deep Field South (full circles), 2MASS (open squares), SIMBAD database (eight pointed stars), IRAS (open circles), ESO/Uppsala (full triangles), APM (full squares), RC3 (full triangles), ISOPHOT (five pointed stars), Siding Spring Observatory (five pointed stars), GALEX (full triangles), HIPASS catalogue (full circles), Palomar/Las Campanas Imaging Atlas of Blue Compact Dwarf Galaxies (full squares), IUE (open diamonds), Spitzer (open squares), FUSE (upside-down light triangles) and UV: 1650, 2500, 315 (upside-down dark triangles) were fitted by three different models of dust emission: modified blackbody (short-dashed line) model

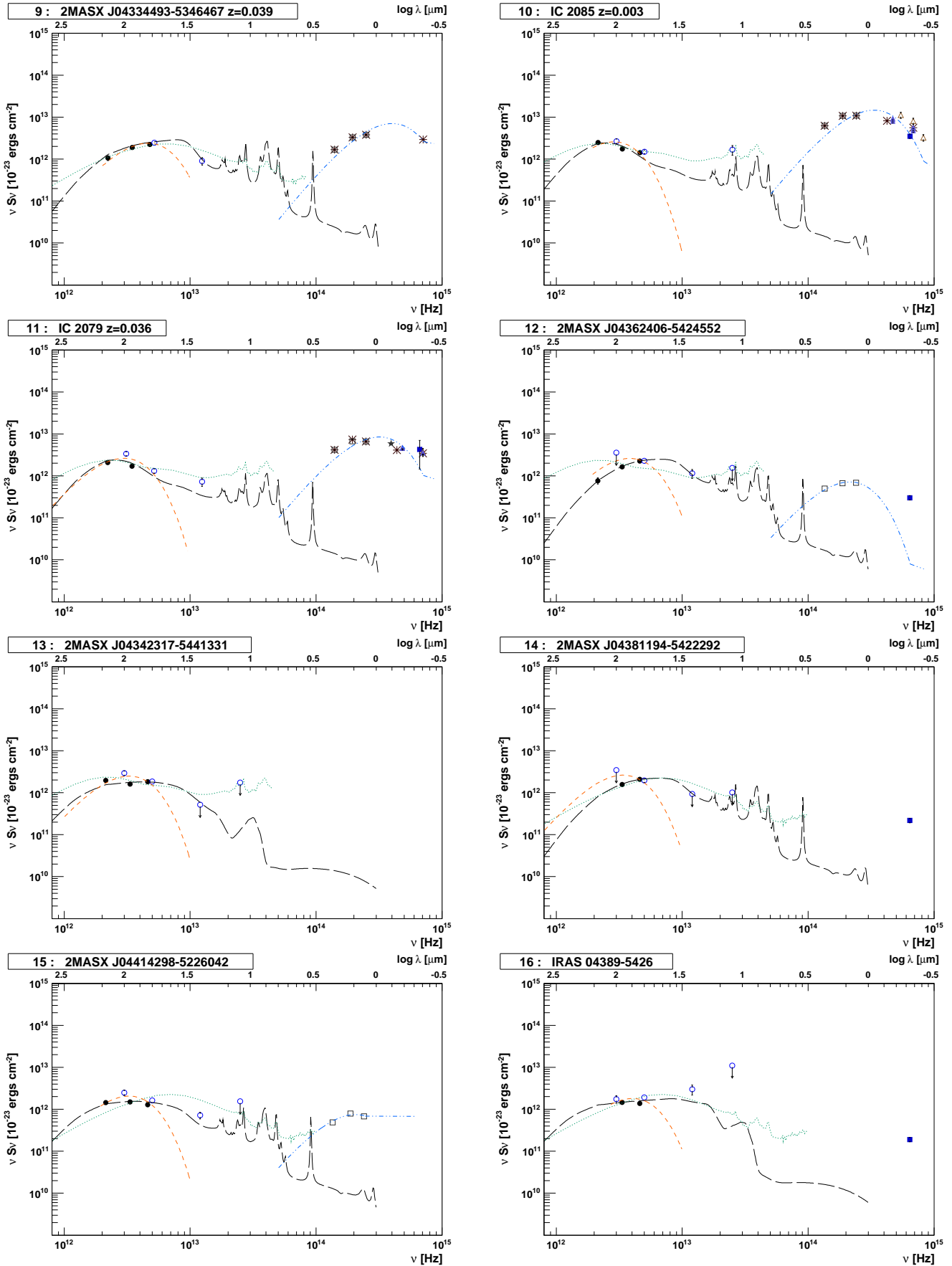


Fig. 15. Next 8 SEDs of ADF-S galaxies, with symbols as in Figure 14. SEDs of galaxies with a given redshift (objects number 9, 10, 11) are fitted after shifting to the rest frame and presented in the rest frame. The remaining objects are shown in the observed frame.

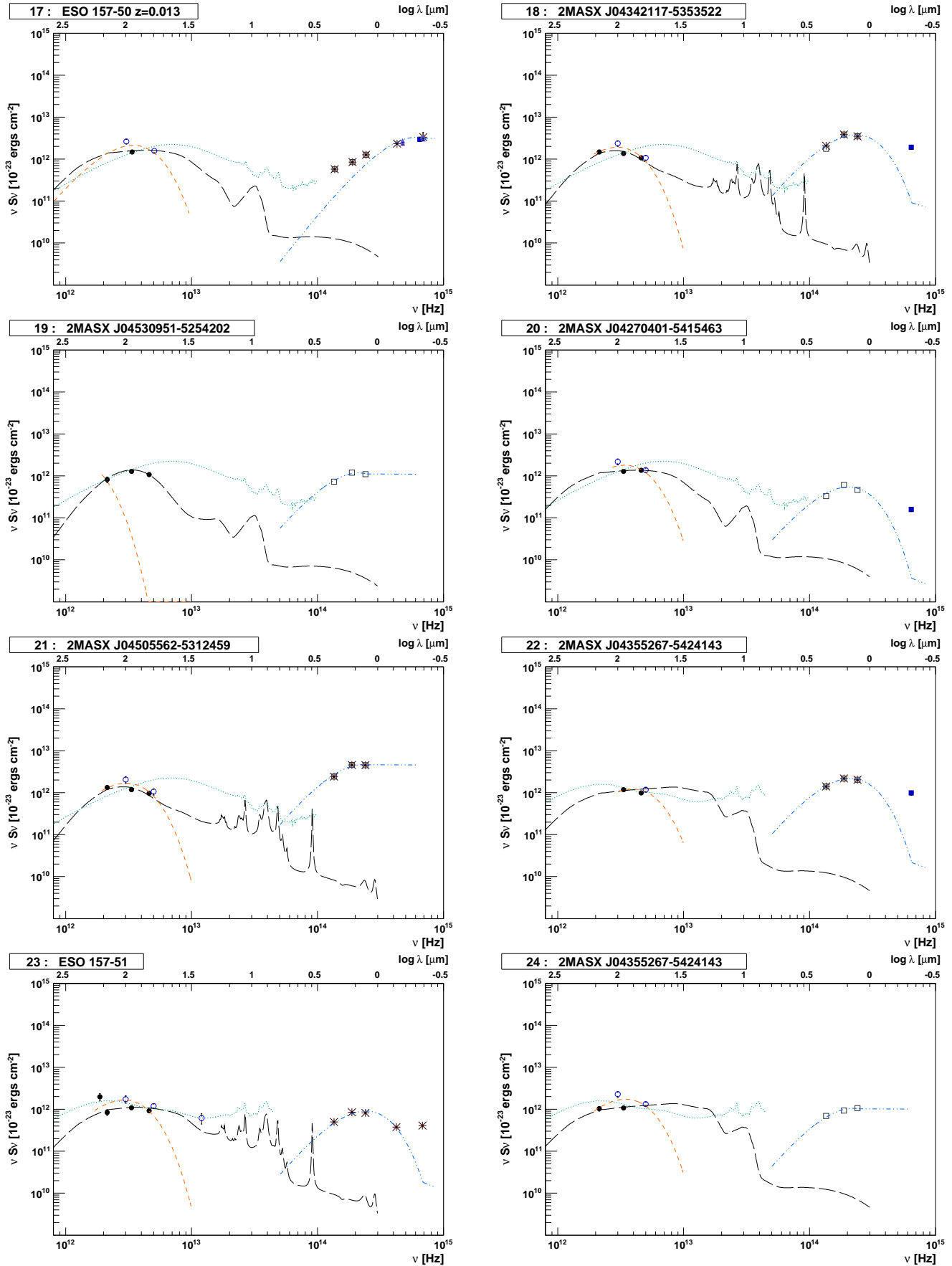


Fig. 16. Next 8 SEDs of ADF-S galaxies, with symbols as in Figure 14. SED of a galaxy number 17, for which the redshift is known, is fitted after shifting to the rest frame and presented in the rest frame. The remaining objects are shown in the observed frame.

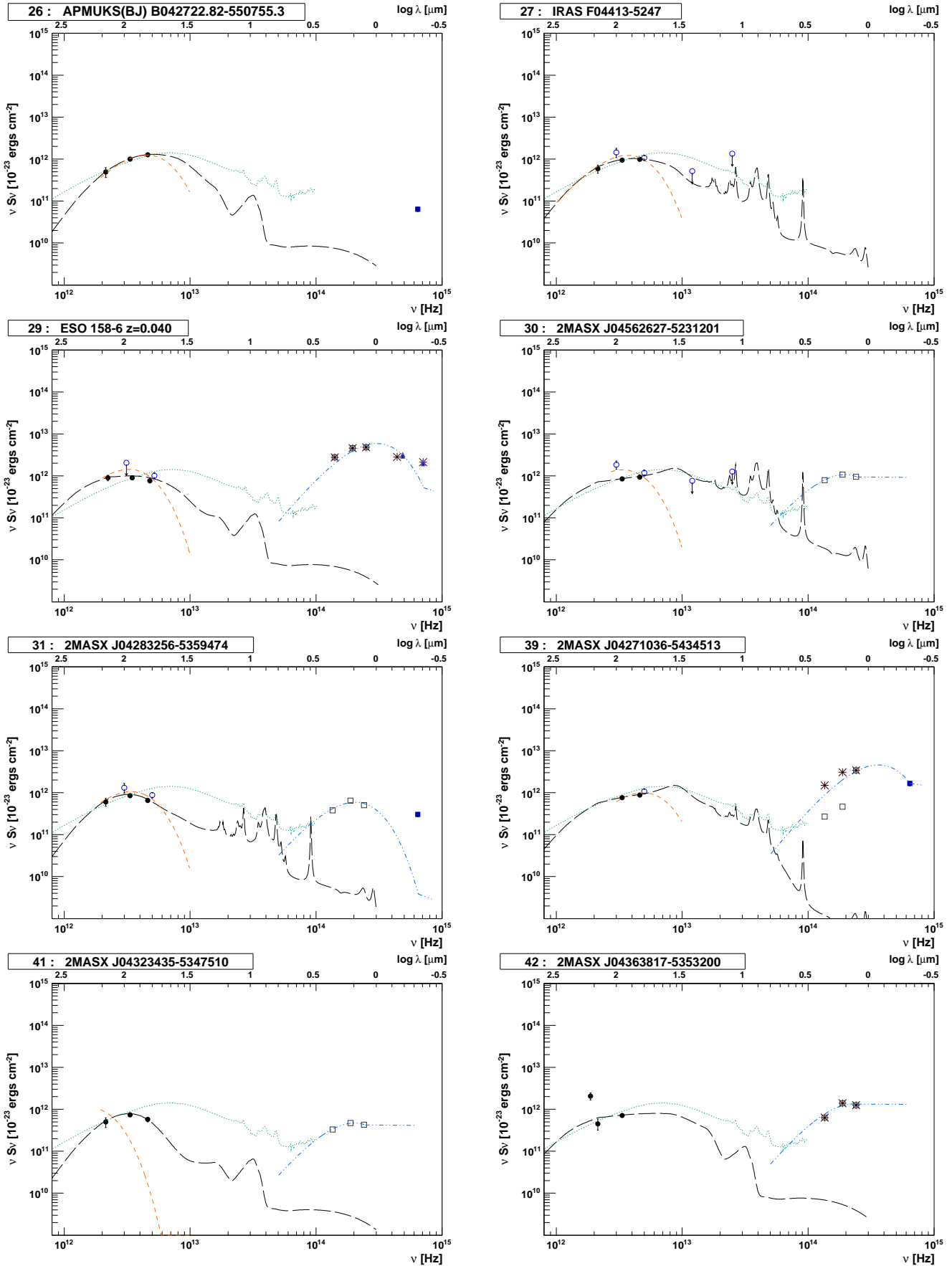


Fig. 17. Next 8 SEDs of ADF-S galaxies, with symbols as in Figure 14. SED of a galaxy number 29, for which the redshift is known, is fitted after shifting to the rest frame and presented in the rest frame. The remaining objects are shown in the observed frame.

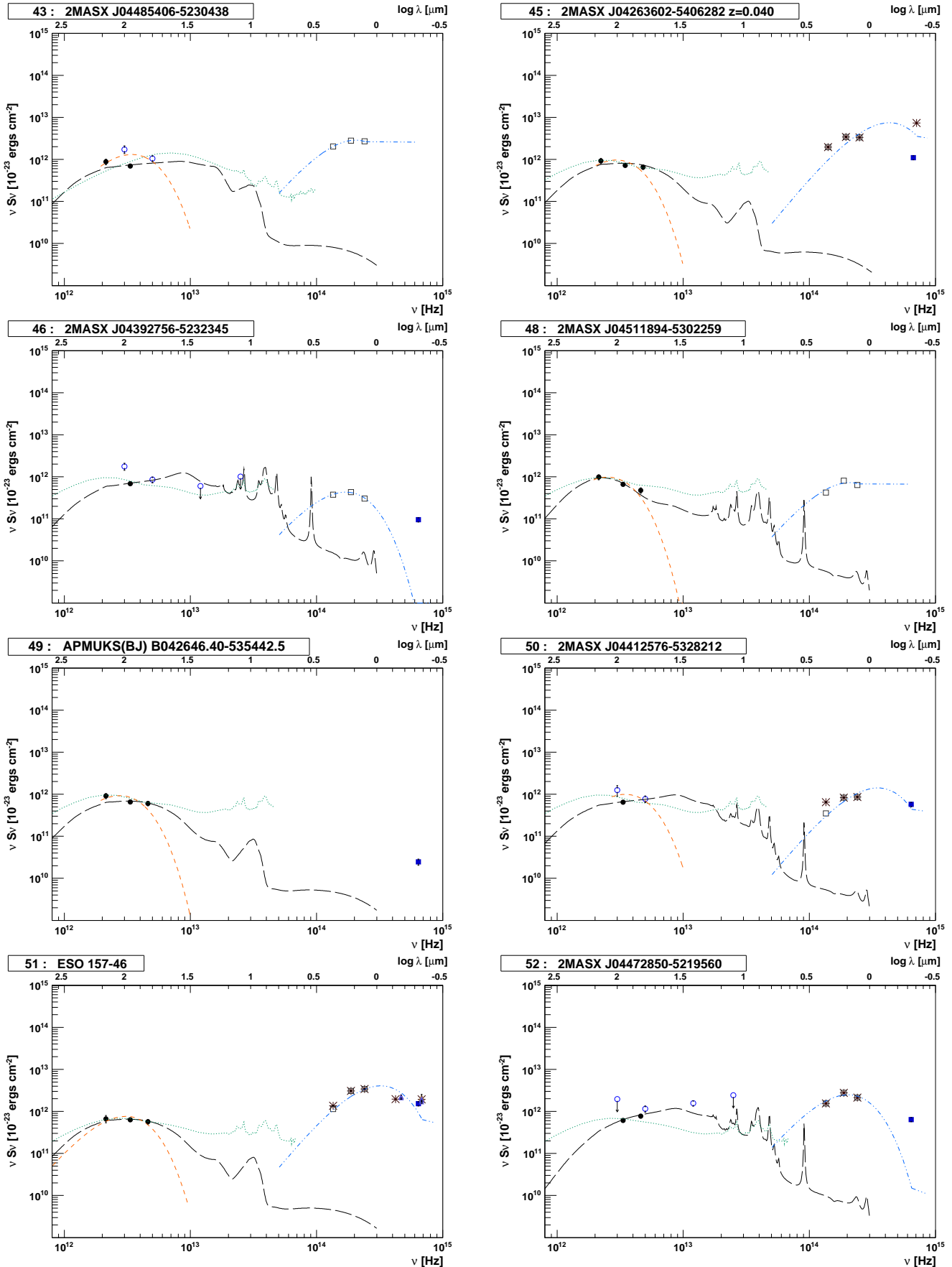


Fig. 18. Next 8 SEDs of ADF-S galaxies, with symbols as in Figure 14. SED of a galaxy number 45, for which the redshift is known, is fitted after shifting to the rest frame and presented in the rest frame. The remaining galaxy objects are shown in the observed frame.

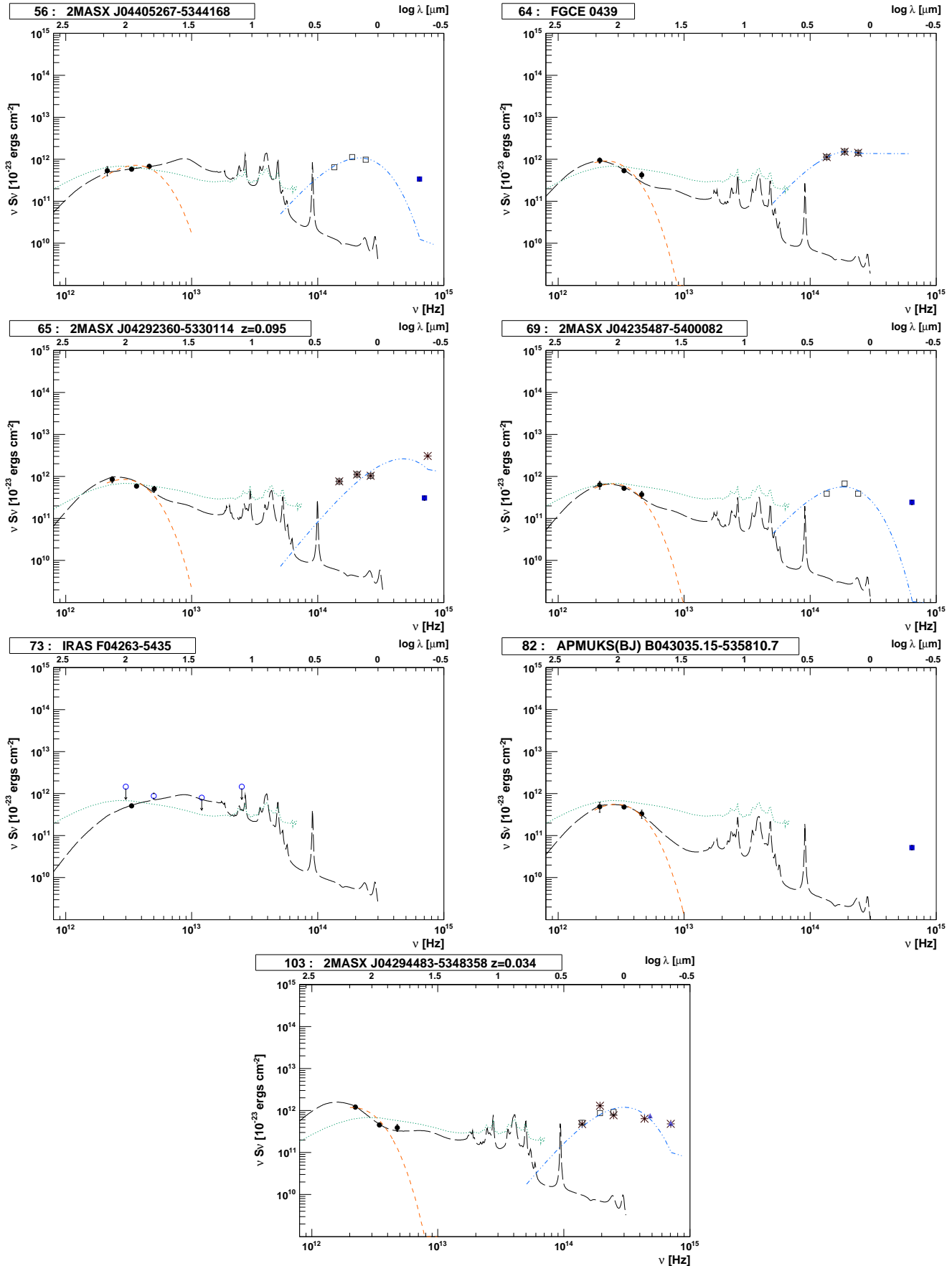


Fig. 19. Next 7 SEDs of ADF-S galaxies, with symbols as in Figure 14. SEDs of galaxies number 65 and 103, with known redshifts, are fitted after shifting to the rest frame and presented in the rest frame. The remaining objects are shown in the observed frame.

Table 6. Morphological and environmental properties of 47 ADF-S galaxies used for fitting of SED models. After the ADF-S identification number, in the second column we give the object's classification: "Galaxy" means that it has been identified as a galaxy, IRS means that it has been previously identified as the infra-red source, RS means that it has been identified as the radio source, "other" means that it has been observed in some other (UV or X-ray) wavelengths. This column contains also the available information about the object's environment - whether it is an object from the cluster of galaxies (in this case it always applies to Abell S0463) or an interacting group of galaxies. The third column gives the object's indicative morphological type, as provided by the NED. The galaxies whose morphological types were determined by Dressler (1980a) are indicated. The last column gives the number of counterparts found for each object in our 40" search range, which may be treated as a very crude indicator of a local environment of an investigated object.

ID (ADFS)	Type of source	Morphological type	Number of counterparts
1	Galaxy/IRS/RS	Sb	1
2	Galaxy in Pair of Interacting Galaxies/IRS/RS	E	1
3	Galaxy/IRS/RS/other	Sa	1
4	Stardust Galaxy IR emission line up with Super Star Cluster/IRS/RS/other	S0, SA0- pec: HII BCDG	1
5	Galaxy/IRS/RS	S	2
6	Galaxy/IRS	-	4
7	Galaxy in Cluster of Galaxies/IRS	S0 ^a	1
8	Galaxy in Cluster of Galaxies/IRS	Sb ^a	2
9	Galaxy in Cluster of Galaxies	Sb ^a	3
10	Galaxy in Cluster of Galaxies/IRS/RS	S00 pec ^a	1
11	Galaxy in Cluster of Galaxies/IRS/RS	SB ^a	1
12	IRS	-	1
13	Galaxy/IRS	-	2
14	Galaxy/IRS/RS	-	2
15	Galaxy/IRS	-	3
16	IRS/Galaxy in Pair of Galaxies	-	2
17	Interacting Galaxies/IR/RS	Sbc pec	3
18	Galaxy/IRS	S	1
19	Galaxy/IRS	-	2
20	Galaxy/IRS	-	1
21	Galaxy/IRS	SAB	1
22	Galaxy/IRS	S	2
23	Interacting Galaxies	cG (compact G), Chain of 3 galaxies	1
24	Galaxy/IRS	S	2
26	Galaxy	-	2
27	IRS	-	1
29	Galaxy/IRS	S0a	1
30	IRS/Galaxy	-	1
31	IRS/Galaxy	-	1
39	Galaxy/IRS	S0	3
41	Galaxy/IRS	-	2
42	Galaxy/IRS	-	1
43	IRS/Galaxy	-	1
45	Galaxy in Cluster of Galaxies/IRS	Sbp ^a	1
46	Galaxy/IRS	-	1
48	Galaxy/IRS	-	1
49	Galaxy	-	2
50	Galaxy/IRS	S	1
51	Galaxy/IRS/RS	SB	1
52	IRS/Galaxy	-	1
56	Galaxy/IRS	-	5
64	Galaxy/IRS	Sc	1
65	Galaxy in Cluster of Galaxies/IRS	S0 ^a	1
69	Galaxy/ IRS	-	2
72	Galaxy in Cluster of Galaxies/IRS	Sbb pec ^a	2
73	IRS	-	1
82	Galaxy	-	1
103	Galaxy in Cluster of Galaxies/IRS	Sb ^a	2

^a Dressler (1980a)

Table 7. Nearest counterparts of 10 brightest ADF-S sources (full version of the table in the online material). In this table we present: the ADF-S identification number, the name of the nearest identified counterpart, right ascension and declination of both ADF-S source and the counterpart, the angular distance between them and the redshift of the counterpart, when available.

ID (ADF-S)	Name	$\alpha_{\text{ADF-S}}$ (J2000)	$\delta_{\text{ADF-S}}$ (J2000)	$\alpha_{\text{counterpart}}$ (J2000)	$\delta_{\text{counterpart}}$ (J2000)	Dist [arc sec]	redshift
1	ESO 157-49	69.90448	-53.01348	69.90300	-53.01294	3.74	0.00578 ¹
2	ESO 157-IGA040	67.90437	-53.28733	67.90467	-53.28825	3.37	0.05881 ²
3	NGC 1617	67.91312	-54.60001	67.91417	-54.60167	6.35	0.00355 ³
4	NGC 1705	73.55990	-53.36119	73.55708	-53.36111	6.06	0.00210 ¹
5	ESO 157-43	68.81647	-54.31440	68.81460	-54.31580	6.51	0.04104 ¹
6	2MASX J04325340-5312021	68.22050	-53.19939	68.22210	-53.20190	9.81	
7	2MASX J04335902-5410074	68.49623	-54.16840	68.49579	-54.16861	2.52	0.04041 ¹
8	2MASX J04293931-5352464	67.41413	-53.87810	67.41540	-53.88000	7.36	0.03910 ¹
9	2MASX J04334493-5346467	68.43882	-53.77891	68.43960	-53.77940	2.52	0.03944 ⁴
10	IC 2085	67.85253	-54.41524	67.84979	-54.41708	8.77	0.00328 ⁵

1 - Lawrence et al. (2001)

2 - Karl et al. (1995)

3 - de Vaucouleurs et al. (1991)

4 - Dressler & Shectman (1988)

5 - Mathewson et al. (1992)

Table 8. Flux densities of 10 brightest ADF-S objects with identified counterparts, measured by AKARI (the full table is available in the online material).

ID (ADF-S)	Flux densities [Jy]			
	N60 (65 μm)	WIDE-S (90 μm)	WIDE-L (140 μm)	N160 (160 μm)
1	1.65E+00 \pm 5.83E-02	2.72E+00 \pm 9.14E-02	5.04E+00 \pm 1.53E-01	4.87E+00 \pm 3.42E-01
2	1.15E+00 \pm 4.18E-02	1.45E+00 \pm 4.79E-02	2.59E+00 \pm 9.43E-02	1.26E+00 \pm 2.12E-01
3	-	1.24E+00 \pm 4.12E-02	3.93E+00 \pm 1.25E-01	5.09E+00 \pm 3.52E-01
4	9.12E-01 \pm 3.44E-02	1.16E+00 \pm 3.84E-02	1.05E+00 \pm 6.74E-02	6.08E-01 \pm 2.00E+00
5	6.22E-01 \pm 2.60E-02	8.89E-01 \pm 2.96E-02	-	-
6	4.46E-01 \pm 2.16E-02	8.66E-01 \pm 2.89E-02	1.25E+00 \pm 7.01E-02	-
7	-	7.58E-01 \pm 2.54E-02	4.56E-01 \pm 6.21E-02	-
8	5.18E-01 \pm 2.33E-02	6.37E-01 \pm 2.15E-02	8.65E-01 \pm 6.54E-02	-
9	4.66E-01 \pm 2.20E-02	5.48E-01 \pm 1.87E-02	4.77E-01 \pm 6.22E-02	-

Table 9. Photometric data for 10 brightest ADF-S sources with identified counterparts, collected from public databases (full version of the corresponding tables are available in the online material).

ID (ADF-S)	0.44 μm	0.47 μm^C	0.55 μm	0.64 μm	0.71 μm		
1	7.05E-03±6.09E-04 ^A	5.16E-03±6.03E-04	-	1.39E-02±1.20E-03 ^A	1.41E-02 ^D		
	7.35E-03±6.35E-03 ^A			1.44E-02±1.25E-03 ^A			
	7.59E-03±6.56E-04 ^A			1.47E-02±1.27E-03 ^D			
	7.90E-03±1.69E-03 ^B						
	7.38E-03 ^D						
2	1.38E-03±1.19E-14 ^A	1.50E-03±1.23E-04	-	2.46E-03±2.13E-04 ^A	2.63E-03 ^D		
	1.46E-03±1.27E-04 ^A			2.62E-03±2.26E-04 ^A			
	1.53E-03±1.32E-04 ^A			2.76E-03±2.38E-04 ^D			
	1.49E-03 ^D						
3	1.19E-01 ^D	-	2.43E-01±2.85E-02 ^B	-	3.54E-01 ^D		
	1.20E-01±1.40E-02 ^B		2.98E-01 ^D	-			
4	2.89E-02±2.50E-03 ^A	2.47E-02±2.29E-04	4.03E-02±3.49E-03 ^B	4.04E-02±3.49E-03 ^A	4.33E-02 ^D		
	3.03E-02±2.62E-03 ^A			4.31E-02±3.73E-03 ^A		3.50E-02±9.81E-04 ^F	
	3.16E-02±2.74E-03 ^A			4.55E-02 ^D		4.55E-02±3.93E-03 ^D	8.63E-03±2.42E-04 ^F
	3.08E-02 ^D			4.10E-02±2.33E-03 ^E		2.73E-02±7.65E-04 ^F	
	3.20E-02±6.83E-03 ^B						
	3.32E-02±4.23E-03 ^B						
	3.69E-02 ^B						
	2.47E-02±2.29E-04 ^E						
5	3.58E-03±3.09E-04 ^A	3.14E-03±3.67E-04	-	3.12E-03±5.29E-04 ^A	6.20E-03 ^D		
	3.91E-03±3.09E-04 ^A			6.38E-03±5.51E-04 ^A			
	4.04E-03±3.49E-04 ^A			6.51E-03±5.63E-04 ^D			
	3.91E-03 ^D						
6	-	5.26E-04±6.14E-05	-	-	-		
7	4.13E-03 ^D	-	-	-	-		
8	4.13E-03 ^D	-	-	-	-		
9	4.13E-03 ^D	-	-	-	-		
10	6.95E-03±6.01E-04 ^A	5.45E-03±6.37E-04	2.06E-02±3.54E-03 ^B	1.70E-02±1.47E-03 ^A	1.93E-02 ^D		

A - Lauberts & Valentijn (1989)

B - de Vaucouleurs et al. (1991)

C - Maddox et al. (1990)

D - The SIMBAD astronomical database, Wenger et al. (2000)

E - Gil de Paz et al. (2003)

Table 1. The list of 330 nearest counterparts of the ADF-S sources from the 10σ catalog ($S_{90\mu m} > 0.0482$ Jy). In this table we present: the ADF-S identification number, the name of the nearest identified counterpart, right ascension and declination of both ADF-S source and the identified counterpart, the angular distance between them and the redshift of the counterpart, when available.

ID (ADF-S)	Name	$\alpha_{\text{ADF-S}}$ (J2000)	$\delta_{\text{ADF-S}}$ (J2000)	$\alpha_{\text{counterpart}}$ (J2000)	$\delta_{\text{counterpart}}$ (J2000)	Dist [arc sec]	redshift
1	ESO 157-49	69.90448	-53.01348	69.90300	-53.01294	3.74	0.00578 ¹
2	ESO 157-IGA040	67.90437	-53.28733	67.90467	-53.28825	3.37	0.05881 ²
3	NGC 1617	67.91312	-54.60001	67.91417	-54.60167	6.35	0.00355 ³
4	NGC 1705	73.55990	-53.36119	73.55708	-53.36111	6.06	0.00210 ¹
5	ESO 157-43	68.81647	-54.31440	68.81460	-54.31580	6.51	0.04104 ¹
6	2MASX J04325340-5312021	68.22050	-53.19939	68.22210	-53.20190	9.81	
7	2MASX J04335902-5410074	68.49623	-54.16840	68.49579	-54.16861	2.52	0.04041 ¹
8	2MASX J04293931-5352464	67.41413	-53.87810	67.41540	-53.88000	7.36	0.03910 ¹
9	2MASX J04334493-5346467	68.43882	-53.77891	68.43960	-53.77940	2.52	0.03944 ⁴
10	IC 2085	67.85253	-54.41524	67.84979	-54.41708	8.77	0.00328 ⁵
11	IC 2079	67.13040	-53.73701	67.12808	-53.73836	6.93	0.03587 ⁶
12	2MASX J04362406-5424552	69.10183	-54.41481	69.09830	-54.41560	7.80	
13	2MASX J04342317-5441331	68.59812	-54.69248	68.60380	-54.68830	18.98	
14	2MASX J04381194-5422292	69.55033	-54.37286	69.54830	-54.37530	9.66	
15	2MASX J04414298-5226042	70.42883	-52.43447	70.42420	-52.43780	0.42	
16	IRAS 04389-5426	70.02874	-54.34237	70.01830	-54.34580	25.15	
17	ESO 157-50	70.18614	-52.75576	70.18346	-52.75794	9.800	0.01291 ⁷
18	2MASX J04342117-5353522	68.59095	-53.89671	68.58796	-53.89858	9.26	
19	2MASX J04530951-5254202	73.29128	-52.90457	73.28971	-52.90567	5.22	
20	2MASX J04270401-5415463	66.76948	-54.26188	66.77120	-54.26440	9.95	
21	2MASX J04505562-5312459	72.73329	-53.21298	72.73040	-53.21310	6.20	
22	2MASX J04355267-5424143	68.96996	-54.40260	68.96958	-54.40472	7.68	
23	ESO 157-51	70.35754	-52.99852	70.35500	-52.99720	7.22	
24	2MASX J04355267-5424143	68.87662	-53.31383	68.87540	-53.31080	11.09	
25	2MASX J04443205-5159435	71.13398	-51.99556	71.13367	-51.99542	0.84	
26	APMUKS(BJ) B042722.82-550755.3	67.11937	-55.02170	67.11858	-55.02311	5.34	
27	IRAS F04413-5247	70.63097	-52.70025	70.62900	-52.69700	13.49	
28	APMUKS(BJ) B043113.80-532142.7	68.10404	-53.25604	68.10169	-53.25731	6.84	
29	ESO 158-6	72.17160	-53.91163	72.16817	-53.91220	7.25	0.03986 ⁸
30	2MASX J04562627-5231201	74.10889	-52.52112	74.10954	-52.52300	8.06	
31	2MASX J04283256-5359474	67.13429	-53.99541	67.12900	-53.99700	11.75	
32	2MASX J04530696-5137502	73.28234	-51.62975	73.27879	-51.63108	9.27	
34	2MASX J04423354-5409225	70.63893	-54.15480	70.63975	-54.15619	5.28	
35	CD-52 1004	71.78421	-52.67601	71.79536	-52.68111	30.48	
36	2MASX J04333071-5350287	68.37965	-53.84017	68.38000	-53.84190	6.43	
37	APMUKS(BJ) B043911.16-534920.2	70.08152	-53.72516	70.08002	-53.72672	6.48	
39	2MASX J04271036-5434513	66.79475	-54.57972	66.80221	-54.57892	15.83	
40	2MASX J04535756-5334123	73.49273	-53.56788	73.48992	-53.57011	10.02	
41	2MASX J04323435-5347510	68.14438	-53.79695	68.14321	-53.79753	3.24	
42	2MASX J04363817-5353200	69.16301	-53.88961	69.15863	-53.88744	12.14	
43	2MASX J04485406-5230438	72.22507	-52.51171	72.21700	-52.51700	25.64	
44	2MASX J04580280-5241390	74.51363	-52.69329	74.51183	-52.69417	5.04	
45	2MASX J04263602-5406282	66.65028	-54.10592	66.65029	-54.10833	8.69	0.04039 ⁴
46	2MASX J04392756-5232345	69.86474	-52.54273	69.86200	-52.54200	6.22	
47	APMUKS(BJ) B042911.18-534903.9	67.58768	-53.70834	67.58626	-53.71089	9.66	
48	2MASX J04511894-5302259	72.82909	-53.04030	72.82892	-53.04058	1.08	
49	APMUKS(BJ) B042646.40-535442.5	66.98278	-53.80051	66.98338	-53.80000	6.36	
50	2MASX J04412576-5328212	70.36013	-53.47367	70.35996	-53.47631	9.50	
51	ESO 157-46	69.72732	-52.86293	69.72562	-52.86392	5.12	
52	2MASX J04472850-5219560	71.87208	-52.33306	71.86790	-52.33280	9.21	
53	2MASX J04292162-5404154	67.34102	-54.07068	67.34040	-54.07170	3.77	
54	2MASX J04375009-5321353	69.45880	-53.35792	69.45883	-53.35972	6.48	
55	2MASX J05023480-5311321	75.64549	-53.19288	75.64500	-53.19222	2.58	
56	2MASX J04405267-5344168	70.22185	-53.73692	70.21958	-53.73806	6.30	
57	ESO 158-14	73.69590	-53.09938	73.69250	-53.09940	7.35	
58	2MASX J04423923-5413495	70.66383	-54.22974	70.66329	-54.23039	2.58	
59	APMUKS(BJ) B043219.97-543942.2	68.36949	-54.55663	68.35978	-54.55837	21.24	

Table 1. continued.

ID (ADF-S)	Name	$\alpha_{\text{ADF-S}}$ (J2000)	$\delta_{\text{ADF-S}}$ (J2000)	$\alpha_{\text{counterpart}}$ (J2000)	$\delta_{\text{counterpart}}$ (J2000)	Dist [arc sec]	redshift
60	2MASX J04285263-5316337	67.22106	-53.27556	67.22830	-53.27190	20.36	
61	2MASX J05002294-5238446	75.09628	-52.64538	75.09554	-52.64572	2.04	
63	2MASX J04320736-5309369	68.03277	-53.15993	68.03079	-53.16025	4.44	
64	FGCE 0439	72.01226	-53.43721	72.01000	-53.43810	5.72	
65	2MASX J04292360-5330114	67.34874	-53.50135	67.35080	-53.50360	9.29	0.09474 ⁴
66	2MASX J04415576-5311041	70.48498	-53.18364	70.48229	-53.18447	6.54	
67	ESO 157-48	69.86035	-53.04714	69.85496	-53.04939	14.20	
68	2MASX J05003472-5319056	75.14589	-53.31892	75.14454	-53.31831	3.66	
69	2MASX J04235487-5400082	65.97959	-54.00145	65.97863	-54.00247	4.20	
70	HD 30294 / IRAS F04423-5238	70.88903	-52.54870	70.87350	-52.54602	35.02	
71	HD 30294 / IRAS F04423-5238	70.88720	-52.54720	70.87350	-52.54602	29.96	
72	IC 2083	67.68344	-53.97832	67.68371	-53.98164	11.96	0.04304 ⁹
73	IRAS F04263-5435	66.85402	-54.47111	66.85400	-54.47800	26.01	
74	APMUKS(BJ) B042510.28-534732.0	66.58741	-53.67844	66.58547	-53.68088	9.72	
75	ESO 157-30	66.88647	-54.19446	66.88671	-54.19656	7.56	0.00494 ¹⁰
76	ESO 157-42	68.79978	-54.20307	68.80008	-54.20603	10.67	0.04056 ⁹
78	APMBGC 157-030-071	67.20383	-53.64476	67.20204	-53.64606	6.03	
79	APMUKS(BJ) B042737.45-541754.3	67.19068	-54.18911	67.19051	-54.18979	2.46	
82	APMUKS(BJ) B043035.15-535810.7	67.92904	-53.86149	67.93328	-53.86434	13.68	
83	APMUKS(BJ) B045146.99-521333.6	73.24695	-52.14472	73.24307	-52.14499	8.64	
85	2MASX J04295759-5345139	67.48984	-53.75289	67.49170	-53.75390	5.30	0.04235 ⁴
86	2MASX J04514200-5345126	72.93302	-53.75262	72.92504	-53.75347	17.28	
88	APMUKS(BJ) B045515.33-513104.6	74.11658	-51.44151	74.11824	-51.44100	4.14	
89	2MASX J04293886-5350073	67.41208	-53.83412	67.41370	-53.83560	6.27	0.04248 ⁶
90	APMUKS(BJ) B043728.10-523446.5	69.66810	-52.48122	69.66733	-52.48210	3.60	
92	APMUKS(BJ) B042945.36-541136.8	67.72319	-54.08570	67.72344	-54.08732	5.88	
93	2MASX J04590078-5310503	74.76365	-53.18383	74.75342	-53.18069	24.78	
94	ESO 158-10	73.31383	-52.79802	73.31380	-52.79920	4.13	0.06238 ¹¹
95	2MASX J04283658-5324357	67.15359	-53.40855	67.15250	-53.41069	8.07	0.04392 ¹⁰
96	APMUKS(BJ) B042539.30-541513.0	66.70094	-54.14094	66.70012	-54.14279	6.90	
97	ESO 158-1	70.41578	-53.90530	70.41370	-53.90750	9.01	
98	APMUKS(BJ) B043929.71-540702.4	70.15527	-54.02161	70.15326	-54.02212	4.62	
99	APMUKS(BJ) B045703.85-520618.0	74.56881	-52.03221	74.56247	-52.03015	15.90	
100	ESO 158-7	72.40226	-53.90726	72.40540	-53.91170	17.22	0.05037 ¹¹
101	2MASX J04574983-5240363	74.45489	-52.67251	74.45758	-52.67667	16.08	
102	APMUKS(BJ) B043804.54-530301.8	69.81444	-52.95298	69.81296	-52.95370	4.14	
103	2MASX J04294483-5348358	67.43672	-53.80925	67.43675	-53.81006	6.38	0.03425 ¹²
104	2MASX J04514705-5140366	72.94480	-51.67736	72.94625	-51.67686	3.72	
105	2MASX J04285253-5351237	67.21962	-53.85499	67.21879	-53.85714	7.93	0.04168 ¹⁰
106	2MASX J04234523-5400303	65.93882	-54.00620	65.93754	-54.00908	10.73	0.05731 ¹³
107	2MASX J04313921-5417353	67.91369	-54.29195	67.91250	-54.29330	5.57	0.05634 ⁴
108	2MASX J04421266-5355520	70.55337	-53.92965	70.55279	-53.93108	5.28	
109	2MASX J04490335-5327208	72.26323	-53.45538	72.26400	-53.45581	2.28	
110	FAIRALL 0303	67.66770	-53.61456	67.66667	-53.61556	4.21	0.04008 ⁴
111	2MASX J04380870-5400502	69.53889	-54.01321	69.53629	-54.01400	6.18	
112	APMUKS(BJ) B044902.90-520912.2	72.56152	-52.06839	72.56154	-52.06921	2.94	
113	2MASX J04305049-5347492	67.71205	-53.79554	67.71042	-53.79688	6.00	
114	2MASX J04305608-5521557	67.73132	-55.36489	67.73358	-55.36547	5.10	
115	APMUKS(BJ) B045257.07-513701.9	73.54550	-51.53891	73.54197	-51.53756	9.30	
117	2MASX J05004165-5243575	75.17566	-52.73285	75.17354	-52.73261	4.68	
118	2MASX J04452961-5308249	71.37499	-53.14088	71.37346	-53.14022	4.08	
119	2MASX J04451081-5219279	71.29812	-52.32486	71.29513	-52.32433	6.84	
120	2MASX J04290394-5335353	67.26548	-53.59278	67.26630	-53.59330	2.58	0.03831 ⁴
121	APMUKS(BJ) B043959.72-525222.9	70.29596	-52.77711	70.29403	-52.77842	6.30	
122	2MASX J04460539-5349550	71.52372	-53.83169	71.52238	-53.83197	3.06	
123	2MASX J04530553-5144012	73.27410	-51.73525	73.27300	-51.73378	5.82	
124	APMUKS(BJ) B044705.27-515231.5	72.09156	-51.78451	72.07575	-51.78898	38.70	
126	2MASX J04324535-5416011	68.18842	-54.26613	68.18908	-54.26706	3.60	
127	APMUKS(BJ) B042222.45-540758.9	65.88531	-54.01707	65.88373	-54.01857	6.36	

Table 1. continued.

ID (ADF-S)	Name	$\alpha_{\text{ADF-S}}$ (J2000)	$\delta_{\text{ADF-S}}$ (J2000)	$\alpha_{\text{counterpart}}$ (J2000)	$\delta_{\text{counterpart}}$ (J2000)	Dist [arc sec]	redshift
130	APMUKS(BJ) B042521.71-544622.0	66.62769	-54.66091	66.62019	-54.66162	15.84	
132	APMUKS(BJ) B043315.43-532831.6	68.60911	-53.37203	68.60580	-53.37317	8.22	
133	APMUKS(BJ) B043600.31-533542.7	69.29238	-53.49516	69.28962	-53.49603	6.72	
134	2MASX J04284021-5350297	67.16472	-53.84081	67.16771	-53.84156	6.98	0.04366 ⁴
135	ESO 157-47	69.83011	-54.21004	69.82971	-54.21150	5.32	0.00580 ¹³
136	2MASX J04284021-5350297	67.16305	-53.84024	67.16771	-53.84156	10.97	0.04366 ⁴
138	APMUKS(BJ) B043347.45-543821.5	68.72561	-54.53669	68.72366	-54.53760	5.22	
139	APMUKS(BJ) B043023.58-541057.6	67.89508	-54.07494	67.89035	-54.07841	16.02	
140	HD 31640	73.63885	-52.51938	73.63937	-52.52365	15.42	
142	APMUKS(BJ) B045035.16-514343.1	72.95174	-51.64787	72.95040	-51.64625	6.54	
143	2MASX J04471047-5346049	71.79445	-53.76829	71.79363	-53.76797	2.10	
146	2MASX J04591744-5251052	74.82765	-52.85153	74.82258	-52.85156	11.04	
147	2MASX J04480825-5325397	72.03197	-53.42830	72.03442	-53.42758	5.82	
148	2MASX J04525430-5135421	73.22942	-51.59712	73.22629	-51.59506	10.20	
149	2MASX J04304494-5317352	67.68447	-53.29083	67.69000	-53.29280	13.81	0.04418 ⁴
151	APMUKS(BJ) B043059.13-540056.2	68.03200	-53.91074	68.03235	-53.91076	0.72	
152	APMUKS(BJ) B043558.36-524505.1	69.29376	-52.65209	69.29214	-52.65224	3.60	
154	2MASX J04563217-5256058	74.13599	-52.93473	74.13417	-52.93492	4.02	
155	2MASX J04352368-5251141	68.85089	-52.85245	68.84863	-52.85386	7.08	
156	2MASX J04284027-5443284	67.17062	-54.72146	67.16779	-54.72458	12.66	
158	2MASX J04440021-5236197	70.99959	-52.60612	71.00100	-52.60558	3.66	
159	2MASX J04471047-5346049	71.79180	-53.76501	71.79363	-53.76797	11.34	
160	APMUKS(BJ) B042547.03-541005.4	66.73270	-54.05464	66.73336	-54.05749	10.38	
162	APMUKS(BJ) B043856.28-530429.4	70.02933	-52.97845	70.02775	-52.97902	3.96	
165	2MASX J04265073-5424153	66.71423	-54.40252	66.71040	-54.40330	8.51	
166	2MASX J04410494-5402486	70.27108	-54.04732	70.27038	-54.04747	1.59	
168	APMUKS(BJ) B043353.83-535751.6	68.76165	-53.86014	68.75911	-53.86277	10.92	
169	ESO 203-3	72.00570	-51.86009	72.00710	-51.85970	3.35	
170	APMUKS(BJ) B045627.32-521846.4	74.41248	-52.23736	74.40794	-52.23732	10.02	
171	APMUKS(BJ) B043753.93-534325.8	69.75842	-53.62484	69.76026	-53.62681	8.10	
172	APMUKS(BJ) B042627.72-534818.4	66.91254	-53.69633	66.90711	-53.69521	12.24	
173	2MASX J04574286-5220093	74.43239	-52.33703	74.42875	-52.33592	8.94	
175	2MASX J04582396-5327481	74.60095	-53.46246	74.59975	-53.46331	3.96	
176	2MFGC 03850	70.46936	-53.70160	70.46926	-53.70338	6.42	
177	2MASX J04574760-5233553	74.45272	-52.56456	74.44833	-52.56539	10.08	
179	2MASX J04372100-5305373	69.33923	-53.09289	69.33738	-53.09369	4.92	
181	2MASX J04464078-5254573	71.66973	-52.91634	71.66988	-52.91586	1.74	
183	2MASX J04405458-5316478	70.22602	-53.27953	70.22742	-53.27992	3.30	
184	2MASX J04493865-5300585	72.41068	-53.01573	72.41104	-53.01633	2.28	
185	APMUKS(BJ) B043657.27-530237.8	69.53704	-52.93796	69.53340	-52.94576	29.16	
190	2MASX J04574760-5233553	74.45093	-52.56502	74.44833	-52.56539	5.82	
191	2MASX J04490850-5346307	72.29425	-53.77261	72.28538	-53.77519	21.06	
192	2MASX J04484409-5230548	72.19001	-52.51645	72.18371	-52.51533	14.40	
194	2MASX J04354249-5435532	68.93092	-54.59782	68.92683	-54.59861	8.89	
195	APMUKS(BJ) B042840.69-532541.8	67.46576	-53.31926	67.46449	-53.32086	6.36	
196	SUMSS J043254-530942	68.23480	-53.16584	68.22558	-53.16181	24.66	
198	APMUKS(BJ) B045439.83-513456.4	73.97142	-51.50573	73.96980	-51.50469	5.22	
199	APMUKS(BJ) B043421.76-532917.5	68.88030	-53.38824	68.88134	-53.38717	4.44	
200	2MASX J04531957-5242323	73.33489	-52.70886	73.33170	-52.70920	7.12	
201	2MASX J04490138-5341108	72.25711	-53.68664	72.25579	-53.68639	2.94	
203	APMUKS(BJ) B045044.73-522017.4	72.97690	-52.26350	72.98275	-52.25595	30.06	
204	APMUKS(BJ) B042826.36-532910.2	67.41056	-53.37303	67.40421	-53.37848	23.88	
205	2MASX J04413259-5221482	70.38938	-52.36417	70.38588	-52.36341	8.16	
206	APMUKS(BJ) B043131.27-543152.8	68.16271	-54.42572	68.15913	-54.42707	8.94	
210	2MASX J04423732-5232100	70.65664	-52.53704	70.65580	-52.53690	1.80	
211	APMUKS(BJ) B044423.99-520906.3	71.40170	-52.06353	71.40173	-52.06221	4.74	
212	APMUKS(BJ) B044627.85-520656.1	71.91896	-52.02849	71.91722	-52.02842	3.84	
213	2MASX J04341529-5356052	68.56086	-53.93207	68.56367	-53.93472	11.22	
214	APMUKS(BJ) B043755.22-542116.1	69.76002	-54.25675	69.75732	-54.25746	6.24	
215	2MASX J04424423-5216587	70.68093	-52.28554	70.68450	-52.28297	12.12	

Table 1. continued.

ID (ADF-S)	Name	$\alpha_{\text{ADF-S}}$ (J2000)	$\delta_{\text{ADF-S}}$ (J2000)	$\alpha_{\text{counterpart}}$ (J2000)	$\delta_{\text{counterpart}}$ (J2000)	Dist [arc sec]	redshift
216	APMUKS(BJ) B042435.33-535704.6	66.44136	-53.83852	66.43821	-53.83928	7.26	
218	SUMSS J045154-530306	72.98235	-53.05317	72.97879	-53.05183	9.06	
219	2MASX J05003677-5301536	75.15276	-53.03395	75.15325	-53.03153	8.76	
222	APMUKS(BJ) B043943.07-541847.8	70.20829	-54.21960	70.20618	-54.21831	6.42	
223	2MASX J04422172-5406124	70.59052	-54.10171	70.59063	-54.10333	5.82	
224	APMUKS(BJ) B042236.02-535852.7	65.94722	-53.86546	65.94206	-53.86710	12.48	
225	2MASX J04494618-5258085	72.44701	-52.96709	72.44258	-52.96917	12.18	
226	SUMSS J045415-532810	73.56898	-53.46973	73.56500	-53.46964	8.52	
228	2MASX J04401313-5345111	70.05479	-53.75264	70.05479	-53.75322	2.10	
232	APMUKS(BJ) B042557.98-535929.4	66.78292	-53.87938	66.78114	-53.88104	7.08	
233	APMUKS(BJ) B043308.86-543930.5	68.56484	-54.55507	68.56301	-54.55604	5.16	
234	APMUKS(BJ) B045159.43-522906.2	73.29361	-52.40390	73.29158	-52.40428	4.68	
239	2MASX J05003518-5253136	75.14851	-52.88652	75.14658	-52.88714	4.74	
244	APMUKS(BJ) B042918.72-541022.9	67.61081	-54.06459	67.61500	-54.06690	12.26	0.03910 ⁴
247	2MASX J04540432-5242323	73.52169	-52.70868	73.51800	-52.70903	8.16	
252	2MASX J04593486-5214335	74.89770	-52.24227	74.89533	-52.24272	5.46	
253	2MASX J04290665-5401202	67.28018	-54.02152	67.27767	-54.02286	7.18	0.04375 ¹⁰
254	APMUKS(BJ) B043633.67-543652.4	69.40996	-54.51643	69.41485	-54.51599	10.32	
255	APMUKS(BJ) B043611.90-544317.3	69.31957	-54.62213	69.32292	-54.62249	7.08	
256	APMUKS(BJ) B042854.03-541153.6	67.51079	-54.09198	67.51006	-54.09103	3.78	
257	APMUKS(BJ) B042558.96-545615.8	66.77398	-54.82432	66.77276	-54.82725	10.86	
258	APMUKS(BJ) B045450.67-514332.9	74.01620	-51.64883	74.01316	-51.64837	7.02	
259	APMUKS(BJ) B043944.90-525126.3	70.23297	-52.76020	70.23262	-52.76242	8.04	
260	APMUKS(BJ) B043214.79-544545.0	68.34128	-54.65844	68.33690	-54.65905	9.36	
261	APMUKS(BJ) B042537.42-533804.7	66.70274	-53.52143	66.70250	-53.52420	9.87	
262	2MASX J04340104-5439380	68.50713	-54.65857	68.50450	-54.66061	9.18	
265	2MASX J04403699-5241268	70.15438	-52.68969	70.15413	-52.69086	4.26	
267	2MASX J04301619-5329218	67.57381	-53.48777	67.56790	-53.48940	13.99	0.04301 ⁶
270	2MASX J04561850-5316271	74.07610	-53.27351	74.07700	-53.27436	3.60	
271	APMUKS(BJ) B042216.82-542920.7	65.84951	-54.37235	65.85572	-54.37451	15.18	
275	2MFGC 04065	74.48129	-52.73308	74.47787	-52.73146	9.46	
277	APMUKS(BJ) B043322.81-534857.5	68.63391	-53.71269	68.63211	-53.71383	5.64	
279	APMUKS(BJ) B043942.07-541151.9	70.20235	-54.10799	70.20357	-54.10277	15.80	
280	2MASX J04534840-5143272	73.45410	-51.72363	73.45163	-51.72422	5.94	
281	2MASX J04441330-5216254	71.05696	-52.27307	71.05550	-52.27369	3.90	
283	2MFGC 04065	74.48148	-52.73146	74.47787	-52.73146	7.88	
287	APMUKS(BJ) B043418.86-525557.5	68.87811	-52.83036	68.87628	-52.83158	5.94	
288	2MASX J04435115-5336267	70.96343	-53.60689	70.96329	-53.60742	1.92	
290	APMUKS(BJ) B042925.07-541825.2	67.63763	-54.19932	67.63763	-54.20038	3.84	
292	2MASX J04530717-5300562	73.27931	-53.01341	73.27983	-53.01556	7.80	
294	APMUKS(BJ) B043800.04-533229.9	69.78693	-53.44552	69.78801	-53.44474	3.66	
295	SUMSS J043022-531827	67.59581	-53.30611	67.59433	-53.30758	6.18	
297	2MASX J04512417-5248164	72.85443	-52.80152	72.85079	-52.80461	13.68	
299	ESO 158-8	72.45620	-52.99195	72.46290	-52.99360	15.73	
300	SUMSS J043022-531827	67.59472	-53.30648	67.59433	-53.30758	4.08	
301	APMBGC 203+094+086	72.50380	-51.57808	72.50250	-51.57808	2.91	0.04178 ¹³
302	APMUKS(BJ) B043418.09-541550.0	68.85643	-54.16143	68.85601	-54.16277	4.92	
304	2MASX J04530717-5300562	73.28107	-53.01502	73.27983	-53.01556	3.30	
306	2MASX J04273110-5325175	66.88170	-53.42038	66.88210	-53.42190	5.69	
307	APMUKS(BJ) B043530.62-534435.9	69.16690	-53.64334	69.16429	-53.64357	5.64	
308	APMBGC 157-064-039	68.30619	-54.23282	68.30483	-54.23264	2.93	
310	APMUKS(BJ) B044402.43-520918.9	71.31695	-52.06377	71.31204	-52.06530	12.24	
311	2MASX J04412672-5216182	70.36453	-52.27106	70.36150	-52.27169	7.08	
312	APMUKS(BJ) B044821.46-521256.3	72.39039	-52.12973	72.38844	-52.13066	5.46	
314	2MASX J04214716-5401037	65.44834	-54.02333	65.44617	-54.01825	18.86	
317	APMUKS(BJ) B042751.09-543439.7	67.24214	-54.46798	67.24351	-54.46932	5.58	
318	APMUKS(BJ) B043250.85-540414.2	68.50505	-53.97703	68.49596	-53.96786	38.22	
323	2MASX J04520572-5317105	73.02602	-53.28517	73.02400	-53.28622	5.76	
324	APMUKS(BJ) B044434.94-522746.4	71.44468	-52.37471	71.44344	-52.37355	4.98	
327	2MASX J04462107-5237519	71.59688	-52.63095	71.58779	-52.63114	19.86	

Table 1. continued.

ID (ADF-S)	Name	$\alpha_{\text{ADF-S}}$ (J2000)	$\delta_{\text{ADF-S}}$ (J2000)	$\alpha_{\text{counterpart}}$ (J2000)	$\delta_{\text{counterpart}}$ (J2000)	Dist [arc sec]	redshift
328	APMUKS(BJ) B044019.37-531128.3	70.37244	-53.09899	70.37172	-53.09695	7.50	
329	APMUKS(BJ) B042736.63-535622.1	67.19034	-53.82932	67.19176	-53.83084	6.24	0.02880 ¹²
334	APMUKS(BJ) B042642.12-541813.5	66.95881	-54.19608	66.96052	-54.19410	7.98	
335	2MASX J04355196-5428453	68.96558	-54.47802	68.96650	-54.47917	4.56	
336	2MASX J04392010-5414002	69.83261	-54.23137	69.83388	-54.23342	7.86	
337	2MFGC 04056	74.33976	-52.78110	74.33929	-52.78308	7.39	
338	2MASX J04543585-5259324	73.65145	-52.99201	73.64938	-52.99231	4.62	
339	2MASX J04584230-5255532	74.68303	-52.93082	74.67629	-52.93153	14.82	
340	2MASX J04480984-5234037	72.04061	-52.56774	72.04100	-52.56761	0.96	
341	APMUKS(BJ) B044314.88-521920.5	71.11088	-52.23186	71.11228	-52.23149	3.36	
342	2MASX J04284373-5438274	67.18368	-54.64102	67.18246	-54.64156	3.19	
343	APMUKS(BJ) B042622.16-535122.2	66.88225	-53.74597	66.88336	-53.74616	2.46	
344	APMUKS(BJ) B043710.84-541121.1	69.57432	-54.09065	69.57504	-54.09134	2.94	
345	2MASX J04284373-5438274	67.18237	-54.64156	67.18246	-54.64156	0.18	
348	APMUKS(BJ) B044923.33-514901.4	72.65146	-51.73352	72.65060	-51.73328	2.10	
351	APMUKS(BJ) B043910.67-533424.7	70.08365	-53.47755	70.08122	-53.47797	5.40	
352	APMUKS(BJ) B043904.34-534321.6	70.05549	-53.62747	70.05297	-53.62698	5.64	
354	2MASX J04382753-5255136	69.61746	-52.92001	69.61483	-52.92050	5.94	
355	2MASX J04593309-5221265	74.89234	-52.35671	74.88804	-52.35736	9.72	
357	APMUKS(BJ) B044804.81-515700.3	72.32008	-51.86536	72.32245	-51.86479	5.64	
358	APMUKS(BJ) B042940.19-550505.8	67.69161	-54.97771	67.69004	-54.97859	4.50	
360	2MASX J05014122-5313500	75.41968	-53.23214	75.42179	-53.23061	7.14	
364	APMUKS(BJ) B043854.46-534728.7	70.01188	-53.69455	70.01101	-53.69543	3.66	
365	APMUKS(BJ) B044654.05-521810.4	72.02798	-52.21795	72.02387	-52.21622	10.98	
366	APMUKS(BJ) B043544.12-531100.9	69.22910	-53.08460	69.22755	-53.08412	3.78	
368	2MASX J04423139-5335280	70.63145	-53.59040	70.63092	-53.59119	3.06	
369	APMUKS(BJ) B042614.66-541455.1	66.84726	-54.13668	66.84713	-54.13848	6.48	
370	ESO 157-45	69.70902	-52.68121	69.71150	-52.68597	17.98	
373	APMUKS(BJ) B043544.12-531100.9	69.22762	-53.08487	69.22755	-53.08412	2.70	
374	2MASX J04434294-5339377	70.93279	-53.66181	70.92888	-53.66053	9.54	
377	APMUKS(BJ) B045203.87-513208.9	73.32046	-51.45657	73.32168	-51.45514	5.82	
380	2MASX J04434294-5339377	70.93133	-53.66117	70.92888	-53.66053	5.70	
384	APMUKS(BJ) B042559.37-541529.9	66.78135	-54.14568	66.78346	-54.14786	9.00	
386	APMUKS(BJ) B044623.78-515946.9	71.90224	-51.90862	71.90175	-51.90912	2.10	
391	2MASX J04335758-5256401	68.48739	-52.94336	68.48979	-52.94453	6.72	
392	AM 0445-525	71.55168	-52.91181	71.55113	-52.91353	6.30	
393	2MASX J04432156-5339328	70.84140	-53.65834	70.83979	-53.65914	4.50	
394	2MASX J04320733-5338339	68.03035	-53.64190	68.03040	-53.64280	3.16	0.04239 ⁴
396	APMUKS(BJ) B045516.45-514338.5	74.12244	-51.65144	74.12037	-51.65043	5.88	
397	2MASX J04363875-5314550	69.16340	-53.24671	69.16154	-53.24864	8.04	
398	APMUKS(BJ) B042055.13-540458.2	65.52918	-53.96639	65.52156	-53.96677	16.20	
399	APMUKS(BJ) B043829.07-544723.7	69.89615	-54.69458	69.89214	-54.69353	9.18	
400	ESO 158-12	73.43437	-52.98231	73.42790	-52.98140	14.37	
402	2MASX J04314162-5336324	67.92861	-53.60878	67.92500	-53.60733	9.30	
410	APMUKS(BJ) B045248.32-520229.4	73.50112	-51.96065	73.50042	-51.96168	4.02	
414	2MASX J04314165-5455393	67.92544	-54.92660	67.92354	-54.92758	5.28	
415	2MASX J04401020-5333001	70.04279	-53.54679	70.04254	-53.55008	11.88	
416	APMUKS(BJ) B043754.84-535744.3	69.76148	-53.86515	69.76093	-53.86530	1.26	
418	2MASX J04443634-5309345	71.15202	-53.15808	71.15142	-53.15958	5.58	
419	APMUKS(BJ) B045149.13-515321.9	73.25711	-51.80977	73.25610	-51.80846	5.22	
422	APMUKS(BJ) B044205.80-521028.2	70.83334	-52.08386	70.82685	-52.08232	15.42	
423	APMUKS(BJ) B042914.09-533709.2	67.60003	-53.50341	67.60089	-53.51242	32.52	
424	FGCE 0448	73.54250	-52.18200	73.53920	-52.18310	8.28	
426	APMUKS(BJ) B042848.90-544552.8	67.47986	-54.65449	67.48125	-54.65736	10.74	
430	APMUKS(BJ) B045540.53-522331.7	74.21317	-52.31532	74.21233	-52.31566	2.22	
431	2MASX J04352263-5256454	68.84621	-52.94483	68.84417	-52.94594	6.00	
432	2MASX J04500910-5250223	72.53828	-52.84039	72.53800	-52.83956	3.06	
434	APMUKS(BJ) B042858.99-542959.8	67.53165	-54.39562	67.52671	-54.39284	14.40	
436	APMUKS(BJ) B043059.00-531244.4	68.04332	-53.10779	68.04205	-53.10751	2.94	
437	2MASX J04271235-5334048	66.80216	-53.56765	66.80290	-53.56830	2.94	

Table 1. continued.

ID (ADF-S)	Name	$\alpha_{\text{ADF-S}}$ (J2000)	$\delta_{\text{ADF-S}}$ (J2000)	$\alpha_{\text{counterpart}}$ (J2000)	$\delta_{\text{counterpart}}$ (J2000)	Dist [arc sec]	redshift
439	APMUKS(BJ) B045430.50-512448.2	73.92986	-51.33745	73.93303	-51.33557	9.84	
441	SUMSS J042932-540329	67.38691	-54.05859	67.38354	-54.05828	7.20	
443	APMUKS(BJ) B044916.95-522809.0	72.61405	-52.38682	72.61607	-52.38525	7.20	
445	APMUKS(BJ) B042622.79-544319.0	66.87707	-54.61049	66.87467	-54.61192	7.20	
447	APMUKS(BJ) B043243.73-542450.9	68.45982	-54.30985	68.46184	-54.31124	6.54	
448	APMUKS(BJ) B044311.33-522959.6	71.09723	-52.40806	71.09533	-52.40895	5.28	
449	2MASX J04573918-5327133	74.41259	-53.45453	74.41325	-53.45361	3.60	
450	2MASX J04403205-5227377	70.13840	-52.46050	70.13613	-52.46272	9.43	
451	2MASX J04475194-5322236	71.96651	-53.37173	71.96646	-53.37325	5.46	
452	2MASX J04260483-5345379	66.52231	-53.75838	66.52017	-53.76050	8.88	
458	APMUKS(BJ) B045736.37-521950.8	74.69978	-52.25544	74.69493	-52.25655	11.40	
460	APMUKS(BJ) B044746.76-521507.5	72.24600	-52.16607	72.24369	-52.16643	5.28	
462	APMUKS(BJ) B043423.71-535810.1	68.88407	-53.87075	68.88324	-53.86847	8.40	
463	2MASX J04392284-5236225	69.84638	-52.60634	69.84529	-52.60628	2.40	
464	APMUKS(BJ) B043900.64-540403.0	70.03627	-53.97024	70.03307	-53.97174	8.64	
465	APMUKS(BJ) B042525.05-542339.2	66.64104	-54.28117	66.63908	-54.28314	8.22	
466	2MASX J04244795-5414431	66.20098	-54.24302	66.19992	-54.24528	8.46	
467	APMUKS(BJ) B045034.19-520143.6	72.94395	-51.94594	72.94272	-51.94637	3.12	
468	APMUKS(BJ) B045047.69-514058.0	73.00581	-51.60204	73.00307	-51.60064	7.92	
472	APMUKS(BJ) B043758.93-531808.7	69.78640	-53.19883	69.78646	-53.20550	24.00	
473	APMUKS(BJ) B043101.21-540630.5	68.04313	-54.00638	68.03978	-54.00366	12.06	
474	HE 0439-5254	70.04434	-52.80658	70.04960	-52.80500	12.75	1.05300 ¹⁴
477	APMUKS(BJ) B043452.86-530452.0	69.01577	-52.97825	69.01576	-52.98069	8.76	
482	APMUKS(BJ) B043100.70-543132.8	68.03193	-54.41829	68.03216	-54.42094	9.54	
486	APMUKS(BJ) B044505.29-520927.6	71.58091	-52.06306	71.57339	-52.06892	26.88	
488	APMUKS(BJ) B043708.83-545147.7	69.56087	-54.76292	69.55761	-54.76534	11.04	
489	APMUKS(BJ) B042822.06-542438.5	67.36688	-54.30235	67.37441	-54.30289	15.96	
490	2MASX J04284642-5408334	67.19351	-54.14162	67.19500	-54.14356	6.05	0.05475 ⁴
492	APMUKS(BJ) B043630.78-523857.9	69.42959	-52.54774	69.42817	-52.55085	11.64	
493	2MASX J05004929-5323127	75.20856	-53.38928	75.20542	-53.38678	11.28	
494	APMUKS(BJ) B043048.60-541521.4	67.98879	-54.15128	67.98544	-54.15089	7.20	
496	APMUKS(BJ) B044011.52-531303.4	70.34136	-53.12351	70.33875	-53.12322	5.76	
497	APMUKS(BJ) B043803.56-534214.5	69.80277	-53.60627	69.80055	-53.60719	5.76	
499	APMUKS(BJ) B044145.58-521541.3	70.74512	-52.16860	70.74172	-52.16890	7.56	

1 - Lawrence et al. (2001)

2 - Karl et al. (1995)

3 - de Vaucouleurs et al. (1991)

4 - Dressler & Shectman (1988)

5 - Mathewson et al. (1992)

6 - Mathewson & Ford (1996)

7 - di Nella et al. (1996)

8 - de Souza et al. (1997)

9 - da Costa et al. (1991)

10 - Paturel et al. (2002)

11 - Fairall (1984)

12 - Ellis et al. (1984)

13 - Loveday et al. (1996)

14 - Wisotzki et al. (2000)

Table 2. The list of 218 nearest counterparts of the ADF-S sources from the fainter part of the 6σ catalog ($0.0.82 \text{ Jy} < S_{90\mu\text{m}} < 0.0301 \text{ Jy}$). All the columns are ordered as in Table 1.

ID (ADF-S)	Name	$\alpha_{\text{ADF-S}}$ (J2000)	$\delta_{\text{ADF-S}}$ (J2000)	$\alpha_{\text{counterpart}}$ (J2000)	$\delta_{\text{counterpart}}$ (J2000)	Dist [arc sec]	redshift
503	APMUKS(BJ) B042654.63-541839.4	67.01398	-54.19913	67.01242	-54.20153	9.24	
504	APMUKS(BJ) B042901.44-541940.2	67.53602	-54.22007	67.53917	-54.22078	7.1	
507	APMUKS(BJ) B045318.69-512458.0	73.63448	-51.33819	73.63429	-51.33689	4.7	
513	2MASX J04483850-5326377	72.16142	-53.44373	72.16033	-53.44386	2.38	
514	APMUKS(BJ) B042858.99-542959.8	67.53412	-54.40284	67.52671	-54.39283	39.23	
519	2MASX J04554545-5237330	73.93758	-52.62664	73.93946	-52.62581	5.09	
523	APMUKS(BJ) B043801.14-541109.3	69.79368	-54.08956	69.78417	-54.08903	20.18	
524	APMUKS(BJ) B043420.17-533205.3	68.87540	-53.43288	68.87413	-53.43375	4.16	
526	2MASX J04440985-5336563	71.04189	-53.61249	71.04096	-53.61569	11.71	
530	APMUKS(BJ) B043146.09-532540.6	68.23989	-53.32284	68.23504	-53.32400	11.23	
532	APMUKS(BJ) B043443.19-534558.7	68.97556	-53.66877	68.96683	-53.66567	21.71	
533	APMUKS(BJ) B043953.46-543139.8	70.24798	-54.43549	70.24650	-54.43294	9.67	
534	2MASX J04440985-5336563	71.04432	-53.61395	71.04096	-53.61569	9.54	
536	APMUKS(BJ) B042501.03-550051.2	66.52964	-54.90290	66.53100	-54.90267	2.94	
538	2MASX J04483850-5326377	72.15999	-53.44267	72.16033	-53.44386	4.35	
541	APMBGC 157-032-065	67.26548	-53.74777	67.26521	-53.74761	0.81	
543	APMUKS(BJ) B042429.78-535826.6	66.41817	-53.86206	66.41483	-53.86194	7.1	
544	2MASX J05014281-5307250	75.43186	-53.12637	75.42863	-53.12353	12.39	
545	APMUKS(BJ) B043224.59-544231.2	68.38155	-54.59885	68.37833	-54.60539	24.48	
548	2MASX J04402326-5259071	70.09456	-52.98481	70.09688	-52.98544	5.51	
551	IRXS J043507.7-550142	68.78336	-55.02423	68.78208	-55.02847	15.49	
552	APMUKS(BJ) B045332.35-522517.0	73.68139	-52.34446	73.67883	-52.34242	9.26	
554	APMUKS(BJ) B043752.62-531907.1	69.75754	-53.21986	69.76000	-53.22161	8.24	
555	APMUKS(BJ) B045311.59-514715.0	73.60245	-51.70867	73.60029	-51.70814	5.18	
556	2MASX J04414136-5240352	70.42333	-52.67685	70.42242	-52.67639	2.59	
559	APMUKS(BJ) B044715.13-515832.4	72.11958	-51.88959	72.11554	-51.88942	8.99	
560	APMUKS(BJ) B042519.46-533529.8	66.61606	-53.48828	66.62617	-53.48044	35.56	
564	APMUKS(BJ) B043533.09-525409.7	69.18557	-52.80040	69.18521	-52.80303	9.49	
565	APMUKS(BJ) B045550.68-515228.2	74.26064	-51.79898	74.26096	-51.79822	2.82	
567	APMUKS(BJ) B042202.00-540035.2	65.80225	-53.89232	65.80033	-53.89494	10.29	
570	APMUKS(BJ) B042521.77-541818.7	66.62766	-54.19072	66.62658	-54.19406	12.22	
572	APMUKS(BJ) B043829.07-544723.7	69.90291	-54.69659	69.89213	-54.69353	25	
574	RBS 0567	69.90294	-53.19569	69.91125	-53.19194	22.43	0.243 ¹⁵
575	APMUKS(BJ) B043404.34-540727.0	68.79860	-54.02012	68.80071	-54.02281	10.65	
576	2MASX J04341959-5443411	68.57898	-54.72517	68.58167	-54.72819	12.24	
577	APMUKS(BJ) B044026.04-533254.3	70.39531	-53.45258	70.39488	-53.45428	6.18	
578	APMUKS(BJ) B043318.92-543155.2	68.60643	-54.43857	68.60650	-54.42975	31.75	
579	APMUKS(BJ) B043423.86-532253.4	68.89401	-53.28375	68.89142	-53.28053	12.87	
582	APMUKS(BJ) B042915.37-534556.0	67.60615	-53.65793	67.60433	-53.65878	4.93	
583	APMUKS(BJ) B045522.99-522803.1	74.14143	-52.39021	74.13842	-52.39069	6.85	
585	SUMSS J043433-530648	68.62299	-53.11344	68.63771	-53.11350	31.8	
588	APMUKS(BJ) B042257.27-542644.7	66.02506	-54.33116	66.02433	-54.33192	3.12	
593	APMUKS(BJ) B045308.62-512658.3	73.58234	-51.36855	73.59200	-51.37011	22.43	
595	APMUKS(BJ) B043823.64-531450.9	69.89312	-53.15254	69.88988	-53.15103	8.87	
596	APMUKS(BJ) B044013.95-530845.1	70.35242	-53.05032	70.34975	-53.05153	7.23	
598	APMUKS(BJ) B043943.26-523313.3	70.23230	-52.45797	70.22954	-52.45878	6.71	
603	APMUKS(BJ) B045107.76-522934.7	73.08553	-52.41437	73.07658	-52.41119	22.73	
604	SUMSS J050114-533751	75.30992	-53.62303	75.31154	-53.63108	29.2	
606	APMUKS(BJ) B043404.34-540727.0	68.80027	-54.02186	68.80071	-54.02281	3.53	
608	APMUKS(BJ) B043409.84-532221.3	68.82750	-53.26464	68.83325	-53.27133	27.09	
610	RBS 0567	69.91096	-53.19424	69.91125	-53.19194	8.29	0.243 ¹⁵
612	2MASX J04293218-5428334	67.38078	-54.47455	67.38400	-54.47586	8.22	
618	2MASX J04334469-5412145	68.43933	-54.20270	68.43617	-54.20403	8.2	
621	FAIRALL 0773	67.63843	-53.66767	67.63679	-53.66922	6.59	0.0383 ⁴
624	APMBGC 157-033-078	67.30187	-53.50617	67.29800	-53.50997	16	0.0446 ¹³
625	APMUKS(BJ) B043407.80-531350.7	68.82508	-53.12984	68.82658	-53.12947	3.51	
629	APMUKS(BJ) B042834.46-534832.7	67.43480	-53.70201	67.43375	-53.70153	2.83	
632	APMUKS(BJ) B045258.21-521906.2	73.53831	-52.23849	73.53813	-52.23875	1.02	

Table 2. continued.

ID (ADF-S)	Name	$\alpha_{\text{ADF-S}}$ (J2000)	$\delta_{\text{ADF-S}}$ (J2000)	$\alpha_{\text{counterpart}}$ (J2000)	$\delta_{\text{counterpart}}$ (J2000)	Dist [arc sec]	redshift
633	APMUKS(BJ) B043407.80-531350.7	68.82735	-53.13146	68.82658	-53.12947	7.35	
634	APMUKS(BJ) B044503.87-522527.4	71.56534	-52.33635	71.56421	-52.33550	3.94	
636	APMUKS(BJ) B045523.92-522810.8	74.14537	-52.38857	74.14225	-52.39286	16.9	
639	APMUKS(BJ) B042543.71-544450.5	66.71600	-54.63312	66.71196	-54.63661	15.13	
640	APMUKS(BJ) B043612.50-533247.7	69.34277	-53.44730	69.34092	-53.44764	4.16	
644	2MASX J04472616-5325550	71.86765	-53.43946	71.85904	-53.43189	32.92	
648	APMUKS(BJ) B043242.34-534115.8	68.47028	-53.58122	68.46554	-53.58483	16.49	
652	2MASX J04563013-5325268	74.12353	-53.42264	74.12563	-53.42414	7.02	
653	APMUKS(BJ) B043746.05-535235.4	69.72814	-53.77868	69.72550	-53.77933	6.09	
654	2MASX J04394443-5246304	69.93468	-52.77409	69.93500	-52.77508	3.64	
659	APMUKS(BJ) B045434.60-521828.3	73.92934	-52.23260	73.93917	-52.23011	23.45	
662	2MASX J04301532-5357259	67.56354	-53.95683	67.56392	-53.95722	1.62	
664	APMUKS(BJ) B042416.21-534240.8	66.35378	-53.59018	66.36179	-53.59900	36.07	
669	APMUKS(BJ) B042951.26-543155.5	67.74618	-54.42466	67.74350	-54.42594	7.27	
670	APMUKS(BJ) B045348.30-512742.0	73.75091	-51.39339	73.75692	-51.38303	39.67	
675	APMUKS(BJ) B043852.69-532127.8	70.00705	-53.26879	70.00925	-53.26183	25.49	
677	2MASX J04402941-5321430	70.12419	-53.36435	70.12275	-53.36197	9.1	
679	APMUKS(BJ) B045236.97-520206.3	73.46180	-51.95966	73.45329	-51.95506	25.12	
685	2MASX J04444398-5355395	71.18633	-53.92723	71.18321	-53.92761	6.76	
686	APMUKS(BJ) B043807.78-534400.0	69.81245	-53.63520	69.81771	-53.63658	12.28	
690	APMUKS(BJ) B042836.83-534529.5	67.43903	-53.65082	67.44425	-53.65069	11.15	
692	APMUKS(BJ) B043942.46-534647.2	70.20404	-53.68661	70.21071	-53.68481	15.63	
693	APMUKS(BJ) B043430.88-533649.0	68.91153	-53.51361	68.91763	-53.51275	13.41	
694	APMUKS(BJ) B044926.36-515543.8	72.66111	-51.84336	72.66183	-51.84511	6.51	
697	APMUKS(BJ) B043029.27-533427.5	67.91179	-53.46641	67.91392	-53.46892	10.11	
698	APMUKS(BJ) B042111.51-541455.0	65.58419	-54.13001	65.58746	-54.13283	12.28	
699	SUMSS J043632-544704	69.14054	-54.77594	69.13733	-54.78467	32.11	
700	APMUKS(BJ) B043135.34-544540.5	68.17514	-54.65450	68.17296	-54.65706	10.26	
708	APMUKS(BJ) B045406.76-512858.1	73.83552	-51.40292	73.83346	-51.40453	7.41	
709	APMUKS(BJ) B043329.49-533758.9	68.66466	-53.53219	68.66221	-53.53103	6.71	
710	APMUKS(BJ) B043149.23-530443.1	68.25201	-52.97258	68.25250	-52.97475	7.88	
713	APMUKS(BJ) B042859.37-535002.6	67.53143	-53.72512	67.53696	-53.72697	13.53	
715	APMUKS(BJ) B043403.78-544405.8	68.78913	-54.63287	68.79021	-54.63356	3.34	
717	APMUKS(BJ) B044403.66-522653.3	71.31220	-52.35946	71.31354	-52.35819	5.43	
718	APMUKS(BJ) B042324.34-540531.6	66.13691	-53.97337	66.14142	-53.97881	21.77	
720	APMUKS(BJ) B044154.56-521935.7	70.77075	-52.22510	70.77825	-52.23419	36.68	
721	2MASX J04420122-5210309	70.50296	-52.17342	70.50504	-52.17567	9.3	0.0492 ¹³
723	2MASX J04390803-5235114	69.78973	-52.58494	69.78342	-52.58647	14.87	
728	APMUKS(BJ) B044441.23-521150.1	71.47456	-52.10828	71.47288	-52.10803	3.83	
729	2MASX J04530959-5306023	73.29922	-53.09886	73.28992	-53.10064	21.1	
730	APMUKS(BJ) B045017.89-515353.3	72.87813	-51.81742	72.87650	-51.81542	8.07	
734	2MASX J04392549-5437242	69.85679	-54.62364	69.85638	-54.62331	1.48	
738	APMUKS(BJ) B043049.86-533607.8	67.99670	-53.49108	67.99913	-53.49717	22.52	0.0425 ⁴
739	APMUKS(BJ) B042856.35-534622.4	67.52836	-53.66598	67.52521	-53.66575	6.77	
740	APMUKS(BJ) B045746.54-515746.4	74.74375	-51.88504	74.74179	-51.88886	14.43	
743	APMUKS(BJ) B043454.43-525411.6	69.02962	-52.79949	69.02450	-52.80283	16.4	
749	APMUKS(BJ) B043348.20-535146.4	68.73853	-53.75898	68.73704	-53.76122	8.67	
750	2MASX J04583496-5205071	74.64933	-52.08680	74.64817	-52.08664	2.64	
754	APMUKS(BJ) B043603.55-525601.1	69.31320	-52.83293	69.31146	-52.83456	6.97	
758	APMBGC 157-022-077	66.95729	-53.53716	66.95979	-53.53717	5.35	
760	SUMSS J044044-533320	70.18245	-53.54510	70.18463	-53.55561	38.12	
762	APMUKS(BJ) B042203.93-540734.9	65.80509	-54.01008	65.80683	-54.01156	6.47	
763	2MASX J04595928-5243165	75.00042	-52.72174	74.99700	-52.72128	7.64	
764	APMUKS(BJ) B042907.45-552417.5	67.55284	-55.30214	67.54958	-55.29789	16.7	
765	APMUKS(BJ) B043612.19-530612.1	69.34799	-53.00473	69.34525	-53.00444	6.02	
769	APMUKS(BJ) B042348.86-540114.3	66.24735	-53.90644	66.24421	-53.90778	8.22	
770	APMUKS(BJ) B043752.91-541749.0	69.73362	-54.20199	69.74846	-54.19989	32.15	
771	APMUKS(BJ) B042550.44-545956.8	66.73651	-54.88598	66.73654	-54.88847	8.97	
772	APMUKS(BJ) B042840.56-550603.0	67.44489	-54.99255	67.44204	-54.99336	6.57	
774	APMUKS(BJ) B043712.15-543604.0	69.57447	-54.50107	69.57496	-54.50328	8.01	

Table 2. continued.

ID (ADF-S)	Name	$\alpha_{\text{ADF-S}}$ (J2000)	$\delta_{\text{ADF-S}}$ (J2000)	$\alpha_{\text{counterpart}}$ (J2000)	$\delta_{\text{counterpart}}$ (J2000)	Dist [arc sec]	redshift
776	APMUKS(BJ) B042425.37-541844.2	66.40383	-54.19902	66.39217	-54.20008	24.86	
777	APMUKS(BJ) B043447.59-541052.8	68.98686	-54.07445	68.97971	-54.08078	27.33	
778	APMUKS(BJ) B042631.69-541037.5	66.91292	-54.06504	66.91883	-54.06725	14.81	
781	APMUKS(BJ) B043740.43-543937.1	69.68953	-54.56349	69.69171	-54.56300	4.88	
782	NGC 1705:[WMR2006] XMM1	73.73456	-53.41540	73.74000	-53.40653	34.01	
784	APMUKS(BJ) B043956.70-525018.7	70.28688	-52.74273	70.28192	-52.74386	11.56	
789	APMUKS(BJ) B043417.29-530420.7	68.87034	-52.97276	68.86800	-52.97133	7.22	
790	APMUKS(BJ) B045851.55-522827.5	75.00681	-52.40051	75.00583	-52.40156	4.33	
791	APMUKS(BJ) B045420.23-512756.6	73.89813	-51.37848	73.88967	-51.38769	38.24	
794	2MASX J04334449-5351027	68.43692	-53.84855	68.43538	-53.85072	8.48	
795	APMUKS(BJ) B042649.69-542915.0	66.98834	-54.37564	66.98954	-54.37797	8.77	
796	APMUKS(BJ) B042620.20-540248.6	66.87000	-53.93578	66.87275	-53.93678	6.85	
797	2MASX J04524957-5147190	73.20920	-51.78982	73.20671	-51.78867	6.93	
800	APMUKS(BJ) B042753.18-534548.8	67.26301	-53.66325	67.26279	-53.65525	28.8	
801	APMUKS(BJ) B045524.10-522328.8	74.14331	-52.31737	74.14400	-52.31453	10.34	
806	2MASX J04300425-5349489	67.51875	-53.83015	67.51767	-53.83025	2.33	
807	APMUKS(BJ) B043447.59-541052.8	68.98010	-54.07642	68.97971	-54.08078	15.71	
809	2MASX J04453622-5205228	71.40198	-52.08861	71.40096	-52.08958	4.17	
810	2MASX J04405611-5431026	70.23797	-54.51569	70.23371	-54.51736	10.75	
811	APMUKS(BJ) B043020.55-542157.7	67.86929	-54.25696	67.86742	-54.26044	13.15	
812	APMUKS(BJ) B045057.70-513724.3	73.04576	-51.54314	73.04542	-51.54147	6.05	
813	APMUKS(BJ) B042445.89-535343.1	66.48118	-53.78286	66.48279	-53.78350	4.13	
815	APMUKS(BJ) B043536.31-525942.3	69.20455	-52.89880	69.19746	-52.89547	19.51	
816	APMUKS(BJ) B042437.23-541736.5	66.44326	-54.17935	66.44167	-54.18150	8.44	
824	APMUKS(BJ) B042603.80-545154.8	66.79529	-54.75340	66.79383	-54.75483	5.98	
826	APMUKS(BJ) B043731.04-540903.5	69.66320	-54.05268	69.65950	-54.05350	8.36	
827	APMUKS(BJ) B042841.07-535200.5	67.46828	-53.76223	67.46050	-53.75939	19.46	
828	APMUKS(BJ) B044007.45-534256.4	70.31810	-53.61522	70.31542	-53.62119	22.26	
830	2MASX J04515355-5208276	72.97749	-52.14353	72.97300	-52.14100	13.47	
831	SUMSS J042455-540811	66.24654	-54.14212	66.23042	-54.13650	39.57	
833	APMUKS(BJ) B044733.75-520052.0	72.19304	-51.91785	72.19250	-51.92856	38.56	
834	APMUKS(BJ) B045400.85-511938.6	73.79526	-51.25035	73.81071	-51.24900	35.15	
837	HE 0435-5304	69.20986	-52.97659	69.21167	-52.98028	13.84	1.2310 ¹⁴
838	APMUKS(BJ) B045232.52-521708.7	73.41529	-52.21004	73.43167	-52.20561	39.49	
841	APMUKS(BJ) B045712.59-515214.0	74.60704	-51.79300	74.60171	-51.79589	15.78	
843	APMUKS(BJ) B043653.22-533907.5	69.50497	-53.54954	69.50883	-53.55392	17.79	
846	APMUKS(BJ) B043442.47-540916.3	68.96779	-54.05214	68.95879	-54.05386	20	
849	APMUKS(BJ) B042430.24-541305.0	66.40683	-54.10766	66.41363	-54.10594	15.61	
851	APMUKS(BJ) B042819.30-533507.7	67.37472	-53.47842	67.37358	-53.47764	3.72	
853	APMUKS(BJ) B042826.00-540041.7	67.38896	-53.91084	67.39600	-53.90386	29.23	0.2591 ¹²
854	APMUKS(BJ) B045202.65-514903.7	73.31335	-51.74630	73.31321	-51.73700	33.48	
856	CD-53 954	68.00308	-53.70573	68.00470	-53.69988	21.35	
857	SUMSS J045259-512941	73.25041	-51.49198	73.24871	-51.49486	11.05	
858	APMUKS(BJ) B042918.97-533416.8	67.62157	-53.46198	67.62179	-53.46461	9.48	
859	APMUKS(BJ) B042220.39-542942.8	65.88194	-54.38234	65.87046	-54.38072	24.77	
860	APMUKS(BJ) B044329.30-521125.8	71.17753	-52.10047	71.17383	-52.09992	8.41	
865	APMUKS(BJ) B042247.79-542356.5	65.98786	-54.28373	65.98558	-54.28503	6.69	
869	APMUKS(BJ) B043613.92-532009.4	69.35332	-53.23345	69.34950	-53.23706	15.37	
870	APMUKS(BJ) B042409.91-545408.8	66.32996	-54.78892	66.32013	-54.78994	20.74	
874	APMUKS(BJ) B045141.10-521035.3	73.22188	-52.09224	73.21917	-52.09536	12.74	
875	APMUKS(BJ) B042751.62-533545.7	67.26017	-53.49037	67.25842	-53.48769	10.34	
879	APMUKS(BJ) B043518.24-532356.0	69.11987	-53.29794	69.11725	-53.29894	6.7	
882	APMUKS(BJ) B044507.73-521808.2	71.58106	-52.21108	71.58175	-52.21358	9.14	
883	APMUKS(BJ) B042303.35-535313.7	66.05878	-53.77059	66.05679	-53.77344	11.11	
885	APMUKS(BJ) B043338.39-541757.2	68.68914	-54.19741	68.69054	-54.19736	2.96	
886	APMUKS(BJ) B043613.87-543736.6	69.33086	-54.52627	69.33238	-54.52789	6.63	
888	APMUKS(BJ) B043119.02-544545.3	68.10869	-54.65605	68.10513	-54.65808	10.43	
891	APMUKS(BJ) B045406.98-521536.9	73.82994	-52.18879	73.82488	-52.18194	27.06	
892	APMUKS(BJ) B042739.84-534715.2	67.20652	-53.67892	67.20704	-53.67900	1.15	
894	APMUKS(BJ) B045525.56-514938.8	74.15796	-51.74905	74.15704	-51.75069	6.26	

Table 2. continued.

ID (ADF-S)	Name	$\alpha_{\text{ADF-S}}$ (J2000)	$\delta_{\text{ADF-S}}$ (J2000)	$\alpha_{\text{counterpart}}$ (J2000)	$\delta_{\text{counterpart}}$ (J2000)	Dist [arc sec]	redshift
898	APMUKS(BJ) B042116.46-541041.6	65.61560	-54.05734	65.60896	-54.06256	23.44	
902	APMUKS(BJ) B043139.87-540532.4	68.20108	-53.98850	68.20067	-53.98825	1.26	
904	APMUKS(BJ) B044601.80-521635.3	71.80566	-52.19065	71.80692	-52.18881	7.2	
907	APMUKS(BJ) B043536.31-525942.3	69.20734	-52.90101	69.19746	-52.89547	29.29	
908	APMUKS(BJ) B042716.78-534336.1	67.10781	-53.61977	67.11200	-53.61769	11.66	
911	APMUKS(BJ) B043444.25-534916.7	68.96348	-53.72046	68.97054	-53.72069	15.07	
913	APMUKS(BJ) B042401.33-540651.6	66.29212	-54.00489	66.29483	-54.00169	12.86	
917	2MASX J04415103-5320301	70.46281	-53.33947	70.46254	-53.34175	8.23	
920	APMUKS(BJ) B045457.54-512830.8	74.04829	-51.39947	74.04475	-51.39792	9.72	
924	APMUKS(BJ) B044245.39-522915.6	70.98625	-52.39530	70.98763	-52.39622	4.49	
926	APMUKS(BJ) B042943.59-531546.3	67.72859	-53.15836	67.72800	-53.15661	6.42	
928	APMUKS(BJ) B045640.68-520151.5	74.47331	-51.95581	74.46700	-51.95567	14.01	
931	APMUKS(BJ) B042932.92-551400.5	67.65130	-55.12474	67.65779	-55.12697	15.59	
932	APMUKS(BJ) B045458.29-514101.0	74.04758	-51.60854	74.04538	-51.60633	9.35	
935	APMUKS(BJ) B043838.89-524907.2	69.95674	-52.72120	69.95867	-52.72253	6.36	
938	APMUKS(BJ) B042328.58-535428.1	66.16665	-53.79251	66.16138	-53.79458	13.47	0.0415 ⁴
940	APMUKS(BJ) B042425.78-545212.6	66.38807	-54.75342	66.38650	-54.75797	16.71	
942	APMUKS(BJ) B045115.03-515930.7	73.11927	-51.90887	73.11300	-51.91025	14.78	
943	APMUKS(BJ) B042548.46-544015.0	66.73815	-54.56000	66.73271	-54.56017	11.38	
945	HD 031204	72.73552	-53.45908	72.73575	-53.45992	3.05	
947	APMUKS(BJ) B043459.77-540924.9	69.03506	-54.05576	69.03067	-54.05658	9.75	
949	APMUKS(BJ) B045559.67-514914.4	74.29597	-51.74513	74.29900	-51.74458	7.03	
950	APMUKS(BJ) B043726.42-530308.0	69.65317	-52.94978	69.65446	-52.95469	17.91	
951	APMUKS(BJ) B045422.61-514121.3	73.89684	-51.61396	73.89688	-51.61128	9.66	
955	SUMSS J045747-524452	74.46383	-52.74675	74.44588	-52.74797	39.37	
956	APMUKS(BJ) B043853.76-534404.1	70.01478	-53.63596	70.00883	-53.63858	15.82	
959	APMUKS(BJ) B043141.02-532208.1	68.22513	-53.26751	68.21471	-53.26486	24.38	
962	APMUKS(BJ) B043109.02-542144.2	68.07278	-54.25572	68.06892	-54.25761	10.6	
967	APMUKS(BJ) B042249.55-535734.3	65.99677	-53.84594	65.99854	-53.84558	3.98	
968	APMUKS(BJ) B045326.64-521610.0	73.66026	-52.19072	73.65696	-52.19036	7.4	
971	APMUKS(BJ) B042748.44-542705.0	67.23435	-54.34262	67.23417	-54.34297	1.33	
975	APMUKS(BJ) B043234.29-534235.2	68.43556	-53.60327	68.43179	-53.60672	14.81	
978	APMUKS(BJ) B045112.81-514154.6	73.12287	-51.61241	73.10733	-51.61683	38.21	
980	APMUKS(BJ) B045343.93-513245.8	73.73462	-51.46674	73.73771	-51.46733	7.25	
981	APMUKS(BJ) B043819.31-531804.4	69.87264	-53.20681	69.87117	-53.20469	8.25	
982	2MASX J04470733-5207379	71.79652	-52.13210	71.78067	-52.12722	39.19	
983	APMUKS(BJ) B042645.53-534804.0	66.98319	-53.69071	66.98117	-53.69153	5.22	
989	IRAS 04566-5328	74.43930	-53.39197	74.43292	-53.39472	16.91	
996	APMUKS(BJ) B042845.94-534654.9	67.48405	-53.67503	67.48183	-53.67458	4.99	
1000	APMUKS(BJ) B043704.06-531752.9	69.56058	-53.19954	69.55842	-53.20008	5.06	

1 - 14 As in Table 1

15 - Thomas et al. (1998)

Table 3. Flux densities of 330 ADF-S sources from the 10σ catalog with identified counterparts, measured by AKARI.

ID (ADF-S)	Flux densities [Jy]			
	N60 (65 μm)	WIDE-S (90 μm)	WIDE-L (140 μm)	N160 (160 μm)
1	1.65E+00 \pm 5.83E-02	2.72E+00 \pm 9.14E-02	5.04E+00 \pm 1.53E-01	4.87E+00 \pm 3.42E-01
2	1.15E+00 \pm 4.18E-02	1.45E+00 \pm 4.79E-02	2.59E+00 \pm 9.43E-02	1.26E+00 \pm 2.12E-01
3	-	1.24E+00 \pm 4.12E-02	3.93E+00 \pm 1.25E-01	5.09E+00 \pm 3.52E-01
4	9.12E-01 \pm 3.44E-02	1.16E+00 \pm 3.84E-02	1.05E+00 \pm 6.74E-02	6.08E-01 \pm 2.00E+00
5	6.22E-01 \pm 2.60E-02	8.89E-01 \pm 2.96E-02	-	-
6	4.46E-01 \pm 2.16E-02	8.66E-01 \pm 2.89E-02	1.25E+00 \pm 7.01E-02	-
7	-	7.58E-01 \pm 2.54E-02	4.56E-01 \pm 6.21E-02	-
8	5.18E-01 \pm 2.33E-02	6.37E-01 \pm 2.15E-02	8.65E-01 \pm 6.54E-02	-
9	4.66E-01 \pm 2.20E-02	5.48E-01 \pm 1.87E-02	4.77E-01 \pm 6.22E-02	-
10	3.07E-01 \pm 1.86E-02	5.24E-01 \pm 1.80E-02	1.16E+00 \pm 6.88E-02	-
11	-	4.95E-01 \pm 1.71E-02	9.43E-01 \pm 6.62E-02	-
12	4.92E-01 \pm 2.27E-02	4.91E-01 \pm 1.69E-02	3.59E-01 \pm 6.16E-02	-
13	3.97E-01 \pm 2.04E-02	4.79E-01 \pm 1.66E-02	9.17E-01 \pm 6.59E-02	-
14	4.52E-01 \pm 2.17E-02	4.73E-01 \pm 1.64E-02	-	-
15	2.78E-01 \pm 1.81E-02	4.51E-01 \pm 1.57E-02	6.73E-01 \pm 6.36E-02	-
16	3.00E-01 \pm 1.85E-02	4.41E-01 \pm 1.54E-02	-	-
17	-	4.37E-01 \pm 1.53E-02	-	-
18	2.33E-01 \pm 1.73E-02	4.07E-01 \pm 1.44E-02	6.94E-01 \pm 6.38E-02	-
19	2.32E-01 \pm 1.73E-02	3.87E-01 \pm 1.38E-02	3.81E-01 \pm 6.17E-02	-
20	2.94E-01 \pm 1.84E-02	3.84E-01 \pm 1.37E-02	-	-
21	2.08E-01 \pm 1.70E-02	3.56E-01 \pm 1.28E-02	6.18E-01 \pm 6.32E-02	-
22	2.14E-01 \pm 1.70E-02	3.55E-01 \pm 1.28E-02	-	-
23	1.99E-01 \pm 1.68E-02	3.28E-01 \pm 1.20E-02	3.93E-01 \pm 6.18E-02	1.06E+00 \pm 2.08E-01
24	-	3.21E-01 \pm 1.18E-02	4.85E-01 \pm 6.23E-02	-
25	-	3.10E-01 \pm 1.15E-02	-	-
26	2.75E-01 \pm 1.80E-02	3.01E-01 \pm 1.12E-02	2.31E-01 \pm 6.11E-02	-
27	2.14E-01 \pm 1.70E-02	2.84E-01 \pm 1.07E-02	2.76E-01 \pm 6.13E-02	-
28	1.71E-01 \pm 1.65E-02	2.62E-01 \pm 1.01E-02	-	-
29	1.60E-01 \pm 1.63E-02	2.59E-01 \pm 1.00E-02	4.03E-01 \pm 6.18E-02	-
30	2.02E-01 \pm 1.69E-02	2.55E-01 \pm 9.91E-03	-	-
31	1.42E-01 \pm 1.62E-02	2.53E-01 \pm 9.87E-03	2.83E-01 \pm 6.13E-02	-
32	1.33E-01 \pm 1.61E-02	2.50E-01 \pm 9.78E-03	-	-
34	-	2.40E-01 \pm 9.51E-03	3.87E-01 \pm 6.17E-02	-
35	1.46E-01 \pm 1.62E-02	2.37E-01 \pm 9.42E-03	-	-
36	-	2.36E-01 \pm 9.38E-03	-	-
37	1.79E-01 \pm 1.66E-02	2.32E-01 \pm 9.29E-03	-	-
39	1.91E-01 \pm 1.67E-02	2.29E-01 \pm 9.19E-03	-	-
40	-	2.23E-01 \pm 9.05E-03	-	-
41	1.24E-01 \pm 1.60E-02	2.21E-01 \pm 8.98E-03	2.32E-01 \pm 6.11E-02	-
42	-	2.14E-01 \pm 8.81E-03	2.11E-01 \pm 6.11E-02	1.10E+00 \pm 2.09E-01
43	-	2.10E-01 \pm 8.68E-03	4.10E-01 \pm 6.18E-02	-
44	5.88E-02 \pm 1.55E-02	2.08E-01 \pm 8.64E-03	-	-
45	1.36E-01 \pm 1.61E-02	2.07E-01 \pm 8.61E-03	4.14E-01 \pm 6.19E-02	-
46	-	2.06E-01 \pm 8.59E-03	-	-
47	1.72E-01 \pm 1.65E-02	2.01E-01 \pm 8.45E-03	-	-
48	1.04E-01 \pm 1.58E-02	1.99E-01 \pm 8.41E-03	4.60E-01 \pm 6.21E-02	-
49	1.31E-01 \pm 1.61E-02	1.96E-01 \pm 8.32E-03	4.25E-01 \pm 6.19E-02	-
50	-	1.94E-01 \pm 8.28E-03	-	-
51	1.24E-01 \pm 1.60E-02	1.90E-01 \pm 8.18E-03	3.11E-01 \pm 6.14E-02	-
52	1.68E-01 \pm 1.64E-02	1.84E-01 \pm 8.02E-03	-	-
53	1.15E-01 \pm 1.59E-02	1.78E-01 \pm 7.89E-03	-	-
54	1.10E-01 \pm 1.59E-02	1.76E-01 \pm 7.84E-03	-	-
55	9.22E-02 \pm 1.57E-02	1.76E-01 \pm 7.83E-03	-	-
56	1.47E-01 \pm 1.62E-02	1.74E-01 \pm 7.78E-03	2.50E-01 \pm 6.12E-02	-
57	-	1.73E-01 \pm 7.76E-03	3.51E-01 \pm 6.16E-02	-
58	1.59E-01 \pm 1.63E-02	1.73E-01 \pm 7.76E-03	-	-
59	-	1.71E-01 \pm 7.72E-03	3.58E-01 \pm 6.16E-02	-
60	-	1.69E-01 \pm 7.65E-03	-	-
61	-	1.68E-01 \pm 7.63E-03	-	-

Table 3. continued.

ID (ADFS)	Flux densities [Jy]			
	N60 (65 μm)	WIDE-S (90 μm)	WIDE-L (140 μm)	N160 (160 μm)
63	6.31E-02 \pm 1.55E-02	1.63E-01 \pm 7.52E-03	-	-
64	9.19E-02 \pm 1.57E-02	1.61E-01 \pm 7.48E-03	4.39E-01 \pm 6.20E-02	-
65	9.97E-02 \pm 1.58E-02	1.61E-01 \pm 7.46E-03	3.63E-01 \pm 6.16E-02	-
66	-	1.59E-01 \pm 7.44E-03	-	-
67	-	1.58E-01 \pm 7.41E-03	-	-
68	1.22E-01 \pm 1.60E-02	1.58E-01 \pm 7.40E-03	-	-
69	8.06E-02 \pm 1.56E-02	1.57E-01 \pm 7.38E-03	2.93E-01 \pm 6.13E-02	-
70	9.76E-02 \pm 1.58E-02	1.56E-01 \pm 7.36E-03	-	-
71	-	1.55E-01 \pm 7.34E-03	-	-
72	-	1.53E-01 \pm 7.29E-03	5.19E-01 \pm 6.25E-02	-
73	-	1.53E-01 \pm 7.29E-03	-	-
74	1.25E-01 \pm 1.60E-02	1.50E-01 \pm 7.23E-03	-	-
75	-	1.49E-01 \pm 7.19E-03	-	-
76	-	1.48E-01 \pm 7.18E-03	3.59E-01 \pm 6.16E-02	-
78	1.00E-01 \pm 1.58E-02	1.47E-01 \pm 7.15E-03	-	-
79	1.03E-01 \pm 1.58E-02	1.47E-01 \pm 7.14E-03	-	-
82	7.15E-02 \pm 1.56E-02	1.44E-01 \pm 7.09E-03	2.28E-01 \pm 6.11E-02	-
83	1.29E-01 \pm 1.60E-02	1.43E-01 \pm 7.07E-03	-	-
85	1.30E-01 \pm 1.60E-02	1.43E-01 \pm 7.05E-03	-	-
86	-	1.42E-01 \pm 7.05E-03	-	-
88	1.15E-01 \pm 1.59E-02	1.40E-01 \pm 7.00E-03	-	-
89	-	1.40E-01 \pm 7.00E-03	3.34E-01 \pm 6.15E-02	-
90	-	1.40E-01 \pm 7.00E-03	-	-
92	-	1.40E-01 \pm 6.99E-03	-	-
93	-	1.40E-01 \pm 6.99E-03	2.41E-01 \pm 6.12E-02	-
94	-	1.39E-01 \pm 6.97E-03	-	-
95	-	1.37E-01 \pm 6.94E-03	5.30E-01 \pm 6.25E-02	-
96	-	1.37E-01 \pm 6.94E-03	2.53E-01 \pm 6.12E-02	-
97	4.95E-02 \pm 1.55E-02	1.35E-01 \pm 6.90E-03	-	-
98	1.08E-01 \pm 1.58E-02	1.35E-01 \pm 6.89E-03	-	-
99	1.17E-01 \pm 1.59E-02	1.35E-01 \pm 6.88E-03	-	-
100	-	1.33E-01 \pm 6.84E-03	-	-
101	-	1.32E-01 \pm 6.82E-03	-	-
102	-	1.32E-01 \pm 6.81E-03	-	-
103	8.21E-02 \pm 1.57E-02	1.32E-01 \pm 6.81E-03	5.45E-01 \pm 6.27E-02	-
104	-	1.30E-01 \pm 6.77E-03	3.28E-01 \pm 6.15E-02	-
105	-	1.29E-01 \pm 6.75E-03	-	-
106	-	1.28E-01 \pm 6.74E-03	-	-
107	8.29E-02 \pm 1.57E-02	1.27E-01 \pm 6.71E-03	-	-
108	8.40E-02 \pm 1.57E-02	1.27E-01 \pm 6.71E-03	-	-
109	-	1.27E-01 \pm 6.71E-03	1.89E-01 \pm 6.10E-02	-
110	1.32E-01 \pm 1.61E-02	1.25E-01 \pm 6.68E-03	-	-
111	1.03E-01 \pm 1.58E-02	1.25E-01 \pm 6.67E-03	-	-
112	-	1.25E-01 \pm 6.67E-03	-	-
113	-	1.25E-01 \pm 6.67E-03	-	-
114	8.23E-02 \pm 1.57E-02	1.24E-01 \pm 6.66E-03	-	-
115	-	1.23E-01 \pm 6.63E-03	-	-
117	-	1.22E-01 \pm 6.62E-03	-	-
118	-	1.21E-01 \pm 6.60E-03	2.62E-01 \pm 6.12E-02	-
119	-	1.21E-01 \pm 6.59E-03	-	-
120	-	1.18E-01 \pm 6.53E-03	-	-
121	1.08E-01 \pm 1.58E-02	1.17E-01 \pm 6.51E-03	-	-
122	-	1.16E-01 \pm 6.49E-03	-	-
123	-	1.16E-01 \pm 6.49E-03	-	-
124	-	1.15E-01 \pm 6.48E-03	-	-
126	7.50E-02 \pm 1.56E-02	1.13E-01 \pm 6.44E-03	-	-
127	-	1.13E-01 \pm 6.43E-03	-	-
130	-	1.10E-01 \pm 6.38E-03	-	-
132	-	1.09E-01 \pm 6.35E-03	-	-
133	-	1.07E-01 \pm 6.32E-03	-	-

Table 3. continued.

ID (ADFS)	Flux densities [Jy]			
	N60 (65 μm)	WIDE-S (90 μm)	WIDE-L (140 μm)	N160 (160 μm)
134	-	1.06E-01 \pm 6.30E-03	-	-
135	-	1.06E-01 \pm 6.30E-03	-	-
136	-	1.06E-01 \pm 6.30E-03	-	-
138	-	1.05E-01 \pm 6.29E-03	-	-
139	8.47E-02 \pm 1.57E-02	1.04E-01 \pm 6.26E-03	-	-
140	-	1.04E-01 \pm 6.26E-03	-	-
142	-	1.03E-01 \pm 6.25E-03	-	-
143	-	1.03E-01 \pm 6.25E-03	2.45E-01 \pm 6.12E-02	-
146	-	1.01E-01 \pm 6.22E-03	-	-
147	-	1.01E-01 \pm 6.22E-03	-	-
148	-	1.01E-01 \pm 6.21E-03	-	-
149	-	1.01E-01 \pm 6.21E-03	-	-
151	-	9.98E-02 \pm 6.19E-03	2.30E-01 \pm 6.11E-02	-
152	-	9.97E-02 \pm 6.19E-03	-	-
154	-	9.91E-02 \pm 6.18E-03	-	-
155	-	9.89E-02 \pm 6.17E-03	-	-
156	-	9.88E-02 \pm 6.17E-03	-	-
158	-	9.81E-02 \pm 6.16E-03	2.72E-01 \pm 6.13E-02	-
159	-	9.74E-02 \pm 6.15E-03	2.45E-01 \pm 6.12E-02	-
160	-	9.74E-02 \pm 6.15E-03	-	-
162	-	9.70E-02 \pm 6.14E-03	-	-
165	6.91E-02 \pm 1.56E-02	9.54E-02 \pm 6.11E-03	-	-
166	-	9.52E-02 \pm 6.11E-03	-	-
168	-	9.48E-02 \pm 6.10E-03	-	-
169	-	9.40E-02 \pm 6.09E-03	-	-
170	-	9.36E-02 \pm 6.08E-03	-	-
171	-	9.30E-02 \pm 6.07E-03	-	-
172	-	9.24E-02 \pm 6.06E-03	-	-
173	-	9.23E-02 \pm 6.06E-03	-	-
175	6.20E-02 \pm 1.55E-02	9.20E-02 \pm 6.05E-03	-	-
176	-	9.20E-02 \pm 6.05E-03	-	-
177	-	9.19E-02 \pm 6.05E-03	-	-
179	-	9.12E-02 \pm 6.04E-03	-	-
181	-	9.09E-02 \pm 6.04E-03	-	-
183	-	9.08E-02 \pm 6.03E-03	-	-
184	5.71E-02 \pm 1.55E-02	9.08E-02 \pm 6.03E-03	-	-
185	7.33E-02 \pm 1.56E-02	9.07E-02 \pm 6.03E-03	-	-
190	-	8.99E-02 \pm 6.02E-03	-	-
191	-	8.98E-02 \pm 6.02E-03	-	-
192	-	8.95E-02 \pm 6.01E-03	-	-
194	-	8.87E-02 \pm 6.00E-03	-	-
195	-	8.86E-02 \pm 6.00E-03	-	-
196	-	8.84E-02 \pm 5.99E-03	-	-
198	6.01E-02 \pm 1.55E-02	8.81E-02 \pm 5.99E-03	-	-
199	-	8.79E-02 \pm 5.99E-03	-	-
200	-	8.78E-02 \pm 5.98E-03	-	-
201	-	8.76E-02 \pm 5.98E-03	-	-
203	-	8.75E-02 \pm 5.98E-03	-	-
204	-	8.74E-02 \pm 5.98E-03	-	-
205	6.97E-02 \pm 1.56E-02	8.61E-02 \pm 5.96E-03	-	-
206	5.58E-02 \pm 1.55E-02	8.54E-02 \pm 5.95E-03	-	-
210	-	8.43E-02 \pm 5.93E-03	-	-
211	-	8.42E-02 \pm 5.93E-03	-	-
212	-	8.41E-02 \pm 5.92E-03	2.12E-01 \pm 6.11E-02	-
213	4.97E-02 \pm 1.55E-02	8.31E-02 \pm 5.91E-03	-	-
214	-	8.29E-02 \pm 5.91E-03	-	-
215	-	8.28E-02 \pm 5.90E-03	-	-
216	-	8.21E-02 \pm 5.89E-03	2.87E-01 \pm 6.13E-02	-
218	-	8.19E-02 \pm 5.89E-03	-	-
219	-	8.18E-02 \pm 5.89E-03	-	-

Table 3. continued.

ID (ADFS)	Flux densities [Jy]			
	N60 (65 μm)	WIDE-S (90 μm)	WIDE-L (140 μm)	N160 (160 μm)
222	4.66E-02 \pm 1.55E-02	8.14E-02 \pm 5.88E-03	-	-
223	-	8.14E-02 \pm 5.88E-03	-	-
224	-	8.12E-02 \pm 5.88E-03	-	-
225	-	8.12E-02 \pm 5.88E-03	-	-
226	8.06E-02 \pm 1.56E-02	8.10E-02 \pm 5.88E-03	-	-
228	-	8.09E-02 \pm 5.88E-03	-	-
232	-	8.03E-02 \pm 5.87E-03	-	-
233	-	7.94E-02 \pm 5.85E-03	-	-
234	-	7.93E-02 \pm 5.85E-03	-	-
239	8.39E-02 \pm 1.57E-02	7.83E-02 \pm 5.84E-03	-	-
244	-	7.77E-02 \pm 5.83E-03	-	-
247	-	7.74E-02 \pm 5.82E-03	-	-
252	5.99E-02 \pm 1.55E-02	7.65E-02 \pm 5.81E-03	-	-
253	-	7.64E-02 \pm 5.81E-03	-	-
254	6.67E-02 \pm 1.56E-02	7.63E-02 \pm 5.81E-03	-	-
255	-	7.59E-02 \pm 5.80E-03	-	-
256	-	7.56E-02 \pm 5.79E-03	-	-
257	-	7.47E-02 \pm 5.78E-03	-	-
258	-	7.45E-02 \pm 5.78E-03	-	-
259	-	7.43E-02 \pm 5.78E-03	-	-
260	-	7.37E-02 \pm 5.77E-03	2.60E-01 \pm 6.12E-02	-
261	-	7.33E-02 \pm 5.76E-03	-	-
262	-	7.32E-02 \pm 5.76E-03	-	-
265	-	7.28E-02 \pm 5.76E-03	-	-
267	-	7.25E-02 \pm 5.75E-03	-	-
270	-	7.16E-02 \pm 5.74E-03	-	-
271	-	7.15E-02 \pm 5.74E-03	-	-
275	-	7.12E-02 \pm 5.73E-03	-	-
277	-	7.10E-02 \pm 5.73E-03	-	-
279	-	7.07E-02 \pm 5.73E-03	-	-
280	-	7.06E-02 \pm 5.72E-03	-	-
281	-	7.06E-02 \pm 5.72E-03	-	-
283	-	7.03E-02 \pm 5.72E-03	-	-
287	-	7.00E-02 \pm 5.72E-03	-	-
288	-	6.99E-02 \pm 5.71E-03	-	-
290	-	6.93E-02 \pm 5.71E-03	-	-
292	-	6.91E-02 \pm 5.70E-03	-	-
294	-	6.88E-02 \pm 5.70E-03	-	-
295	-	6.87E-02 \pm 5.70E-03	-	-
297	-	6.86E-02 \pm 5.70E-03	-	-
299	-	6.84E-02 \pm 5.69E-03	-	-
300	-	6.83E-02 \pm 5.69E-03	-	-
301	-	6.82E-02 \pm 5.69E-03	-	-
302	-	6.80E-02 \pm 5.69E-03	-	-
304	-	6.80E-02 \pm 5.69E-03	-	-
306	-	6.76E-02 \pm 5.68E-03	-	-
307	-	6.76E-02 \pm 5.68E-03	-	-
308	-	6.75E-02 \pm 5.68E-03	-	-
310	-	6.74E-02 \pm 5.68E-03	-	-
311	-	6.74E-02 \pm 5.68E-03	-	-
312	-	6.73E-02 \pm 5.68E-03	-	-
314	-	6.71E-02 \pm 5.68E-03	-	-
317	-	6.66E-02 \pm 5.67E-03	-	-
318	-	6.64E-02 \pm 5.67E-03	-	-
323	-	6.57E-02 \pm 5.66E-03	-	-
324	-	6.56E-02 \pm 5.66E-03	-	-
327	-	6.52E-02 \pm 5.65E-03	-	-
328	-	6.49E-02 \pm 5.65E-03	-	-
329	5.66E-02 \pm 1.55E-02	6.49E-02 \pm 5.65E-03	-	-
334	-	6.42E-02 \pm 5.64E-03	-	-

Table 3. continued.

ID (ADFS)	Flux densities [Jy]			
	N60 (65 μm)	WIDE-S (90 μm)	WIDE-L (140 μm)	N160 (160 μm)
335	-	6.41E-02 \pm 5.64E-03	-	-
336	-	6.40E-02 \pm 5.64E-03	-	-
337	-	6.40E-02 \pm 5.64E-03	-	-
338	-	6.39E-02 \pm 5.64E-03	-	-
339	-	6.38E-02 \pm 5.63E-03	-	-
340	-	6.38E-02 \pm 5.63E-03	-	-
341	-	6.35E-02 \pm 5.63E-03	-	-
342	6.39E-02 \pm 1.56E-02	6.34E-02 \pm 5.63E-03	-	-
343	-	6.34E-02 \pm 5.63E-03	-	-
344	-	6.32E-02 \pm 5.63E-03	-	-
345	6.39E-02 \pm 1.56E-02	6.31E-02 \pm 5.63E-03	-	-
348	-	6.28E-02 \pm 5.62E-03	-	-
351	-	6.23E-02 \pm 5.61E-03	-	-
352	-	6.23E-02 \pm 5.61E-03	-	-
354	-	6.20E-02 \pm 5.61E-03	-	-
355	-	6.20E-02 \pm 5.61E-03	-	-
357	-	6.18E-02 \pm 5.61E-03	-	-
358	-	6.18E-02 \pm 5.61E-03	-	-
360	-	6.16E-02 \pm 5.61E-03	-	-
364	-	6.07E-02 \pm 5.60E-03	-	-
365	-	6.06E-02 \pm 5.59E-03	-	-
366	-	6.06E-02 \pm 5.59E-03	-	-
368	-	6.03E-02 \pm 5.59E-03	-	-
369	-	6.02E-02 \pm 5.59E-03	-	-
370	-	6.00E-02 \pm 5.59E-03	-	-
373	-	5.99E-02 \pm 5.58E-03	-	-
374	-	5.98E-02 \pm 5.58E-03	-	-
377	-	5.94E-02 \pm 5.58E-03	-	-
380	-	5.91E-02 \pm 5.58E-03	-	-
384	-	5.90E-02 \pm 5.57E-03	-	-
386	-	5.88E-02 \pm 5.57E-03	-	-
391	-	5.83E-02 \pm 5.57E-03	-	-
392	-	5.82E-02 \pm 5.57E-03	-	-
393	-	5.82E-02 \pm 5.56E-03	-	-
394	-	5.81E-02 \pm 5.56E-03	-	-
396	-	5.80E-02 \pm 5.56E-03	-	-
397	-	5.80E-02 \pm 5.56E-03	-	-
398	-	5.80E-02 \pm 5.56E-03	-	-
399	-	5.80E-02 \pm 5.56E-03	-	-
400	-	5.79E-02 \pm 5.56E-03	-	-
402	-	5.74E-02 \pm 5.56E-03	-	-
410	-	5.63E-02 \pm 5.54E-03	-	-
414	-	5.58E-02 \pm 5.54E-03	-	-
415	-	5.56E-02 \pm 5.53E-03	-	-
416	-	5.56E-02 \pm 5.53E-03	-	-
418	-	5.54E-02 \pm 5.53E-03	-	-
419	-	5.54E-02 \pm 5.53E-03	-	-
422	-	5.51E-02 \pm 5.53E-03	-	-
423	-	5.51E-02 \pm 5.53E-03	-	-
424	-	5.51E-02 \pm 5.53E-03	-	-
426	-	5.50E-02 \pm 5.53E-03	-	-
430	-	5.45E-02 \pm 5.52E-03	-	-
431	-	5.44E-02 \pm 5.52E-03	-	-
432	-	5.44E-02 \pm 5.52E-03	-	-
434	-	5.40E-02 \pm 5.52E-03	-	-
436	-	5.39E-02 \pm 5.52E-03	-	-
437	-	5.39E-02 \pm 5.52E-03	-	-
439	-	5.38E-02 \pm 5.51E-03	-	-
441	-	5.36E-02 \pm 5.51E-03	-	-
443	6.67E-02 \pm 1.56E-02	5.33E-02 \pm 5.51E-03	-	-

Table 3. continued.

ID (ADFS)	Flux densities [Jy]			
	N60 (65 μm)	WIDE-S (90 μm)	WIDE-L (140 μm)	N160 (160 μm)
445	-	5.31E-02 \pm 5.51E-03	-	-
447	-	5.30E-02 \pm 5.51E-03	-	-
448	-	5.30E-02 \pm 5.51E-03	-	-
449	-	5.29E-02 \pm 5.50E-03	-	-
450	-	5.29E-02 \pm 5.50E-03	2.09E-01 \pm 6.11E-02	-
451	-	5.29E-02 \pm 5.50E-03	-	-
452	-	5.29E-02 \pm 5.50E-03	-	6.94E-01 \pm 2.03E-01
458	-	5.24E-02 \pm 5.50E-03	-	-
460	-	5.21E-02 \pm 5.50E-03	-	-
462	-	5.20E-02 \pm 5.49E-03	-	-
463	-	5.20E-02 \pm 5.49E-03	-	-
464	-	5.19E-02 \pm 5.49E-03	-	-
465	-	5.18E-02 \pm 5.49E-03	-	-
466	-	5.17E-02 \pm 5.49E-03	-	-
467	-	5.13E-02 \pm 5.49E-03	-	-
468	-	5.13E-02 \pm 5.49E-03	-	-
472	-	5.09E-02 \pm 5.48E-03	-	-
473	-	5.09E-02 \pm 5.48E-03	-	-
474	-	5.09E-02 \pm 5.48E-03	-	-
477	-	5.06E-02 \pm 5.48E-03	-	-
482	-	4.98E-02 \pm 5.47E-03	-	-
486	-	4.97E-02 \pm 5.47E-03	-	-
488	-	4.92E-02 \pm 5.47E-03	-	-
489	-	4.91E-02 \pm 5.46E-03	-	-
490	-	4.90E-02 \pm 5.46E-03	-	-
492	-	4.88E-02 \pm 5.46E-03	-	-
493	-	4.87E-02 \pm 5.46E-03	-	-
494	4.96E-02 \pm 1.55E-02	4.86E-02 \pm 5.46E-03	-	-
496	-	4.84E-02 \pm 5.46E-03	-	-
497	-	4.83E-02 \pm 5.46E-03	-	-
499	-	4.82E-02 \pm 5.46E-03	-	-

Table 4. Flux densities of 218 ADF-S sources from the fainter part of the 6σ catalog, measured by AKARI.

ID (ADF-S)	Flux densities [Jy]			
	N60 (65 μm)	WIDE-S (90 μm)	WIDE-L (140 μm)	N160 (160 μm)
503	-	4.79E-02 \pm 5.45E-03	-	-
504	-	4.78E-02 \pm 5.45E-03	-	-
507	-	4.75E-02 \pm 5.45E-03	-	-
513	-	4.70E-02 \pm 5.44E-03	-	-
514	-	4.69E-02 \pm 5.44E-03	-	-
519	-	4.68E-02 \pm 5.44E-03	-	-
523	-	4.65E-02 \pm 5.44E-03	-	-
524	-	4.65E-02 \pm 5.44E-03	-	-
526	-	4.64E-02 \pm 5.44E-03	-	-
530	6.38E-02 \pm 1.56E-02	4.62E-02 \pm 5.44E-03	-	-
532	-	4.61E-02 \pm 5.43E-03	-	-
533	-	4.61E-02 \pm 5.43E-03	-	-
534	-	4.60E-02 \pm 5.43E-03	-	-
536	-	4.60E-02 \pm 5.43E-03	-	-
538	-	4.59E-02 \pm 5.43E-03	-	-
541	-	4.57E-02 \pm 5.43E-03	-	-
543	-	4.55E-02 \pm 5.43E-03	-	-
544	-	4.54E-02 \pm 5.43E-03	2.49E-01 \pm 6.12E-02	-
545	-	4.53E-02 \pm 5.43E-03	-	-
548	-	4.51E-02 \pm 5.42E-03	-	-
552	-	4.49E-02 \pm 5.42E-03	-	-
554	-	4.48E-02 \pm 5.42E-03	-	-
555	-	4.48E-02 \pm 5.42E-03	-	-
556	-	4.47E-02 \pm 5.42E-03	-	-
559	-	4.46E-02 \pm 5.42E-03	-	-
560	-	4.46E-02 \pm 5.42E-03	-	-
564	-	4.41E-02 \pm 5.42E-03	-	-
565	-	4.39E-02 \pm 5.41E-03	-	-
567	-	4.37E-02 \pm 5.41E-03	-	-
570	-	4.36E-02 \pm 5.41E-03	-	-
572	-	4.35E-02 \pm 5.41E-03	-	-
574	-	4.35E-02 \pm 5.41E-03	-	-
575	-	4.35E-02 \pm 5.41E-03	-	-
576	-	4.35E-02 \pm 5.41E-03	-	-
577	-	4.34E-02 \pm 5.41E-03	-	-
578	-	4.33E-02 \pm 5.41E-03	-	-
579	-	4.31E-02 \pm 5.41E-03	-	-
582	-	4.30E-02 \pm 5.40E-03	-	-
583	-	4.30E-02 \pm 5.40E-03	-	-
585	-	4.29E-02 \pm 5.40E-03	-	-
588	-	4.28E-02 \pm 5.40E-03	-	-
593	-	4.27E-02 \pm 5.40E-03	-	-
595	-	4.27E-02 \pm 5.40E-03	-	-
596	-	4.27E-02 \pm 5.40E-03	-	-
598	-	4.26E-02 \pm 5.40E-03	-	-
603	-	4.23E-02 \pm 5.40E-03	-	-
604	-	4.23E-02 \pm 5.40E-03	-	-
606	-	4.22E-02 \pm 5.40E-03	-	-
608	-	4.21E-02 \pm 5.40E-03	-	-
610	-	4.20E-02 \pm 5.40E-03	-	-
612	-	4.19E-02 \pm 5.39E-03	-	-
618	-	4.17E-02 \pm 5.39E-03	-	-
621	-	4.16E-02 \pm 5.39E-03	-	-
624	-	4.15E-02 \pm 5.39E-03	-	-
625	-	4.15E-02 \pm 5.39E-03	-	-
629	-	4.14E-02 \pm 5.39E-03	-	-
632	-	4.13E-02 \pm 5.39E-03	-	-
633	-	4.12E-02 \pm 5.39E-03	-	-
634	-	4.11E-02 \pm 5.39E-03	-	-

Table 4. continued.

ID (ADFS)	Flux densities [Jy]			
	N60 (65 μm)	WIDE-S (90 μm)	WIDE-L (140 μm)	N160 (160 μm)
636	-	4.11E-02 \pm 5.39E-03	-	-
639	-	4.08E-02 \pm 5.38E-03	-	-
640	-	4.07E-02 \pm 5.38E-03	-	-
644	-	4.06E-02 \pm 5.38E-03	-	-
648	-	4.05E-02 \pm 5.38E-03	-	-
652	-	4.04E-02 \pm 5.38E-03	-	-
653	-	4.04E-02 \pm 5.38E-03	-	-
654	-	4.03E-02 \pm 5.38E-03	-	-
659	-	4.01E-02 \pm 5.38E-03	-	-
662	-	3.99E-02 \pm 5.38E-03	-	-
664	-	3.98E-02 \pm 5.38E-03	-	-
669	-	3.95E-02 \pm 5.37E-03	-	-
670	-	3.94E-02 \pm 5.37E-03	-	-
675	-	3.93E-02 \pm 5.37E-03	-	-
677	-	3.92E-02 \pm 5.37E-03	-	-
679	-	3.91E-02 \pm 5.37E-03	-	-
685	-	3.90E-02 \pm 5.37E-03	-	-
686	-	3.89E-02 \pm 5.37E-03	-	-
690	-	3.87E-02 \pm 5.37E-03	-	-
692	-	3.86E-02 \pm 5.37E-03	-	-
693	-	3.86E-02 \pm 5.37E-03	-	-
694	-	3.85E-02 \pm 5.37E-03	-	-
697	-	3.84E-02 \pm 5.36E-03	-	-
698	-	3.84E-02 \pm 5.36E-03	-	-
699	-	3.83E-02 \pm 5.36E-03	-	-
700	-	3.83E-02 \pm 5.36E-03	-	-
708	-	3.79E-02 \pm 5.36E-03	-	-
709	-	3.79E-02 \pm 5.36E-03	-	-
710	-	3.79E-02 \pm 5.36E-03	-	-
713	-	3.78E-02 \pm 5.36E-03	-	-
715	-	3.78E-02 \pm 5.36E-03	-	-
717	-	3.76E-02 \pm 5.36E-03	-	-
718	-	3.76E-02 \pm 5.36E-03	-	-
720	-	3.76E-02 \pm 5.36E-03	-	-
721	-	3.75E-02 \pm 5.36E-03	-	-
723	-	3.75E-02 \pm 5.36E-03	-	-
728	-	3.73E-02 \pm 5.36E-03	-	-
729	-	3.73E-02 \pm 5.36E-03	-	-
730	-	3.73E-02 \pm 5.36E-03	-	-
734	-	3.72E-02 \pm 5.35E-03	-	-
738	-	3.70E-02 \pm 5.35E-03	-	-
739	-	3.70E-02 \pm 5.35E-03	-	-
740	-	3.70E-02 \pm 5.35E-03	-	-
743	-	3.70E-02 \pm 5.35E-03	-	-
749	-	3.68E-02 \pm 5.35E-03	-	-
750	-	3.68E-02 \pm 5.35E-03	-	-
754	-	3.67E-02 \pm 5.35E-03	-	-
758	-	3.65E-02 \pm 5.35E-03	-	-
760	-	3.64E-02 \pm 5.35E-03	-	-
762	-	3.63E-02 \pm 5.35E-03	-	-
763	-	3.63E-02 \pm 5.35E-03	-	-
764	-	3.63E-02 \pm 5.35E-03	-	-
765	-	3.61E-02 \pm 5.35E-03	-	-
769	-	3.60E-02 \pm 5.35E-03	-	-
770	-	3.60E-02 \pm 5.35E-03	-	-
771	4.96E-02 \pm 1.55E-02	3.60E-02 \pm 5.34E-03	-	-
772	-	3.59E-02 \pm 5.34E-03	-	-
774	-	3.58E-02 \pm 5.34E-03	-	-
776	-	3.58E-02 \pm 5.34E-03	-	-
777	-	3.58E-02 \pm 5.34E-03	-	-

Table 4. continued.

ID (ADFS)	Flux densities [Jy]			
	N60 (65 μm)	WIDE-S (90 μm)	WIDE-L (140 μm)	N160 (160 μm)
778	-	3.57E-02 \pm 5.34E-03	-	-
781	-	3.56E-02 \pm 5.34E-03	-	-
782	-	3.56E-02 \pm 5.34E-03	-	-
784	-	3.55E-02 \pm 5.34E-03	-	-
789	-	3.51E-02 \pm 5.34E-03	-	-
790	-	3.51E-02 \pm 5.34E-03	-	-
791	-	3.51E-02 \pm 5.34E-03	-	-
794	-	3.51E-02 \pm 5.34E-03	-	-
795	-	3.51E-02 \pm 5.34E-03	-	-
796	-	3.51E-02 \pm 5.34E-03	-	-
797	-	3.51E-02 \pm 5.34E-03	-	-
800	-	3.49E-02 \pm 5.34E-03	-	-
801	-	3.49E-02 \pm 5.34E-03	-	-
806	-	3.48E-02 \pm 5.34E-03	-	-
807	-	3.47E-02 \pm 5.34E-03	-	-
809	-	3.46E-02 \pm 5.33E-03	-	-
810	-	3.46E-02 \pm 5.33E-03	-	-
811	-	3.46E-02 \pm 5.33E-03	-	-
812	-	3.46E-02 \pm 5.33E-03	-	-
813	-	3.46E-02 \pm 5.33E-03	-	-
815	-	3.46E-02 \pm 5.33E-03	-	-
816	-	3.45E-02 \pm 5.33E-03	-	7.82E-01 \pm 2.04E-01
824	-	3.43E-02 \pm 5.33E-03	-	-
826	-	3.42E-02 \pm 5.33E-03	-	-
827	-	3.42E-02 \pm 5.33E-03	-	-
828	-	3.42E-02 \pm 5.33E-03	-	-
830	-	3.41E-02 \pm 5.33E-03	-	-
831	-	3.40E-02 \pm 5.33E-03	-	-
833	-	3.40E-02 \pm 5.33E-03	-	-
834	-	3.40E-02 \pm 5.33E-03	-	-
837	-	3.38E-02 \pm 5.33E-03	-	-
838	-	3.38E-02 \pm 5.33E-03	-	-
841	-	3.36E-02 \pm 5.33E-03	-	-
843	-	3.36E-02 \pm 5.33E-03	-	-
846	-	3.34E-02 \pm 5.33E-03	-	-
849	-	3.33E-02 \pm 5.32E-03	-	-
851	-	3.33E-02 \pm 5.32E-03	-	-
853	-	3.33E-02 \pm 5.32E-03	-	-
854	-	3.33E-02 \pm 5.32E-03	-	-
857	-	3.32E-02 \pm 5.32E-03	-	-
858	-	3.32E-02 \pm 5.32E-03	-	-
859	5.52E-02 \pm 1.55E-02	3.32E-02 \pm 5.32E-03	-	-
860	-	3.32E-02 \pm 5.32E-03	-	-
865	-	3.31E-02 \pm 5.32E-03	-	-
869	-	3.31E-02 \pm 5.32E-03	-	-
870	-	3.30E-02 \pm 5.32E-03	-	-
874	-	3.30E-02 \pm 5.32E-03	-	-
875	-	3.30E-02 \pm 5.32E-03	-	-
879	-	3.29E-02 \pm 5.32E-03	-	-
882	-	3.29E-02 \pm 5.32E-03	-	-
883	-	3.28E-02 \pm 5.32E-03	-	-
885	-	3.28E-02 \pm 5.32E-03	-	-
886	-	3.28E-02 \pm 5.32E-03	-	-
888	-	3.27E-02 \pm 5.32E-03	-	-
891	-	3.26E-02 \pm 5.32E-03	-	-
892	-	3.26E-02 \pm 5.32E-03	-	-
894	-	3.25E-02 \pm 5.32E-03	-	-
898	-	3.24E-02 \pm 5.32E-03	-	-
902	-	3.24E-02 \pm 5.32E-03	-	-
904	-	3.24E-02 \pm 5.32E-03	-	-

Table 4. continued.

ID (ADFS)	Flux densities [Jy]			
	N60 (65 μm)	WIDE-S (90 μm)	WIDE-L (140 μm)	N160 (160 μm)
907	-	3.23E-02 \pm 5.32E-03	-	-
908	-	3.23E-02 \pm 5.32E-03	-	-
911	-	3.22E-02 \pm 5.32E-03	-	-
913	-	3.21E-02 \pm 5.32E-03	-	-
917	-	3.20E-02 \pm 5.32E-03	-	-
920	-	3.19E-02 \pm 5.31E-03	-	-
924	-	3.18E-02 \pm 5.31E-03	-	-
926	-	3.17E-02 \pm 5.31E-03	-	-
928	-	3.16E-02 \pm 5.31E-03	-	-
931	-	3.15E-02 \pm 5.31E-03	-	-
932	-	3.15E-02 \pm 5.31E-03	-	-
935	-	3.15E-02 \pm 5.31E-03	-	-
938	-	3.14E-02 \pm 5.31E-03	-	-
940	-	3.14E-02 \pm 5.31E-03	-	-
942	-	3.14E-02 \pm 5.31E-03	-	-
943	-	3.13E-02 \pm 5.31E-03	-	-
945	-	3.13E-02 \pm 5.31E-03	-	-
947	-	3.13E-02 \pm 5.31E-03	-	-
949	-	3.13E-02 \pm 5.31E-03	-	-
950	-	3.12E-02 \pm 5.31E-03	-	-
951	-	3.12E-02 \pm 5.31E-03	-	-
955	-	3.12E-02 \pm 5.31E-03	-	-
956	-	3.11E-02 \pm 5.31E-03	-	-
959	-	3.11E-02 \pm 5.31E-03	-	-
962	-	3.10E-02 \pm 5.31E-03	-	-
967	-	3.09E-02 \pm 5.31E-03	-	-
968	-	3.09E-02 \pm 5.31E-03	-	-
971	-	3.08E-02 \pm 5.31E-03	-	-
975	-	3.07E-02 \pm 5.31E-03	-	-
978	-	3.07E-02 \pm 5.31E-03	-	-
980	-	3.07E-02 \pm 5.31E-03	-	-
981	-	3.07E-02 \pm 5.31E-03	-	-
982	-	3.06E-02 \pm 5.31E-03	-	-
983	-	3.06E-02 \pm 5.31E-03	-	-
996	-	3.02E-02 \pm 5.30E-03	-	-
1000	-	3.01E-02 \pm 5.30E-03	-	-

Table 5. Flux densities in other wavelengths, found for the counterparts of the ADFS sources in the public databases, for the 10σ catalog - part 1.

ID (ADF-S)	0.44 μm	0.47 μm^c	0.55 μm	0.64 μm	0.71 μm
1	7.05E-03±6.09E-04 ^A 7.35E-03±6.35E-03 ^A 7.59E-03±6.56E-04 ^A 7.90E-03±1.69E-03 ^B 7.38E-03 ^D	5.16E-03±6.03E-04	-	1.39E-02±1.20E-03 ^A 1.44E-02±1.25E-03 ^A 1.47E-02±1.27E-03 ^D	1.41E-02 ^D
2	1.38E-03±1.19E-14 ^A 1.46E-03±1.27E-04 ^A 1.53E-03±1.32E-04 ^A 1.49E-03 ^D	1.50E-03±1.23E-04	-	2.46E-03±2.13E-04 ^A 2.62E-03±2.26E-04 ^A 2.76E-03±2.38E-04 ^D	2.63E-03 ^D
3	1.19E-01 ^D 1.20E-01±1.40E-02 ^B	-	2.43E-01±2.85E-02 ^B 2.98E-01 ^D	-	3.54E-01 ^D
4	2.89E-02±2.50E-03 ^A 3.03E-02±2.62E-03 ^A 3.16E-02±2.74E-03 ^A 3.08E-02 ^D 3.20E-02±6.83E-03 ^B 3.32E-02±4.23E-03 ^B 3.69E-02 ^B 2.47E-02±2.29E-04 ^E	2.47E-02±2.29E-04	4.03E-02±3.49E-03 ^B 4.55E-02 ^D	4.04E-02±3.49E-03 ^A 4.31E-02±3.73E-03 ^A 4.55E-02±3.93E-03 ^D 4.10E-02±2.33E-03 ^E	4.33E-02 ^D 3.50E-02±9.81E-04 ^F 8.63E-03±2.42E-04 ^F 2.73E-02±7.65E-04 ^F
5	3.58E-03±3.09E-04 ^A 3.91E-03±3.09E-04 ^A 4.04E-03±3.49E-04 ^A 3.91E-03 ^D	3.14E-03±3.67E-04	-	3.12E-03±5.29E-04 ^A 6.38E-03±5.51E-04 ^A 6.51E-03±5.63E-04 ^D	6.20E-03 ^D
6	-	5.26E-04±6.14E-05	-	-	-
7	4.13E-03 ^D	-	-	-	-
8	4.13E-03 ^D	-	-	-	-
9	4.13E-03 ^D	-	-	-	-
10	6.95E-03±6.01E-04 ^A 7.59E-03±6.56E-04 ^A 8.43E-03±7.29E-04 ^A 8.16E-03 ^D 1.18E-02±2.01E-03 ^B	5.45E-03±6.37E-04	2.06E-02±3.54E-03 ^B	1.70E-02±1.47E-03 ^A 1.87E-02±1.62E-03 ^A 2.01E-02±1.73E-03 ^D	1.93E-02 ^D
11	5.07E-03±4.38E-04 ^A 5.00E-03±4.32E-04 ^A 5.07E-03±4.38E-04 ^A 4.92E-03 ^D 5.31E-03±1.13E-03 ^B	6.41E-03±4.21E-03	-	9.34E-03±8.07E-04 ^A 9.81E-03±8.48E-04 ^A 9.94E-03±8.59E-04 ^D	9.47E-03 ^D
12	-	4.71E-04±5.50E-05	-	-	-
14	-	3.41E-04±3.98E-05	-	-	-
16	-	2.97E-04±3.47E-05	-	-	-
17	4.39E-03±3.80E-04 ^A 4.97E-03±4.29E-04 ^A 4.83E-03 ^D 5.22E-03±1.11E-03 ^B	4.54E-03±5.30E-04	-	5.06E-03±4.37E-04 ^A 5.76E-03±4.98E-04 ^D	5.50E-03 ^D
18	-	3.00E-03±3.50E-04	-	-	-
19	-	-	-	-	-
20	-	2.49E-04±2.91E-05	-	-	-
22	-	1.54E-03±1.80E-04	-	-	-
23	6.02E-04 ^D	-	-	-	8.88E-04 ^D
26	-	1.00E-04±1.17E-05	-	-	-
28	-	1.11E-04±1.30E-05	-	-	-
29	2.77E-03±2.39E-04 ^A 2.94E-03±2.54E-04 ^A 3.13E-03±2.70E-04 ^A 3.02E-03 ^D	-	-	6.07E-03±5.25E-04 ^A 6.49E-03±5.61E-04 ^A 6.73E-03±5.81E-04 ^D	6.43E-03 ^D
30	-	-	-	-	-
31	-	4.75E-04±5.55E-05	-	-	-

Table 5. continued.

ID (ADF-S)	0.44 μm	0.47 μm^C	0.55 μm	0.64 μm	0.71 μm
32	-	2.49E-03±2.91E-04	-	-	-
35	2.86E-01 ^D	-	8.66E-01 ^D	-	-
36	1.64E-03 ^D	2.25E-04±2.63E-05	-	-	-
37	-	1.42E-04±1.66E-05	-	-	-
39	-	2.59E-03±3.02E-04	-	-	-
45	1.04E-02 ^D	1.65E-03±1.92E-04	-	-	-
46	-	1.49E-04±1.74E-05	-	-	-
47	-	5.71E-05±7.86E-06	-	-	-
49	-	3.84E-05±6.51E-06	-	-	-
50	-	8.97E-04±1.05E-04	-	-	-
51	2.49E-03±2.15E-04 ^A 2.74E-03±2.37E-04 ^A 2.91E-03±2.51E-04 ^A 2.83E-03 ^D 3.09E-03±6.59E-04 ^B	2.38E-03±2.78E-04	-	4.56E-03±3.94E-04 ^A 4.68E-03±4.82E-04 ^A 4.87E-03±4.21E-04 ^D	4.66E-03 ^D
52	-	1.00E-03±1.17E-04	-	-	-
53	1.64E-03 ^D	4.97E-04±5.81E-05	-	-	-
54	-	1.79E-04±2.09E-05	-	-	-
56	-	5.30E-04±6.20E-05	-	-	-
57	3.16E-03±2.73E-04 ^A 3.30E-03±2.85E-04 ^A 3.37E-03±2.91E-04 ^A 3.25E-03 ^D	-	-	6.90E-03±5.97E-04 ^A 6.71E-03±5.80E-04 ^A 6.90E-03±5.97E-04 ^D	6.61E-03 ^D
59	-	1.26E-04±1.47E-05	-	-	-
60	1.64E-03 ^D	3.29E-04±3.84E-05	-	-	-
63	-	2.00E-04±2.34E-05	-	-	-
65	-	4.37E-04±5.11E-05	-	-	-
	4.13E-03 ^D				
67	1.88E-03±1.62E-04 ^A 1.94E-03±1.68E-04 ^A 2.02E-03±1.74E-05 ^A 1.96E-03 ^D	1.19E-03±1.39E-04	-	1.84E-03±1.90E-04 ^A 1.94E-03±1.68E-04 ^A 2.02E-03±1.75E-04 ^D	1.93E-03 ^D
69	-	3.77E-04±4.41E-05	-	-	-
70	1.56E+00 ^D	-	5.02E+00 ^D	-	-
71	1.56E+00 ^D	-	5.02E+00 ^D	-	-
72	4.23E-03±3.65E-04 ^A 4.44E-03±3.83E-04 ^A 4.59E-03±3.96E-04 ^A 4.45E-03 ^D 4.80E-03±1.03E-03 ^B	3.08E-03±3.60E-04	-	7.27E-03±6.28E-04 ^A 7.69E-03±6.65E-04 ^A 7.92E-03±6.85E-04 ^D	7.59E-03 ^D
74	-	2.05E-04±2.40E-05	-	-	-
75	7.33E-03±6.33E-04 ^A 7.73E-03±6.68E-04 ^A 8.13E-03±7.02E-04 ^A 7.87E-03 ^D 8.42E-04±1.80E-04 ^B 5.83E-03±8.02E-05 ^B	3.74E-03±4.37E-04	-	1.31E-02±1.12E-03 ^A 1.40E-02±1.21E-03 ^A 1.49E-02±1.29E-03 ^D	1.42E-02 ^D
76	4.35E-03±3.76E-04 ^A 4.55E-03±3.93E-04 ^A 4.83E-03±4.18E-04 ^A 4.70E-03 ^D 5.07E-03±1.08E-04 ^B	4.14E-03±4.83E-04	-	7.24E-03±6.25E-04 ^A 4.63E-03±6.60E-04 ^A 8.39E-03±7.25E-04 ^D	8.03E-03 ^D
78	1.64E-03 ^D	1.17E-03±1.17E-04	-	-	-
79	-	2.91E-05±4.94E-06	-	-	-
82	-	8.10E-05±9.47E-06	-	-	-
83	-	4.06E-05±5.59E-06	-	-	-
85	1.64E-03 ^D	3.17E-04±3.70E-05	-	-	-
88	-	1.15E-04±1.34E-05	-	-	-

Table 5. continued.

ID (ADF-S)	0.44 μm	0.47 μm^C	0.55 μm	0.64 μm	0.71 μm
89	1.64E-03 ^D	6.99E-04±2.51E-04	-	-	-
90	-	2.17E-04±2.54E-05	-	-	-
92	-	5.82E-05±8.00E-06	-	-	-
94	2.31E-03±2.00E-04 ^A 2.63E-03±2.27E-04 ^A 2.88E-03±1.49E-04 ^A 2.81E-03 ^D	-	-	4.08E-03±3.52E-04 ^A 4.50E-03±3.89E-04 ^A -	-
95	1.04E-02 ^D 2.10E-03±1.40E-04 ^B	2.15E-03±2.51E-04	3.64E-03±2.81E-04 ^B	-	-
96	-	7.67E-05±8.96E-06	-	-	-
97	1.59E-03±1.37E-04 ^A 1.68E-03±1.45E-04 ^A 1.72E-03±1.48E-04 ^A 1.66E-03 ^D	-	-	3.21E-03±2.77E-04 ^A 3.38E-03±2.92E-04 ^A 3.49E-03±3.02E-04 ^D	3.35E-03 ^D
98	-	8.64E-05±1.01E-05	-	-	-
99	-	4.75E-05±6.54E-06	-	-	-
100	4.91E-03±4.24E-04 ^A 5.48E-03±4.74E-04 ^A 5.95E-03±5.14E-04 ^A 5.75E-03 ^D 6.16E-03±1.31E-03 ^B	-	-	1.01E-02±8.69E-04 ^A 1.11E-02±9.66E-04 ^A 1.23E-02±1.06E-03 ^D	1.17E-02 ^D
102	-	7.53E-05±8.80E-06	-	-	-
103	7.09E-04±6.12E-05 ^A 6.85E-04 ^D	-	-	1.55E-03±1.34E-04 ^D	1.47E-03 ^D
104	-	1.04E-03±1.21E-04	-	-	-
105	1.04E-02 ^D	1.24E-03±2.51E-04	-	-	-
106	-	5.30E-04±6.20E-05	-	-	-
107	4.13E-03 ^D	4.66E-04±5.45E-05	-	-	-
110	6.55E-03 ^D	4.93E-04±5.76E-05	1.25E-03 ^D	-	-
111	-	5.16E-04±6.03E-05	-	-	-
112	-	2.94E-05±4.99E-06	-	-	-
113	-	3.64E-04±4.25E-05	-	-	-
114	-	2.86E-04±3.34E-05	-	-	-
115	-	1.69E-04±1.98E-05	-	-	-
120	4.13E-03 ^D	4.79E-04±5.60E-05	-	-	-
121	-	4.75E-05±6.54E-06	-	-	-
123	-	8.56E-04±1.00E-04	-	-	-
124	-	2.97E-05±5.03E-06	-	-	-
126	-	2.68E-04±3.14E-05	-	-	-
127	-	5.82E-05±8.00E-06	-	-	-
130	-	4.58E-05±6.30E-06	-	-	-
132	-	6.38E-05±7.45E-06	-	-	-
133	-	9.30E-05±1.09E-05	-	-	-
134	4.13E-03 ^D	5.11E-03±5.97E-05	-	-	-
135	2.35E-03±2.03E-04 ^A 2.52E-03±2.18E-04 ^A 2.78E-03±5.95E-04 ^A 2.56E-03 ^D	2.38E-03±2.78E-04	-	2.85E-03±2.47E-04 ^A 3.10E-03±2.67E-04 ^A 3.23E-03±2.87E-04 ^D	3.17E-03 ^D
136	4.13E-03 ^D	5.11E-03±5.97E-05	-	-	-
138	-	4.02E-04±4.70E-05	-	-	-
139	-	2.42E-04±2.83E-05	-	-	-
140	2.01E+00 ^D	-	2.24E+00 ^D	-	-
142	-	7.74E-05±9.04E-06	-	-	-
148	-	1.23E-04±1.43E-05	-	-	-
149	1.64E-03 ^D	3.64E-04±4.25E-05	-	-	-
151	-	1.01E-04±1.01E-04	-	-	-
152	-	8.10E-05±9.47E-06	-	-	-
155	-	7.53E-04±8.80E-05	-	-	-
156	-	7.53E-04±8.80E-05	-	-	-

Table 5. continued.

ID (ADF-S)	0.44 μm	0.47 μm^C	0.55 μm	0.64 μm	0.71 μm
160	-	8.18E-05±9.56E-06	-	-	-
162	-	1.34E-04±1.57E-05	-	-	-
165	1.64E-03 ^D	-	-	-	-
166	1.14E-01 ^D	1.10E-03±1.28E-04	-	-	-
168	-	1.72E-04±2.02E-05	-	-	-
169	7.65E-04±6.61E-05 ^A 8.03E-04±6.94E-05 ^A 8.16E-04±7.08E-05 ^A 7.94E-04 ^D	8.56E-04±1.00E-04	-	1.18E-03±1.02E-04 ^A 1.25E-03±1.08E-04 ^A 1.27E-03±1.10E-04 ^D	1.21E-03 ^D
170	-	2.63E-05±4.46E-06	-	-	-
171	-	9.48E-05±1.11E-05	-	-	-
172	-	3.47E-05±5.89E-06	-	-	-
179	-	1.86E-04±2.17E-05	-	-	-
183	-	3.32E-04±3.88E-05	-	-	-
185	-	3.41E-05±5.78E-06	-	-	-
194	-	1.34E-03±1.57E-04	-	-	-
195	-	7.95E-05±9.30E-06	-	-	-
198	-	7.60E-05±8.88E-06	-	-	-
199	-	3.77E-05±6.39E-06	-	-	-
203	-	6.32E-05±7.38E-06	-	-	-
204	-	3.44E-05±5.83E-06	-	-	-
205	-	4.33E-04±5.06E-05	-	-	-
206	-	4.54E-05±6.24E-06	-	-	-
211	-	1.12E-04±1.31E-05	-	-	-
212	-	1.59E-04±1.85E-05	-	-	-
213	-	2.17E-04±2.54E-05	-	-	-
214	-	1.37E-04±1.60E-05	-	-	-
215	-	4.29E-04±5.02E-05	-	-	-
216	-	1.14E-04±1.33E-05	-	-	-
222	-	2.84E-05±4.81E-06	-	-	-
224	-	3.95E-05±5.44E-06	-	-	-
228	-	8.18E-05±9.56E-06	-	-	-
232	-	1.11E-04±1.30E-05	-	-	-
233	-	2.21E-04±2.58E-05	-	-	-
234	-	5.92E-05±8.15E-06	-	-	-
244	1.64E-03 ^D	3.38E-04±3.95E-05	-	-	-
252	-	3.47E-04±4.06E-05	-	-	-
253	1.64E-03 ^D	1.17E-03±1.37E-04	-	-	-
254	-	2.71E-05±4.59E-06	-	-	-
255	-	1.28E-04±1.50E-05	-	-	-
256	-	2.89E-05±4.90E-06	-	-	-
257	-	9.22E-05±1.08E-05	-	-	-
258	-	4.66E-05±6.42E-06	-	-	-
259	-	9.30E-05±1.09E-05	-	-	-
260	-	1.47E-04±1.72E-05	-	-	-
261	1.64E-03 ^D	1.91E-04±2.20E-05	-	-	-
265	-	2.86E-04±3.34E-05	-	-	-
267	1.64E-03 ^D	5.98E-04±6.99E-05	-	-	-
271	-	3.60E-07±4.62E-05	-	-	-
277	-	3.05E-05±5.17E-06	-	-	-
279	-	2.84E-05±4.81E-06	-	-	-
280	-	1.47E-04±1.72E-05	-	-	-
281	-	4.37E-04±5.11E-05	-	-	-
287	-	2.07E-04±2.42E-05	-	-	-
290	-	1.08E-04±1.26E-05	-	-	-
294	-	5.21E-05±7.17E-06	-	-	-
299	1.49E-03±1.28E-04 ^A 1.56E-03±1.35E-04 ^A 1.58E-03±1.36E-04 ^A	-	4.18E-03±7.74E-04 ^B	2.48E-03±2.14E-04 ^A 2.60E-03±2.24E-04 ^A 2.65E-03±2.29E-04 ^D	2.51E-03 ^D

Table 5. continued.

ID (ADF-S)	0.44 μm	0.47 μm^C	0.55 μm	0.64 μm	0.71 μm
	1.53E-03 ^D				
	1.68E-03±3.59E-04 ^B				
	2.95E-03±5.31E-04 ^B				
301	-	1.02E-03±1.19E-04	-	-	-
302	-	1.33E-04±1.56E-05	-	-	-
306	1.64E-03 ^D	2.24E-04±2.78E-05	-	-	-
307	-	3.84E-05±6.51E-06	-	-	-
310	-	2.97E-05±5.03E-06	-	-	-
311	-	3.17E-04±3.70E-05	-	-	-
312	-	5.82E-05±8.00E-06	-	-	-
314	-	9.39E-04±1.10E-04	-	-	-
317	-	9.30E-05±1.09E-05	-	-	-
318	-	3.23E-05±5.47E-06	-	-	-
324	-	2.34E-04±2.73E-05	-	-	-
328	-	2.15E-04±2.51E-05	-	-	-
329	-	3.91E-04±4.57E-05	-	-	-
334	-	8.33E-05±9.73E-06	-	-	-
341	-	6.62E-05±7.73E-06	-	-	-
342	-	1.31E-03±1.53E-04	-	-	-
343	-	4.02E-04±4.70E-05	-	-	-
344	-	1.33E-04±1.56E-05	-	-	-
345	-	1.31E-03±1.53E-04	-	-	-
348	-	1.15E-04±1.34E-05	-	-	-
351	-	2.11E-04±2.47E-05	-	-	-
352	-	1.15E-04±7.71E-06	-	-	-
354	-	3.99E-04±4.66E-05	-	-	-
355	-	4.10E-04±4.79E-05	-	-	-
357	-	3.32E-05±5.62E-06	-	-	-
358	-	6.44E-05±7.52E-06	-	-	-
364	-	1.86E-04±2.17E-05	-	-	-
365	-	1.23E-04±1.43E-05	-	-	-
366	-	6.20E-05±8.54E-06	-	-	-
369	-	6.93E-05±8.10E-06	-	-	-
370	1.89E-03±1.63E-04 ^A	2.05E-03±2.40E-04	-	2.20E-03±1.90E-04 ^A	2.49E-03 ^D
	2.01E-03±1.74E-04 ^A			2.41E-03±2.27E-04 ^A	
	2.08E-03±1.80E-04 ^A			2.62E-03±2.27E-04 ^D	
	2.01E-03 ^D				
373	-	6.20E-05±8.54E-06	-	-	-
377	-	1.09E-04±1.27E-05	-	-	-
384	-	1.71E-04±2.00E-05	-	-	-
386	-	1.11E-04±1.30E-05	-	-	-
391	-	2.13E-04±2.49E-05	-	-	-
394	1.64E-03 ^D	8.10E-04±4.45E-05	-	-	-
396	-	4.37E-05±6.02E-06	-	-	-
397	-	3.35E-04±3.91E-05	-	-	-
398	-	1.16E-04±1.36E-05	-	-	-
399	-	3.47E-05±5.89E-06	-	-	-
400	9.24E-04±7.98E-05 ^A	-	-	1.17E-03±1.09E-04 ^A	1.24E-03 ^D
	1.01E-03±8.76E-05 ^A			1.26E-03±1.09E-04 ^A	
	1.06E-03±9.15E-05 ^A			1.30E-03±1.12E-04 ^D	
	1.03E-03 ^D				
410	-	1.14E-04±1.33E-05	-	-	-
415	-	8.41E-04±9.82E-05	-	-	-
416	-	1.34E-04±1.57E-05	-	-	-
419	-	3.95E-05±5.44E-06	-	-	-
422	-	2.54E-05±4.30E-06	-	-	-
423	-	4.37E-05±6.02E-06	-	-	-
424	-	1.87E-03±2.19E-04	-	-	-
426	-	1.09E-04±1.27E-05	-	-	-

Table 5. continued.

ID (ADF-S)	0.44 μm	0.47 μm^C	0.55 μm	0.64 μm	0.71 μm
430	-	8.64E-05±1.01E-05	-	-	-
434	-	2.97E-05±5.03E-06	-	-	-
436	-	5.35E-05±7.37E-06	-	-	-
437	1.64E-03 ^D	3.77E-04±4.41E-05	-	-	-
439	-	2.89E-05±4.90E-06	-	-	-
443	-	1.18E-04±1.38E-05	-	-	-
445	-	1.19E-04±1.39E-05	-	-	-
447	-	1.43E-04±1.68E-05	-	-	-
448	-	6.99E-05±8.17E-06	-	-	-
452	-	1.27E-04±1.49E-05	-	-	-
458	-	4.79E-05±6.60E-06	-	-	-
460	-	3.50E-05±5.94E-06	-	-	-
462	-	3.08E-05±5.22E-06	-	-	-
463	-	2.91E-04±3.41E-05	-	-	-
464	-	1.93E-04±2.25E-05	-	-	-
465	-	5.11E-05±7.04E-06	-	-	-
466	-	1.69E-04±1.98E-05	-	-	-
467	-	3.99E-05±5.49E-06	-	-	-
468	-	6.93E-05±8.10E-06	-	-	-
472	-	8.56E-05±1.00E-05	-	-	-
473	-	3.08E-04±3.60E-05	-	-	-
474	-	-	1.37E-03 ^D	-	-
477	-	5.98E-05±8.23E-06	-	-	-
482	-	4.97E-05±6.84E-06	-	-	-
486	-	2.61E-05±4.42E-06	-	-	-
488	-	3.91E-05±6.63E-06	-	-	-
489	-	3.00E-05±5.08E-06	-	-	-
490	4.13E-03 ^D	3.32E-04±3.88E-05	-	-	-
492	-	9.05E-05±1.06E-05	-	-	-
494	-	1.24E-04±1.45E-05	-	-	-
496	-	8.48E-05±9.91E-06	-	-	-
497	-	3.08E-04±3.60E-05	-	-	-
499	-	1.11E-04±1.30E-05	-	-	-

A - Lauberts & Valentijn (1989)

B - de Vaucouleurs et al. (1991)

C - Maddox et al. (1990)

D - The SIMBAD astronomical database, Wenger et al. (2000)

E - Gil de Paz et al. (2003)

F - Sandage (1975)

Table 6. Flux densities in other wavelengths found for the counterparts of the ADFS sources in the public databases, for the 10σ catalog - part 2.

ID (ADF-S)	0.79 μm	1.25 μm	1.65 μm	2.22 μm	12 μm^I
1	2.38E-02±1.19E-03 ^G	4.31E-02±1.13E-04 ^H 4.31E-02±1.13E-04 ^D	5.66E-02±1.85E-04 ^H 5.66E-02±1.85E-04 ^D	5.37E-02±2.31E-04 ^H 5.37E-02±2.31E-04 ^D	1.25E-01±1.38E-02
2	-	8.17E-03±3.21E-05 ^H 8.17E-03±3.89E-05 ^D	1.04E-02±6.71E-05 ^H 1.04E-02±6.71E-05 ^D	7.71E-03±6.75E-05 ^H 7.71E-03±6.75E-05 ^D	6.45E-02±1.81E-01
3	-	1.02E+00±2.17E-03 ^D	1.26E+00±3.27E-03 ^D	9.85E-01±3.06E-03 ^D	-
4	2.02E+15±1.24E-02 ^J	5.24E-02±1.54E-04 ^H 5.24E-02±1.54E-02 ^D	3.30E-02±5.34E-02 ^H 5.34E-02±2.23E-04 ^D	4.50E-02±4.11E-02 ^H 4.11E-04±2.38E-04 ^D	2.38E-04±2.50E-01
5	-	1.62E-02±6.35E-05 ^H 1.62E-02±6.35E-05 ^D	1.73E-02±1.05E-04 ^H 1.75E-02±1.07E-04 ^D	1.83E-02±1.10E-04 ^H 1.83E-02±1.10E-04 ^D	< 5.48E-02
6	-	3.42E-03±3.11E-05 ^H 3.42E-03 ^D	3.07E-03±5.11E-05 ^H 3.07E-03 ^D	4.61E-03±5.18E-05 ^H 4.61E-03 ^D	<5.02E-02
7	-	4.07E-03±2.21E-05 ^H 4.07E-03±2.21E-05 ^D	5.22E-03±3.93E-05 ^H 5.22E-03±3.93E-05 ^D	4.19E-03±4.09E-05 ^H 4.19E-03±4.09E-05 ^D	<8.02E-02
8	-	8.75E-03±4.19E-05 ^H 8.75E-03±4.19E-05 ^D	1.30E-02±7.52E-05 ^H 1.30E-02±7.52E-05 ^D	1.22E-02±7.75E-05 ^H 1.22E-02±7.75E-05 ^D	-
9	-	1.53E-02±6.23E-05 ^H 1.53E-02±6.23E-05 ^D	1.69E-02±9.87E-05 ^H 1.69E-02±9.87E-05 ^D	1.20E-02±1.01E-04 ^H 1.20E-02±1.01E-04 ^D	-
10	-	4.50E-02±1.38E-04 ^H 4.50E-02±1.38E-04 ^D	5.69E-02±1.76E-04 ^H 5.69E-02±1.76E-04 ^D	4.62E-02±2.22E-04 ^H 4.62E-02±2.22E-04 ^D	6.69E-02±1.74E-02
11	1.49E-02±7.44E-04 ^G	2.66E-02±9.14E-05 ^H 2.66E-02±9.14E-05 ^D	3.45E-02±1.54E-04 ^H 3.78E-02±1.70E-04 ^D	2.97E-02±1.61E-04 ^H 2.97E-02±1.61E-04 ^D	-
12	-	2.86E-03±2.11E-05 ^H	3.57E-03±3.91E-05 ^H	3.71E-03±4.01E-05 ^H	< 6.17E-02
13	-	-	-	-	< 6.96E-02
14	-	-	-	-	< 4.05E-02±2.50E-01
15	-	2.83E-03±2.21E-05 ^H	4.20E-03±3.48E-05 ^H	3.61E-03±3.97E-05 ^H	< 6.17E-02
16	-	-	-	-	< 7.03E-02
17	-	5.24E-03±3.90E-05 ^H 5.24E-03±3.90E-05 ^D	4.49E-03±5.88E-05 ^H 4.49E-03±5.88E-05 ^D	4.20E-03±6.43E-05 ^H 4.20E-03±6.43E-05 ^D	-
18	-	1.45E-02±6.79E-05 ^H 1.45E-02±6.79E-05 ^D	2.04E-02±1.12E-04 ^H 2.04E-02±1.12E-04 ^D	1.31E-02±1.00E-04 ^H 1.55E-02±1.16E-04 ^D	-
19	-	4.59E-03±2.88E-05 ^H	6.41E-03±4.66E-05 ^H	5.38E-03±5.02E-05 ^H	-
20	-	1.93E-03±2.01E-05 ^H	3.27E-03±3.06E-05 ^H	2.46E-03±2.13E-05 ^H	-
21	-	1.88E-02±5.34E-05 ^H 1.88E-02±5.34E-05 ^D	2.45E-02±8.66E-05 ^H 2.45E-02±8.66E-05 ^D	1.80E-02±9.28E-05 ^H 1.80E-02±9.28E-05 ^D	-
22	-	8.47E-03±4.63E-05 ^H 8.47E-03±4.63E-05 ^D	1.17E-02±8.48E-05 ^H 1.17E-02±8.48E-05 ^D	1.04E-02±8.64E-05 ^H 1.04E-02±8.64E-05 ^D	-
23	-	3.40E-03±2.54E-05 ^D	4.54E-03±4.02E-05 ^D	3.70E-03±4.57E-05 ^D	-
24	-	4.45E-03±2.82E-05 ^H	4.95E-03±4.46E-05 ^H	5.15E-03±4.79E-05 ^H	-
25	-	2.93E-03±2.10E-05 ^H	3.01E-03±3.19E-05 ^H	3.28E-03±3.73E-05 ^H	-
27	-	-	-	-	< 5.40E-02
29	-	1.93E-02±6.44E-05 ^H 1.93E-02±6.44E-05 ^D	2.35E-02±1.05E-04 ^H 2.35E-02±1.05E-04 ^D	1.96E-02±1.12E-04 ^H 1.96E-02±1.12E-04 ^D	-
30	-	4.00E-03±2.68E-05 ^H	5.76E-03±4.11E-05 ^H	5.85E-03±4.72E-05 ^H	< 5.05E-02
31	-	2.11E-03±1.68E-05 ^H	3.46E-03±2.39E-05 ^H	2.81E-03±3.15E-05 ^H	-
32	-	8.25E-03±4.56E-05 ^H 8.25E-03±4.56E-05 ^D	1.13E-02±7.23E-05 ^H 1.13E-02±7.23E-05 ^D	7.66E-03±7.81E-05 ^H 7.66E-03±7.81E-05 ^D	-
34	-	6.58E-03±3.57E-05 ^H	1.03E-02±6.41E-05 ^H	1.17E-02±7.07E-05 ^H	-
35	-	3.44E+00±1.08E-02 ^D	2.30E+00±1.31E-02 ^D	1.63E+00±4.48E-03 ^D	-
36	-	4.37E-03±3.48E-05 ^H 4.37E-03±3.48E-05 ^D	4.90E-03±5.66E-05 ^H 4.90E-03±5.66E-05 ^D	4.43E-03±5.89E-05 ^H 4.43E-03±5.89E-05 ^D	-
39	-	1.42E-02±4.71E-05 ^H 1.42E-02±4.71E-05 ^D	2.48E-03±2.61E-05 ^H 1.64E-02±7.09E-05 ^D	2.01E-03±3.37E-05 ^H 1.11E-02±8.96E-05 ^D	-
40	-	3.21E-03±2.21E-05 ^H	3.70E-03±3.38E-05 ^H	4.26E-03±4.01E-05 ^H	-
41	-	1.79E-03±1.18E-05 ^H	2.52E-03±2.02E-05 ^H	2.45E-03±1.98E-05 ^H	-
42	-	5.24E-03±3.29E-05 ^H 5.24E-03±3.29E-05 ^D	7.44E-03±5.37E-05 ^H 7.44E-03±5.37E-05 ^D	4.66E-03±5.64E-05 ^H 4.66E-03±5.64E-05 ^D	-
43	-	1.12E-02±4.15E-05 ^H	1.50E-02±6.80E-05 ^H	1.50E-02±7.35E-05 ^H	-

Table 6. continued.

ID (ADF-S)	0.79 μm	1.25 μm	1.65 μm	2.22 μm	12 μm^I
44	-	5.30E-03±2.98E-05 ^H	6.28E-03±4.71E-05 ^H	5.90E-03±5.28E-05 ^H	-
45	-	1.34E-02±5.08E-05 ^H	1.75E-02±7.89E-05 ^H	1.40E-02±9.80E-05 ^H	-
		1.34E-02±5.08E-05 ^D	1.75E-02±7.89E-05 ^D	1.40E-02±9.80E-05 ^D	
46	-	1.27E-03±1.96E-05 ^H	2.32E-03±3.28E-05 ^H	2.78E-03±3.52E-05 ^H	< 4.07E-02
48	-	2.68E-03±2.19E-05 ^H	4.33E-03±3.53E-05 ^H	3.12E-03±3.80E-05 ^H	-
50	-	3.59E-03±3.00E-05 ^H	4.45E-03±4.66E-05 ^H	2.59E-03±3.62E-05 ^H	-
		3.59E-03±3.00E-05 ^D	4.45E-03±4.66E-05 ^D	4.77E-03±5.23E-05 ^D	
51	-	1.43E-02±6.00E-05 ^H	1.63E-02±9.72E-05 ^H	8.47E-03±2.91E-05 ^H	-
		1.43E-02±6.00E-05 ^D	1.63E-02±9.72E-05 ^D	1.01E-02±9.69E-05 ^D	
52	-	8.88E-03±3.79E-05 ^H	1.47E-02±6.29E-05 ^H	1.15E-02±6.78E-05 ^H	< 9.68E-02
		8.88E-03 ^D	1.47E-02 ^D	1.15E-02 ^D	
53	-	4.68E-03±2.50E-05 ^H	7.93E-03±4.64E-05 ^H	4.85E-03±4.57E-06 ^H	-
		4.68E-03±2.50E-05 ^D	7.88E-03±4.60E-05 ^D	4.85E-03±4.57E-05 ^D	
54	-	2.17E-03±2.07E-05 ^H	2.65E-03±3.26E-05 ^H	2.07E-03±3.42E-05 ^H	-
55	-	1.22E-03±8.62E-06 ^H	2.28E-03±2.75E-05 ^H	2.03E-03±3.14E-05 ^H	-
56	-	4.08E-03±2.92E-05 ^H	5.99E-03±4.70E-05 ^H	4.78E-03±5.02E-05 ^H	-
57	-	1.93E-02±5.01E-05 ^H	2.25E-02±7.71E-05 ^H	1.78E-02±8.56E-05 ^H	-
		1.93E-02±5.01E-05 ^D	2.25E-02±7.71E-05 ^D	1.78E-02±8.56E-05 ^D	
58	-	2.23E-03±2.02E-05 ^H	2.78E-03±3.46E-05 ^H	2.64E-03±3.69E-05 ^H	-
60	-	2.52E-03±2.15E-05 ^H	3.11E-03±3.44E-05 ^H	3.18E-03±3.87E-05 ^H	-
61	-	2.51E-03±2.56E-05 ^H	2.15E-03±4.27E-05 ^H	3.89E-03±5.15E-05 ^H	-
63	-	1.71E-03±1.96E-05 ^H	1.93E-03±1.76E-05 ^H	2.45E-03±3.39E-05 ^H	-
64	-	5.93E-03±3.58E-05 ^H	8.05E-03±5.97E-05 ^H	8.30E-03±6.36E-05 ^H	-
		5.93E-03±3.58E-05 ^D	8.05E-03±5.97E-05 ^D	8.30E-03±6.36E-05 ^D	
65	-	3.94E-03±2.50E-05 ^H	5.46E-03±4.13E-05 ^H	5.19E-03±4.10E-05 ^H	-
		3.94E-03±2.50E-05 ^D	5.46E-03±4.13E-05 ^D	5.19E-03±4.10E-05 ^D	
66	-	2.87E-03±2.45E-05 ^H	3.54E-03±3.88E-05 ^H	3.40E-03±4.35E-05 ^H	-
68	-	3.04E-03±1.70E-05 ^H	3.80E-03±2.79E-05 ^H	2.54E-03±3.24E-05 ^H	-
69	-	1.63E-03±1.55E-05 ^H	3.62E-03±3.26E-05 ^H	2.90E-03±3.87E-05 ^H	-
70	-	1.66E+01±8.57E-01 ^D	1.81E+01±3.10E-01 ^D	1.51E+01±8.55E-01 ^D	9.40E-01±3.76E-02
71	-	1.66E+01±8.57E-01 ^D	1.81E+01±3.10E-01 ^D	1.51E+01±8.55E-01 ^D	9.40E-01±3.76E-02
72	-	1.58E-02±5.67E-05 ^H	2.69E-02±1.00E-04 ^H	1.74E-02±9.75E-05 ^H	-
		1.58E-02±5.67E-05 ^D	2.69E-02±1.00E-04 ^D	1.74E-02±9.81E-05 ^D	
73	-	-	-	-	< 5.86E-02
75	-	2.92E-02±7.38E-05 ^H	3.22E-02±1.05E-04 ^H	2.11E-02±1.33E-04 ^H	-
		2.92E-02±7.38E-05 ^D	3.22E-02±1.05E-04 ^D	2.11E-02±1.33E-04 ^D	
76	-	2.29E-02±1.08E-04 ^H	2.49E-02±1.93E-04 ^H	1.98E-02±1.95E-04 ^H	-
		2.29E-02±1.08E-04 ^D	2.49E-02±1.93E-04 ^D	1.98E-02±1.95E-04 ^D	
85	-	2.11E-03±2.15E-05 ^H	3.21E-03±3.75E-05 ^H	2.30E-03±3.74E-05 ^H	-
		2.11E-03±2.15E-05 ^D	3.21E-03±3.75E-05 ^D	2.30E-03±3.74E-05 ^D	
86	-	9.46E-03±5.71E-05 ^H	1.46E-02±9.47E-05 ^H	1.19E-02±1.02E-04 ^H	-
89	2.50E-03±1.03E-04 ^G	3.73E-03±2.25E-05 ^H	4.51E-03±4.63E-05 ^H	2.92E-03±2.47E-05 ^H	-
		3.73E-03 ^D	4.51E-03 ^D	3.68E-03 ^D	
93	-	1.25E-03±1.74E-05 ^H	1.24E-03 ^H	1.95E-03±3.40E-05 ^H	-
94	-	7.65E-03±5.00E-05 ^H	8.80E-03±7.75E-05 ^H	9.64E-03±8.92E-05 ^H	-
		7.65E-03±5.00E-05 ^D	8.80E-03±7.75E-05 ^D	9.64E-03±8.92E-05 ^D	
95	8.33E-03±4.16E-04 ^G	1.64E-02±7.12E-05 ^H	2.18E-02±1.13E-04 ^H	1.64E-02±1.23E-04 ^H	-
		1.64E-02±7.12E-05 ^D	2.18E-02±1.13E-04 ^D	1.64E-02±1.23E-04 ^D	
97	-	1.03E-02±6.12E-05 ^H	1.50E-02±9.75E-05 ^H	1.09E-02±1.05E-04 ^H	-
		1.03E-02±6.12E-05 ^D	1.50E-02±9.75E-05 ^D	1.09E-02±1.05E-04 ^D	
101	-	2.81E-03±2.80E-05 ^H	5.27E-03±4.24E-05 ^H	4.12E-03±4.69E-05 ^H	-
103	-	3.73E-03±2.25E-05 ^H	4.51E-03±4.63E-05 ^H	3.68E-03±4.43E-05 ^H	-
		3.11E-03±2.66E-05 ^D	6.72E-03±4.55E-05 ^D	3.42E-03±4.57E-05 ^D	
104	-	2.49E-03±2.12E-05 ^H	3.07E-03±3.37E-05 ^H	1.68E-03±2.01E-05 ^H	-
105	-	2.12E-02±6.08E-05 ^H	2.86E-02±1.00E-04 ^H	2.24E-02±1.08E-04 ^H	-
		2.12E-02±6.08E-05 ^D	2.86E-02±1.00E-04 ^D	2.24E-02±1.08E-04 ^D	
106	-	2.47E-03±2.32E-05 ^H	2.32E-03±3.46E-05 ^H	2.21E-03±3.96E-05 ^H	-

Table 6. continued.

ID (ADF-S)	0.79 μm	1.25 μm	1.65 μm	2.22 μm	12 μm^I
107	-	2.47E-03±2.32E-05 ^D 3.71E-03±1.63E-05 ^H 3.86E-03±3.02E-05 ^D	2.32E-03±3.46E-05 ^D 5.77E-03±5.48E-05 ^H 5.77E-03±5.48E-05 ^D	2.23E-03±3.99E-05 ^D 4.82E-03±5.63E-05 ^H 4.82E-03±5.63E-05 ^D	-
108	-	5.42E-03±3.21E-05 ^H	5.44E-03±4.85E-05 ^H	4.93E-03±5.45E-05 ^H	-
109	-	2.92E-03±2.67E-05 ^H	3.60E-03±4.23E-05 ^H	3.61E-03±4.60E-05 ^H	-
110	-	4.39E-03±4.51E-05 ^H 4.39E-03±4.51E-05 ^D	5.89E-03±7.93E-05 ^H 5.89E-03±7.93E-05 ^D	8.15E-03±7.96E-05 ^H 8.15E-03±7.96E-05 ^D	-
111	-	2.69E-03±2.33E-05 ^H	4.36E-03±4.40E-05 ^H	3.33E-03±4.43E-05 ^H	-
113	-	4.23E-03±2.64E-05 ^H	4.74E-03±4.43E-05 ^H	4.15E-03±4.46E-05 ^H	-
114	-	1.76E-03±1.85E-05 ^H	3.28E-03±2.66E-05 ^H	2.26E-03±3.48E-05 ^H	-
117	-	2.93E-03±2.43E-05 ^H	3.73E-03±4.02E-05 ^H	3.61E-03±4.90E-05 ^H	-
118	-	1.19E-02±5.47E-05 ^H	1.32E-02±8.49E-05 ^H	1.34E-02±9.58E-05 ^H	-
119	-	1.65E-03±1.91E-05 ^H	1.77E-03±2.96E-05 ^H	1.62E-03±1.75E-05 ^H	-
120	-	3.81E-03±2.38E-05 ^H 3.81E-03 ^D	5.62E-03±3.87E-05 ^H 5.62E-03 ^D	4.19E-03±3.70E-05 ^H 4.19E-03 ^D	-
122	-	1.82E-02±5.15E-05 ^H	2.37E-02±8.34E-05 ^H	1.80E-02±8.98E-05 ^H	-
123	-	3.86E-03±2.28E-05 ^H	4.34E-03±3.64E-05 ^H	3.47E-03±4.02E-05 ^H	-
126	-	2.24E-03±2.24E-03 ^H	3.96E-03±3.73E-05 ^H	2.80E-03±4.18E-05 ^H	-
134	-	4.20E-03±3.04E-05 ^H 4.20E-03±3.04E-05 ^D	5.63E-03±4.86E-05 ^H 5.63E-03±4.86E-05 ^D	5.17E-03±5.38E-05 ^H 5.17E-03±5.38E-05 ^D	-
136	-	4.20E-03±3.04E-05 ^H 4.20E-03±3.04E-05 ^D	5.63E-03±4.86E-05 ^H 5.63E-03±4.86E-05 ^D	5.17E-03±5.38E-05 ^H 5.17E-03±5.38E-05 ^D	-
140	-	1.42E+00 ^D	1.02E+00 ^D	6.73E-01 ^D	-
143	-	5.99E-03±3.35E-05 ^H	8.40E-03±5.46E-05 ^H	6.87E-03±5.95E-05 ^H	-
146	-	2.76E-03±1.92E-05 ^H	3.05E-03±3.44E-05 ^H	3.24E-03±3.73E-05 ^H	-
147	-	2.20E-03±1.99E-05 ^H	2.76E-03±3.31E-05 ^H	2.36E-03±3.54E-05 ^H	-
148	-	1.12E-03±1.42E-05 ^H	9.85E-04 ^H	1.65E-03±3.31E-05 ^H	-
149	-	4.05E-03±2.66E-05 ^H 4.05E-03±2.66E-05 ^D	5.90E-03±4.35E-05 ^H 5.90E-03±4.35E-05 ^D	5.06E-03±4.43E-05 ^H 5.06E-03±4.43E-05 ^D	-
154	-	1.78E-03±2.13E-05 ^H	2.02E-03±1.75E-05 ^H	2.32E-03±3.57E-05 ^H	-
155	-	1.05E-02±4.21E-05 ^H	1.29E-02±6.80E-05 ^H	1.12E-02±7.06E-05 ^H	-
156	-	4.16E-03 ^H	4.20E-03±4.32E-05 ^H	4.68E-03±5.77E-05 ^H	-
158	-	1.92E-03±2.03E-05 ^H	2.68E-03±3.02E-05 ^H	2.40E-03±3.54E-05 ^H	-
159	-	5.99E-03±3.35E-05 ^H	8.40E-03±5.46E-05 ^H	6.87E-03±5.95E-05 ^H	-
165	-	2.25E-03±2.18E-05 ^H 2.25E-03±2.18E-05 ^D	2.32E-03±3.36E-05 ^H 2.32E-03±3.36E-05 ^D	2.61E-03±4.28E-05 ^H 2.61E-03±4.28E-05 ^D	-
166	-	3.75E-03±2.21E-05 ^H 3.75E-03±2.21E-05 ^D	4.94E-03±3.96E-05 ^H 4.94E-03±3.96E-05 ^D	2.70E-03±4.07E-05 ^H 2.70E-03±4.07E-05 ^D	-
173	-	1.36E-03±1.89E-05 ^H	1.99E-03±2.91E-05 ^H	1.94E-03±3.35E-05 ^H	-
175	-	1.72E-03±1.28E-05 ^H	2.99E-03±3.83E-05 ^H	3.25E-03±4.24E-05 ^H	-
176	-	5.90E-03±3.60E-05 ^H 5.90E-03±3.60E-05 ^D	6.70E-03±5.25E-05 ^H 6.70E-03±5.25E-05 ^D	7.41E-03±5.92E-05 ^H 7.41E-03±5.92E-05 ^D	-
177	-	4.78E-03±2.87E-05 ^H	5.96E-03±4.49E-05 ^H	5.00E-03±5.07E-05 ^H	-
179	-	1.49E-03±1.97E-05 ^H	2.12E-03±3.13E-05 ^H	1.89E-03±3.39E-05 ^H	-
181	-	2.44E-03±1.89E-05 ^H	3.96E-03±2.94E-05 ^H	2.48E-03±3.34E-05 ^H	-
183	-	3.31E-03±2.49E-05 ^H	4.08E-03±3.86E-05 ^H	3.88E-03±4.21E-05 ^H	-
184	-	1.51E-03±2.06E-05 ^H	1.98E-03±3.40E-05 ^H	2.31E-03±3.76E-05 ^H	-
190	-	4.78E-03±2.87E-05 ^H	5.96E-03±4.49E-05 ^H	5.00E-03±5.07E-05 ^H	-
191	-	2.25E-03±2.00E-05 ^H	2.25E-03±3.32E-05 ^H	2.67E-03±3.51E-05 ^H	-
192	-	1.80E-03±1.73E-05 ^H	2.37E-03±2.73E-05 ^H	2.07E-03±2.89E-05 ^H	-
194	-	8.48E-03±4.31E-05 ^H 8.48E-03±6.24E-05 ^D	1.28E-02±7.88E-05 ^H 1.28E-02±7.88E-05 ^D	7.02E-03±7.72E-05 ^H 7.02E-03±7.72E-05 ^D	-
200	-	2.24E-03±2.71E-05 ^H 2.24E-03±2.71E-05 ^D	3.78E-03±4.24E-05 ^H 3.78E-03±4.24E-05 ^D	3.34E-03±4.69E-05 ^H 3.34E-03±4.69E-05 ^D	-
201	-	4.29E-03±2.00E-05 ^H	4.60E-03±3.25E-05 ^H	4.32E-03±3.60E-05 ^H	-
205	-	1.89E-03±1.98E-05 ^H	3.05E-03±3.10E-05 ^H	2.35E-03±3.38E-05 ^H	-
210	-	3.48E-03±2.02E-05 ^H	4.77E-03±3.14E-05 ^H	3.33E-03±3.51E-05 ^H	-

Table 6. continued.

ID (ADF-S)	0.79 μm	1.25 μm	1.65 μm	2.22 μm	12 μm^I
		3.48E-03±2.02E-05 ^D	4.77E-03±3.14E-05 ^D	3.33E-03±3.51E-05 ^D	
213	-	1.42E-03±2.04E-05 ^H	2.99E-03±3.43E-05 ^H	1.99E-03±3.57E-05 ^H	-
215	-	2.18E-03±2.26E-05 ^H	2.03E-03±3.36E-05 ^H	2.44E-03±3.83E-05 ^H	-
219	-	1.13E-03±1.62E-05 ^H	1.86E-03±2.70E-05 ^H	1.53E-03±3.20E-05 ^H	-
223	-	1.64E-03±2.05E-05 ^H	2.02E-03±3.56E-05 ^H	2.36E-03±3.88E-05 ^H	-
225	-	1.63E-03±1.88E-05 ^H	2.21E-03±3.06E-05 ^H	1.84E-03±3.28E-05 ^H	-
228	-	8.97E-04±1.43E-05 ^H	1.41E-03±2.27E-05 ^H	2.69E-03±3.87E-05 ^H	-
239	-	2.48E-03±1.71E-05 ^H	2.68E-03±2.79E-05 ^H	2.09E-03±3.22E-05 ^H	-
247	-	3.44E-03±2.31E-05 ^H	4.33E-03±3.53E-05 ^H	3.50E-03±3.96E-05 ^H	-
252	-	3.39E-03±2.32E-05 ^H	3.77E-03±4.01E-05 ^H	4.20E-03±4.55E-05 ^H	-
253	3.26E-03±1.68E-04 ^G	4.49E-03±3.49E-05 ^H	4.69E-03±6.23E-05 ^H	3.86E-03±6.30E-05 ^H	-
		4.49E-03±3.49E-05 ^D	4.69E-03±6.23E-05 ^D	3.86E-03±6.30E-05 ^D	
262	-	2.23E-03±2.30E-05 ^H	2.57E-03±3.98E-05 ^H	3.13E-03±4.23E-05 ^H	-
265	-	3.19E-03±2.48E-05 ^H	1.05E-02±1.13E-02 ^H	4.28E-03±4.48E-05 ^H	-
267	2.78E-03±1.39E-04 ^G	3.41E-03±2.96E-05 ^H	4.09E-03±5.04E-05 ^H	4.03E-03±5.22E-05 ^H	-
		3.41E-03±2.96E-05 ^D	4.09E-03±5.04E-05 ^D	4.03E-03±5.22E-05 ^D	
270	-	1.31E-03±1.94E-05 ^H	1.13E-03 ^H	2.28E-03±3.50E-05 ^H	-
275	-	4.38E-03±2.45E-05 ^H	5.80E-03±3.79E-05 ^H	4.06E-03±4.11E-05 ^H	-
		4.38E-03±2.43E-05 ^D	5.80E-03±3.79E-05 ^D	4.06E-03±4.11E-05 ^D	
280	-	2.25E-03±1.98E-05 ^H	3.41E-03±3.20E-05 ^H	2.03E-03±3.48E-05 ^H	-
281	-	8.96E-04±6.47E-05 ^H	2.24E-03±2.96E-05 ^H	1.90E-03±3.58E-05 ^H	-
283	-	4.38E-03±2.45E-05 ^H	5.80E-03±3.79E-05 ^H	4.06E-03±4.11E-05 ^H	-
		4.38E-03±2.43E-05 ^D	5.80E-03±3.79E-05 ^D	4.06E-03±4.11E-05 ^D	
288	-	1.91E-03±1.78E-05 ^H	3.05E-03±2.78E-05 ^H	1.78E-03±3.03E-05 ^H	-
292	-	1.98E-03±1.85E-05 ^H	1.60E-03±2.66E-05 ^H	1.82E-03±3.06E-05 ^H	-
297	-	3.40E-03±2.13E-05 ^H	4.48E-03±3.40E-05 ^H	3.22E-03±3.61E-05 ^H	-
304	-	1.98E-03±1.85E-05 ^H	1.60E-03±2.66E-05 ^H	1.82E-03±3.06E-05 ^H	-
306	-	2.41E-03±1.99E-05 ^H	3.53E-03±3.32E-05 ^H	2.22E-03±3.64E-05 ^H	-
		2.41E-03±2.15E-05 ^D	3.53E-03±3.32E-05 ^D	2.22E-03±3.64E-05 ^D	
311	-	3.19E-03±4.12E-05 ^H	5.13E-03±6.51E-05 ^H	6.44E-03±7.35E-05 ^H	-
314	-	6.46E-03±3.74E-05 ^H	6.01E-03±5.53E-05 ^H	4.89E-03±6.17E-05 ^H	-
		6.46E-03±3.74E-05 ^D	6.01E-03±5.53E-05 ^D	4.89E-03±6.17E-05 ^D	
323	-	1.97E-03±1.95E-05 ^H	2.22E-03±3.05E-05 ^H	1.81E-03±3.29E-05 ^H	-
327	-	3.23E-03±5.13E-05 ^H	1.68E-03±2.95E-05 ^H	1.98E-03±3.33E-05 ^H	-
335	-	3.14E-03±1.65E-05 ^H	4.05E-03±3.04E-05 ^H	2.84E-03±3.00E-05 ^H	-
336	-	4.93E-03±3.68E-05 ^H	5.81E-03±6.62E-05 ^H	4.68E-03±6.69E-05 ^H	-
337	-	1.15E-02±5.30E-05 ^H	1.59E-02±8.01E-05 ^H	1.23E-02±7.82E-05 ^H	-
		1.15E-02±5.30E-05 ^D	1.59E-02±8.01E-05 ^D	1.23E-02±7.82E-05 ^D	
338	-	1.21E-03±2.03E-05 ^H	9.15E-04 ^H	2.05E-03±3.60E-05 ^H	-
339	-	1.96E-03±1.63E-05 ^H	2.68E-03±3.06E-05 ^H	1.76E-03±3.07E-05 ^H	-
340	-	4.81E-03±2.82E-05 ^H	7.55E-03±4.63E-05 ^H	5.25E-03±4.90E-05 ^H	-
342	-	9.86E-03±3.86E-05 ^H	1.08E-02±5.18E-05 ^H	7.29E-03±6.70E-05 ^H	-
		9.86E-03±3.86E-05 ^D	1.08E-02±5.18E-05 ^D	7.29E-03±6.70E-05 ^D	
345	-	9.86E-03±3.86E-05 ^H	1.08E-02±5.18E-05 ^H	7.29E-03±6.70E-05 ^H	-
		9.86E-03±3.86E-05 ^D	1.08E-02±5.18E-05 ^D	7.29E-03±6.70E-05 ^D	
354	-	2.95E-03±2.10E-05 ^H	3.00E-03±3.42E-05 ^H	2.78E-03±3.61E-05 ^H	-
355	-	1.22E-03±1.52E-05 ^H	1.41E-03±2.55E-05 ^H	1.30E-03±2.91E-05 ^H	-
360	-	1.27E-03±1.27E-05 ^H	1.26E-03±1.98E-05 ^H	1.42E-03±2.46E-05 ^H	-
368	-	1.29E-03±2.08E-05 ^H	1.97E-03±3.37E-05 ^H	2.22E-03±3.72E-05 ^H	-
374	-	1.93E-03±2.22E-05 ^H	1.65E-03±3.16E-05 ^H	2.14E-03±3.78E-05 ^H	-
380	-	1.93E-03±2.22E-05 ^H	1.65E-03±3.16E-05 ^H	2.14E-03±3.78E-05 ^H	-
391	-	1.18E-03±1.11E-05 ^H	2.39E-03±3.55E-05 ^H	1.98E-03±3.69E-05 ^H	-
392	-	6.95E-03±4.25E-05 ^H	6.73E-03±6.52E-05 ^H	6.88E-03±7.34E-05 ^H	-
393	-	1.61E-03±1.92E-05 ^H	2.74E-03±3.08E-05 ^H	1.77E-03±3.34E-05 ^H	-
394	-	3.59E-03±2.62E-05 ^H	4.26E-03±4.58E-05 ^H	3.89E-03±4.40E-05 ^H	-
		3.59E-03±2.62E-05 ^D	4.26E-03±4.58E-05 ^D	3.89E-03±4.40E-05 ^D	
397	-	1.90E-03±1.97E-05 ^H	1.45E-03 ^H	1.57E-03±3.31E-05 ^H	-

Table 6. continued.

ID (ADF-S)	0.79 μm	1.25 μm	1.65 μm	2.22 μm	12 μm^I
400	-	1.32E-03±1.76E-05 ^H 1.32E-03±1.76E-05 ^D	1.49E-03±9.60E-06 ^H 1.49E-03 ^D	1.24E-03±3.05E-05 ^H 9.28E-04±2.24E-05 ^D	-
402	-	3.20E-03±3.30E-05 ^H 3.20E-03±3.30E-05 ^D	5.04E-03±5.45E-05 ^H 5.04E-03±5.45E-05 ^D	4.41E-03±5.46E-05 ^H 4.41E-03±5.46E-05 ^D	-
414	-	3.51E-03±2.30E-05 ^H	5.38E-03±4.22E-05 ^H	3.38E-03±2.45E-05 ^H	-
415	-	3.43E-03±3.17E-05 ^H	5.43E-03±5.08E-05 ^H	3.98E-03±5.45E-05 ^H	-
418	-	1.76E-03±1.83E-05 ^H	2.03E-03±2.70E-05 ^H	1.94E-03±3.17E-05 ^H	-
431	-	1.15E-03±1.90E-05 ^H	2.01E-03±3.11E-05 ^H	1.96E-03±3.40E-05 ^H	-
432	-	3.05E-03±2.64E-05 ^H	5.64E-03±4.36E-05 ^H	4.22E-03±4.80E-05 ^H	-
437	-	2.07E-03±2.37E-05 ^H 2.07E-03±2.34E-05 ^D	2.55E-03±3.59E-05 ^H 2.55E-03±3.59E-05 ^D	2.51E-03±4.16E-05 ^H 2.51E-03±4.16E-05 ^D	-
449	-	2.83E-03±1.95E-05 ^H	3.72E-03±3.08E-05 ^H	2.44E-03±3.39E-05 ^H	-
450	-	2.60E-03±2.07E-05 ^H 2.60E-03±2.07E-05 ^D	2.45E-03±3.22E-05 ^H 2.45E-03±3.22E-05 ^D	2.30E-03±3.62E-05 ^H 2.30E-03±3.62E-05 ^D	-
451	-	2.98E-03±2.50E-05 ^H	3.75E-03±4.04E-05 ^H	2.95E-03±4.38E-05 ^H	-
452	-	1.11E-03±2.01E-05 ^H	9.55E-04 ^H	2.44E-03±3.42E-05 ^H	-
463	-	2.30E-03±2.58E-05 ^H	2.89E-03±3.76E-05 ^H	3.14E-03±4.15E-05 ^H	-
466	-	1.99E-03±1.95E-05 ^H	2.04E-03±3.05E-05 ^H	3.31E-03±3.57E-05 ^H	-
490	-	4.26E-03±2.75E-05 ^H 4.26E-03±2.75E-05 ^D	5.03E-03±3.89E-05 ^H 5.03E-03±3.89E-05 ^D	3.60E-03±2.84E-05 ^H 5.58E-03±5.19E-05 ^D	-
493	-	1.87E-03±1.66E-05 ^H	3.80E-03±2.67E-05 ^H	2.44E-03±3.17E-05 ^H	-

A - F - as in table 5

G - Mathewson & Ford (1996)

H - Skrutskie et al. (2003)

I - Moshir et al. (1990)

J - Kinney et al. (1993)

Table 7. Flux densities in other wavelengths found for the counterparts of the ADFS sources in the public databases, for the 10σ catalog - part 3.

ID (ADF-S)	$25 \mu\text{m}^I$	$60 \mu\text{m}^I$	$100 \mu\text{m}^I$	35.69 cm^K (843 MHz)
2	1.06E-01±1.90E-02	1.32E+00±6.60E-02	2.20E+00±1.32E-01	1.06E-02±1.00E-03
3	7.36E-02±1.84E-02	6.70E-01±3.35E-02	3.65E+00±1.83E-01	-
4	1.50E-01±1.50E-01	8.68E-01±6.07E-02	1.82E+00±1.45E-01	-
5	7.87E-02±1.34E-02	6.07E-01±3.64E-02	1.64E+00±1.31E-01	1.06E-02±1.00E-03
6	9.28E-02±1.60E-01	6.16E-01±4.31E-02	1.16E+00±1.27E-01	-
7	1.69E-01±2.03E-02	7.47E-01±3.73E-02	9.65E-01±1.25E-01	-
8	7.25E-02±1.88E-02	5.81E-01±3.49E-02	1.22E+00±1.22E-01	-
9	7.24E-02±1.45E-02	4.75E-01±3.32E-02	-	-
10	-	2.99E-01±2.99E-02	8.89E-01±1.16E-01	-
11	5.85E-02±1.34E-02	2.54E-01±3.05E-02	1.09E+00±1.20E-01	1.90E-02±2.50E-03
12	9.57E-02±2.30E-02	4.59E-01±3.21E-02	< 1.19E+00	-
13	4.30E-02±4.30E-02	3.71E-01±2.97E-02	9.77E-01±1.17E-01	-
14	7.78E-02±7.78E-02	3.91E-01±3.91E-02	1.15E+00±1.15E+00	8.30E-03±1.20E-03
15	5.98E-02±1.08E-02	3.24E-01±2.60E-02	8.33E-01±1.25E-01	-
16	2.50E-01±6.81E-02	3.85E-01±3.08E-02	5.84E-01±1.17E-01	-
17	-	3.10E-01±2.79E-02	8.67E-01±1.13E-01	7.00E-03±1.10E-03
18	-	2.15E-01±2.79E-02	7.89E-01±1.18E-01	-
20	-	2.75E-01±3.02E-02	7.29E-01±1.17E-01	-
21	-	2.13E-01±3.62E-02	6.83E-01±1.30E-01	-
22	-	2.37E-01±2.84E-02	-	-
23	5.14E-02±1.44E-02	2.39E-01±2.87E-02	5.84E-01±1.17E-01	-
24	-	2.66E-01±2.93E-02	7.62E-01±1.22E-01	-
27	4.29E-02±4.29E-02	2.14E-01±2.99E-02	4.81E-01±1.20E-01	-
29	-	1.96E-01±3.14E-02	< 6.50E-01	-
30	6.34E-02±6.34E-02	2.37E-01±3.79E-02	6.15E-01±1.35E-01	-
31	-	1.75E-01±2.80E-02	4.40E-01±1.15E-01	-
39	-	2.15E-01±2.80E-02	-	-
43	-	2.11E-01±3.37E-02	5.78E-01±1.21E-01	-
46	5.02E-02±5.02E-02	1.71E-01±2.73E-02	5.90E-01±1.12E-01	-
50	-	1.54E-01±2.77E-02	4.16E-01±1.17E-01	-
51	-	-	-	7.70E-03±1.20E-04
52	1.30E-01±1.94E-02	2.30E-01±3.91E-02	< 6.52E-01	-
60	-	1.67E-01±2.85E-02	-	-
70	2.34E-01±1.87E-02	1.39E-01±3.20E-02	< 4.63E-01	-
71	2.34E-01±1.87E-02	1.39E-01±3.20E-02	< 4.63E-01	-
73	6.71E-02±6.71E-02	1.76E-01±2.81E-02	4.87E-01±4.87E-01	-
101	-	-	-	5.20E-02±1.80E-03
134	-	1.60E-01±2.88E-02	-	-
136	-	1.60E-01±2.88E-02	-	-
166	-	-	-	6.40E-03±1.00E-03
196	-	-	-	1.12E-02±1.10E-03
295	-	-	-	4.46E-01±1.34E-02
300	-	-	-	4.46E-01±1.34E-02
441	-	-	-	2.39E-02±1.80E-03

 I - as in table 6 K - Mauch et al. (2003)

Table 8. Flux densities in other wavelengths found for the counterparts of the ADFS sources in the public databases, for the 10 σ catalog - part 4.

ID	λ [μm]	Measurement	Passband
AKARI			
4	0.10	2.41E-03	1030 A ^L
4	0.15	1.60E-02 \pm 2.22E-03	GALEX FUV ^M
4	0.16	2.30E-02 \pm 3.66E-03	UV 1650 ^N
4	0.18	1.68E-02 \pm 2.32E-03	GALEX NUV ^M
4	0.24	1.02E-02 \pm 7.90E-04	2373 A ^J
4	0.25	2.52E-02 \pm 2.42E-03	UV 2500 ^N
4	0.27	9.93E-03 \pm 3.65E-04	2700 A ^J
4	0.31	3.94E-02 \pm 1.02E-02	UV3150 ^N
4	0.36	2.14E-02 \pm 2.73E-03	B-J ^O
4	1.90	1.03E-02 \pm 6.11E-04	1913 A ^J
4	3.60	2.60E-02 \pm 4.00E-03	3.6 IRAC ^P
4	3.60	2.81E-02 \pm 2.00E-04	3.6 IRAC ^P
4	4.50	1.80E-02 \pm 3.00E-03	4.5 IRAC ^P
4	4.50	1.99E-02 \pm 4.00E-04	4.5 IRAC ^P
4	4.50	1.79E-02 \pm 5.80E-03	4.5 IRAC ^P
4	5.80	1.00E-02 \pm 2.00E-03	5.8 IRAC ^P
4	8.00	1.70E-02 \pm 2.00E-03	8 IRAC ^P
4	8.00	2.44E-02 \pm 1.40E-03	8 IRAC ^P
4	24.0	5.20E-02 \pm 5.00E-03	24 MIPS ^P
4	24.0	5.60E-02 \pm 2.00E-03	24 MIPS ^P
4	24.0	5.27E-02 \pm 2.20E-03	24 MIPS ^P
4	70.0	1.38E+00 \pm 1.00E-01	70 MIPS ^P
4	70.0	1.09E+00 \pm 2.20E-01	24 MIPS ^P
4	160.0	1.20E+00 \pm 2.50E-01	160 MIPS ^P
4	160.0	1.66E+00 \pm 2.10E-01	160 MIPS ^P
10	0.36	3.96E-03 \pm 7.02E-04	b.j ^B

B - as in table 5

J - as in table 6

L - Fox et al. (2006)

M - Dale et al. (2007)

N - Rifatto et al. (1995)

O - Doyle et al. (2005)

P - Dale et al. (2005)

Table 9. Flux densities in other wavelengths found for the counterparts of the ADFS sources, in the public databases, for the fainter part of the 6 σ catalog - part 1.

ID (ADF-S)	0.47 μm^C	1.25 μm	1.65 μm	2.22 μm
503	3.17E-05 \pm 5.37E-06	-	-	-
504	1.26E-04 \pm 1.47E-05	-	-	-
507	8.48E-05 \pm 9.91E-06	-	-	-
513	-	2.25E-03 \pm 2.63E-04 ^H	3.14E-03 \pm 3.73E-04 ^H	2.49E-03 \pm 4.31E-04 ^H
514	2.97E-05 \pm 5.03E-06	-	-	-
519	-	1.65E-03 \pm 3.60E-04 ^H	2.68E-03 \pm 5.01E-04 ^H	1.94E-03 \pm 6.37E-04 ^H
523	2.68E-05 \pm 4.55E-06	-	-	-
524	1.86E-04 \pm 2.17E-05	-	-	-
526	-	7.82E-03 \pm 4.82E-04 ^H	9.52E-03 \pm 6.72E-04 ^H	8.91E-03 \pm 7.97E-04 ^H
530	3.54E-04 \pm 4.13E-05	-	-	-
532	3.05E-05 \pm 5.17E-06	-	-	-
533	1.30E-04 \pm 1.51E-05	-	-	-
534	-	7.82E-03 \pm 4.82E-04 ^H	9.52E-03 \pm 6.72E-04 ^H	8.91E-03 \pm 7.97E-04 ^H
538	-	2.25E-03 \pm 2.63E-04 ^H	3.14E-03 \pm 3.73E-04 ^H	2.49E-03 \pm 4.31E-04 ^H
541	1.52E-03 \pm 1.77E-04	-	-	-
543	4.29E-05 \pm 5.91E-06	-	-	-
544	-	1.28E-03 \pm 2.09E-04 ^H	1.23E-03 \pm 3.12E-04 ^H	1.51E-03 \pm 3.98E-04 ^H
545	3.54E-05 \pm 5.99E-06	-	-	-
548	3.88E-04 \pm 4.53E-05	1.50E-03 \pm 1.31E-04 ^H	1.45E-03 \pm 1.90E-04 ^H	1.53E-03 \pm 2.13E-04 ^H
552	5.16E-05 \pm 7.10E-06	-	-	-
554	2.17E-04 \pm 2.54E-05	-	-	-
555	4.66E-05 \pm 6.42E-06	-	-	-
556	-	1.38E-03 \pm 2.37E-04 ^H	1.20E-03 \pm 3.59E-04 ^H	1.54E-03 \pm 3.97E-04 ^H
559	4.97E-05 \pm 6.84E-06	-	-	-
560	6.62E-05 \pm 7.73E-06	-	-	-
564	4.14E-05 \pm 5.69E-06	-	-	-
565	9.83E-05 \pm 1.15E-05	-	-	-
567	3.77E-05 \pm 6.39E-06	-	-	-
570	7.25E-05 \pm 8.48E-06	-	-	-
572	3.47E-05 \pm 5.89E-06	-	-	-
575	1.23E-04 \pm 1.43E-05	-	-	-
576	-	2.65E-03 \pm 3.40E-04 ^H	2.52E-03 \pm 5.94E-04 ^H	2.44E-03 \pm 6.28E-04 ^H
577	9.22E-05 \pm 1.08E-05	-	-	-
578	4.79E-05 \pm 6.60E-06	-	-	-
579	2.66E-05 \pm 4.51E-06	-	-	-
582	1.66E-04 \pm 1.94E-05	-	-	-
583	1.12E-04 \pm 1.31E-05	-	-	-
588	1.52E-04 \pm 1.77E-05	-	-	-
593	8.10E-05 \pm 9.47E-06	-	-	-
595	4.14E-05 \pm 5.69E-06	-	-	-
596	2.56E-04 \pm 2.99E-05	-	-	-
598	2.81E-04 \pm 3.28E-05	-	-	-
603	9.74E-05 \pm 1.14E-05	-	-	-
604	-	5.92E-03 \pm 3.88E-05 ^D	7.01E-03 \pm 6.00E-05 ^D	7.64E-03 \pm 6.80E-05 ^D
606	1.23E-04 \pm 1.43E-05	-	-	-
608	5.66E-05 \pm 7.79E-06	-	-	-
612	4.10E-04 \pm 4.79E-05	4.26E-03 \pm 3.22E-04 ^H	4.83E-03 \pm 5.49E-04 ^H	3.95E-03 \pm 5.65E-04 ^H
618	2.86E-04 \pm 3.34E-05	2.11E-03 \pm 3.24E-04 ^H	2.58E-03 \pm 5.91E-04 ^H	2.95E-03 \pm 5.84E-04 ^H
621	5.66E-04 \pm 6.61E-05	5.07E-03 \pm 3.18E-04 ^H	7.39E-03 \pm 5.07E-04 ^H	4.39E-03 \pm 5.41E-04 ^H
	-	5.11E-03 \pm 2.45E-05 ^D	7.76E-03 \pm 4.35E-05 ^D	4.39E-03 \pm 4.27E-05 ^D
624	6.20E-04 \pm 7.25E-05	-	-	-
625	2.63E-05 \pm 4.46E-06	-	-	-
629	8.88E-05 \pm 1.04E-05	-	-	-
632	2.56E-04 \pm 2.99E-05	-	-	-
633	2.63E-05 \pm 4.46E-06	-	-	-
634	9.22E-05 \pm 1.08E-05	-	-	-
636	6.74E-05 \pm 7.88E-06	-	-	-
639	5.71E-05 \pm 7.86E-06	-	-	-

Table 9. continued.

ID (ADF-S)	0.47 μm^C	1.25 μm	1.65 μm	2.22 μm
640	3.32E-04 \pm 3.88E-05	-	-	-
644	-	1.61E-03 \pm 3.72E-04 ^H	2.08E-03 \pm 5.52E-04 ^H	3.44E-03 \pm 5.98E-04 ^H
648	6.32E-05 \pm 7.38E-06	-	-	-
652	-	2.41E-03 \pm 2.38E-04 ^H	3.14E-03 \pm 3.38E-04 ^H	2.43E-03 \pm 4.04E-04 ^H
653	4.10E-04 \pm 4.79E-05	-	-	-
654	4.79E-05 \pm 6.60E-06	1.34E-03 \pm 2.97E-04 ^H	1.02E-03 \pm ...	2.47E-03 \pm 4.66E-04 ^H
659	3.29E-05 \pm 5.57E-06	-	-	-
662	3.57E-04 \pm 4.17E-05	2.06E-03 \pm 2.51E-04 ^H	2.20E-03 \pm 4.21E-04 ^H	2.40E-03 \pm 4.62E-04 ^H
664	8.33E-05 \pm 9.73E-06	-	-	-
669	1.15E-04 \pm 1.34E-05	-	-	-
670	6.32E-05 \pm 7.38E-06	-	-	-
675	5.61E-05 \pm 7.71E-06	-	-	-
677	2.34E-04 \pm 2.73E-05	1.76E-03 \pm 2.83E-04 ^H	2.04E-03 \pm 4.31E-04 ^H	2.13E-03 \pm 4.59E-04 ^H
679	3.81E-05 \pm 6.45E-06	-	-	-
685	-	8.68E-03 \pm 4.51E-04 ^H	1.05E-02 \pm 6.16E-04 ^H	8.31E-03 \pm 7.35E-04 ^H
686	3.00E-04 \pm 3.50E-05	-	-	-
690	1.46E-04 \pm 1.71E-05	-	-	-
692	4.29E-05 \pm 5.91E-06	-	-	-
693	4.21E-05 \pm 5.80E-06	-	-	-
694	4.84E-05 \pm 6.66E-06	-	-	-
697	1.56E-04 \pm 1.82E-05	-	-	-
698	9.39E-05 \pm 1.10E-05	-	-	-
700	1.42E-04 \pm 1.66E-05	-	-	-
708	3.38E-05 \pm 5.72E-06	-	-	-
709	7.06E-05 \pm 8.25E-06	-	-	-
710	1.31E-04 \pm 1.53E-05	-	-	-
713	7.39E-05 \pm 8.64E-06	-	-	-
715	2.56E-04 \pm 2.99E-05	-	-	-
717	3.41E-05 \pm 5.78E-06	-	-	-
718	3.32E-05 \pm 5.62E-06	-	-	-
720	8.72E-05 \pm 1.02E-05	-	-	-
721	9.30E-04 \pm 1.09E-04	1.91E-03 \pm 2.61E-04 ^H	2.70E-03 \pm 3.75E-04 ^H	2.12E-03 \pm 4.31E-04 ^H
	-	1.93E-03 \pm 1.81E-05 ^D	2.84E-03 \pm 2.87E-05 ^D	2.12E-03 \pm 3.10E-05 ^D
723	7.39E-05 \pm 8.64E-06	7.59E-04 \pm 2.31E-04 ^H	9.39E-04 \pm 3.38E-04 ^H	2.22E-03 \pm 4.57E-04 ^H
728	1.02E-04 \pm 1.19E-05	-	-	-
729	-	1.92E-03 \pm 2.49E-04 ^H	1.70E-03 \pm 3.71E-04 ^H	1.54E-03 \pm 4.26E-04 ^H
730	1.60E-04 \pm 1.87E-05	-	-	-
734	4.84E-04 \pm 5.65E-05	2.98E-03 \pm 3.21E-04 ^H	2.66E-03 \pm 5.64E-04 ^H	3.23E-03 \pm 5.93E-04 ^H
738	1.89E-04 \pm 2.21E-05	-	-	-
739	3.88E-05 \pm 6.57E-06	-	-	-
740	9.56E-05 \pm 1.12E-05	-	-	-
743	3.08E-05 \pm 5.22E-06	-	-	-
749	2.54E-04 \pm 2.97E-05	-	-	-
750	2.94E-04 \pm 3.44E-05	1.70E-03 \pm 2.85E-04 ^H	2.40E-03 \pm 4.12E-04 ^H	2.35E-03 \pm 4.65E-04 ^H
754	6.32E-05 \pm 7.38E-06	-	-	-
762	1.33E-04 \pm 1.56E-05	-	-	-
763	-	2.91E-03 \pm 2.57E-04 ^H	5.11E-03 \pm 3.96E-04 ^H	3.68E-03 \pm 4.72E-04 ^H
764	4.29E-05 \pm 5.91E-06	-	-	-
765	1.23E-04 \pm 1.43E-05	-	-	-
769	2.86E-05 \pm 4.85E-06	-	-	-
770	5.82E-05 \pm 8.00E-06	-	-	-
771	1.15E-04 \pm 1.34E-05	-	-	-
772	2.86E-04 \pm 3.34E-05	-	-	-
774	1.42E-04 \pm 1.66E-05	-	-	-
776	4.33E-05 \pm 5.96E-06	-	-	-
777	6.68E-05 \pm 7.80E-06	-	-	-
778	1.07E-04 \pm 1.25E-05	-	-	-
781	1.26E-04 \pm 1.47E-05	-	-	-
784	4.54E-05 \pm 6.24E-06	-	-	-

Table 9. continued.

ID (ADF-S)	0.47 μm^C	1.25 μm	1.65 μm	2.22 μm
789	9.83E-05 \pm 1.15E-05	-	-	-
790	6.99E-05 \pm 8.17E-06	-	-	-
791	5.21E-05 \pm 7.17E-06	-	-	-
794	3.74E-04 \pm 4.37E-05	2.64E-03 \pm 3.28E-04 ^H	3.15E-03 \pm 4.83E-04 ^H	3.10E-03 \pm 5.35E-04 ^H
	-	2.66E-03 \pm 2.34E-05 ^D	3.30E-03 \pm 3.72E-05 ^D	3.10E-03 \pm 4.02E-05 ^D
795	7.46E-05 \pm 8.72E-06	-	-	-
796	1.94E-04 \pm 2.27E-05	-	-	-
797	3.44E-04 \pm 4.02E-05	1.16E-03 \pm 1.53E-04 ^H	2.31E-03 \pm 4.12E-04 ^H	1.98E-03 \pm 4.88E-04 ^H
800	1.15E-04 \pm 1.34E-05	-	-	-
801	5.66E-05 \pm 7.79E-06	-	-	-
806	6.15E-04 \pm 7.18E-05	2.69E-03 \pm 3.03E-04 ^H	2.82E-03 \pm 4.93E-04 ^H	2.39E-03 \pm 5.12E-04 ^H
	-	2.71E-03 \pm 2.18E-05 ^D	2.96E-03 \pm 3.72E-05 ^D	2.39E-03 \pm 3.70E-05 ^D
807	6.68E-05 \pm 7.80E-06	-	-	-
809	2.40E-04 \pm 2.81E-05	1.33E-03 \pm 2.91E-04 ^H	1.20E-03 \pm ...	1.78E-03 \pm 4.75E-04 ^H
810	2.81E-04 \pm 3.28E-05	2.14E-03 \pm 4.01E-04 ^H	3.93E-03 \pm 6.20E-04 ^H	3.73E-03 \pm 6.89E-04 ^H
811	5.16E-05 \pm 7.10E-06	-	-	-
812	2.36E-04 \pm 2.76E-05	-	-	-
813	1.96E-04 \pm 2.29E-05	-	-	-
815	2.61E-05 \pm 4.42E-06	-	-	-
816	3.08E-04 \pm 3.60E-05	-	-	-
824	9.05E-05 \pm 1.06E-05	-	-	-
826	1.72E-04 \pm 2.02E-05	-	-	-
827	2.94E-05 \pm 4.99E-06	-	-	-
828	1.43E-04 \pm 1.68E-05	-	-	-
830	1.94E-04 \pm 2.27E-05	9.64E-04 \pm 2.22E-04 ^H	1.89E-03 \pm 4.85E-04 ^H	2.04E-03 \pm 5.33E-04 ^H
833	3.35E-05 \pm 5.67E-06	-	-	-
834	3.08E-05 \pm 5.22E-06	-	-	-
838	3.74E-05 \pm 6.34E-06	-	-	-
841	1.96E-04 \pm 2.29E-05	-	-	-
843	3.11E-05 \pm 5.27E-06	-	-	-
846	3.32E-05 \pm 5.62E-06	-	-	-
849	3.05E-05 \pm 5.17E-06	-	-	-
851	6.50E-05 \pm 7.59E-06	-	-	-
853	1.84E-04 \pm 2.15E-05	-	-	-
854	1.98E-04 \pm 2.31E-05	-	-	-
858	3.41E-05 \pm 5.78E-06	-	-	-
859	2.49E-05 \pm 4.22E-06	-	-	-
860	2.89E-05 \pm 4.90E-06	-	-	-
865	2.07E-04 \pm 2.42E-05	-	-	-
869	1.40E-04 \pm 1.63E-05	-	-	-
870	2.91E-05 \pm 4.94E-06	-	-	-
874	4.97E-05 \pm 6.84E-06	-	-	-
875	1.57E-04 \pm 1.84E-05	-	-	-
879	2.97E-05 \pm 5.03E-06	-	-	-
882	2.73E-05 \pm 4.63E-06	-	-	-
883	3.50E-05 \pm 5.94E-06	-	-	-
885	1.45E-04 \pm 1.69E-05	-	-	-
886	1.74E-04 \pm 2.03E-05	-	-	-
888	3.91E-04 \pm 4.57E-05	-	-	-
891	2.73E-05 \pm 4.63E-06	-	-	-
892	3.91E-05 \pm 6.63E-06	-	-	-
	-	2.53E-03 \pm 2.56E-05 ^D	4.03E-03 \pm 4.10E-05 ^D	3.35E-03 \pm 4.55E-05 ^D
894	3.54E-05 \pm 5.99E-06	-	-	-
898	2.78E-04 \pm 3.25E-05	-	-	-
902	3.00E-05 \pm 5.08E-06	-	-	-
904	2.04E-04 \pm 2.38E-05	-	-	-
907	2.61E-05 \pm 4.42E-06	-	-	-
908	3.64E-05 \pm 6.16E-06	-	-	-
911	5.35E-05 \pm 7.37E-06	-	-	-

Table 9. continued.

ID (ADF-S)	0.47 μm^C	1.25 μm	1.65 μm	2.22 μm
913	7.60E-05 \pm 8.88E-06	-	-	-
917	-	3.96E-03 \pm 3.34E-04 ^H	4.55E-03 \pm 4.80E-04 ^H	4.38E-03 \pm 5.34E-04 ^H
920	3.20E-05 \pm 5.42E-06	-	-	-
924	3.11E-05 \pm 5.27E-06	-	-	-
926	3.50E-05 \pm 5.94E-06	-	-	-
928	6.32E-05 \pm 7.38E-06	-	-	-
931	9.39E-05 \pm 1.10E-05	-	-	-
932	8.41E-05 \pm 9.82E-06	-	-	-
935	1.31E-04 \pm 1.53E-05	-	-	-
938	3.50E-04 \pm 4.10E-05	-	-	-
940	8.64E-05 \pm 1.01E-05	-	-	-
942	5.21E-05 \pm 7.17E-06	-	-	-
943	3.23E-04 \pm 3.77E-05	-	-	-
947	7.67E-05 \pm 8.96E-06	-	-	-
949	7.67E-05 \pm 8.96E-06	-	-	-
950	5.55E-05 \pm 7.64E-06	-	-	-
951	1.72E-04 \pm 2.02E-05	-	-	-
956	8.10E-05 \pm 9.47E-06	-	-	-
959	4.88E-05 \pm 6.72E-06	-	-	-
962	4.75E-05 \pm 6.54E-06	-	-	-
967	4.37E-05 \pm 6.02E-06	-	-	-
968	4.33E-05 \pm 5.96E-06	-	-	-
971	2.32E-04 \pm 2.71E-05	-	-	-
975	1.34E-04 \pm 1.57E-05	-	-	-
978	2.81E-05 \pm 4.76E-06	-	-	-
980	2.00E-04 \pm 2.34E-05	-	-	-
981	4.54E-05 \pm 6.24E-06	-	-	-
982	1.56E-04 \pm 1.82E-05	1.89E-03 \pm 2.74E-04 ^H	1.50E-03 \pm 2.17E-04 ^H	1.99E-03 \pm 4.73E-04 ^H
983	1.08E-04 \pm 1.26E-05	-	-	-
996	3.74E-05 \pm 6.34E-06	-	-	-
1000	3.29E-04 \pm 3.84E-05	-	-	-

C, D - as in table 5*H* - as in table 6

Table 10. Flux densities in other wavelengths found for the counterparts of the ADFS sources in the public databases, for the fainter part of the 6σ catalog - part 2.

ID (ADF-S)	$0.44 \mu\text{m}^D$	$0.55 \mu\text{m}^D$	35.69 cm^K (843 MHz)
541	1.94E-03	-	-
574	-	1.25E-03	-
585	-	-	$5.88\text{E-}02 \pm 2.00\text{E-}03$
604	-	-	$6.80\text{E-}03 \pm 8.00\text{E-}04$
610	-	1.25E-03	-
621	4.13E-03	-	-
624	1.64E-03	-	-
699	-	-	$1.32\text{E-}02 \pm 1.20\text{E-}03$
760	-	-	$1.11\text{E-}02 \pm 1.10\text{E-}03$
794	1.64E-03	-	-
806	1.64E-03	-	-
831	-	-	$1.73\text{E-}02 \pm 1.60\text{E-}03$
837	-	1.04E-03	-
856	2.38E-01	3.09E-01	-
857	-	-	$6.31\text{E-}02 \pm 2.30\text{E-}03$
892	1.64E-03	-	-
945	8.63E+000	1.02E+001	-
955	-	-	$5.04\text{E-}02 \pm 1.70\text{E-}03$
989	5.44E-01	1.81E+000	-

D - as in table 5

K - as in table 7

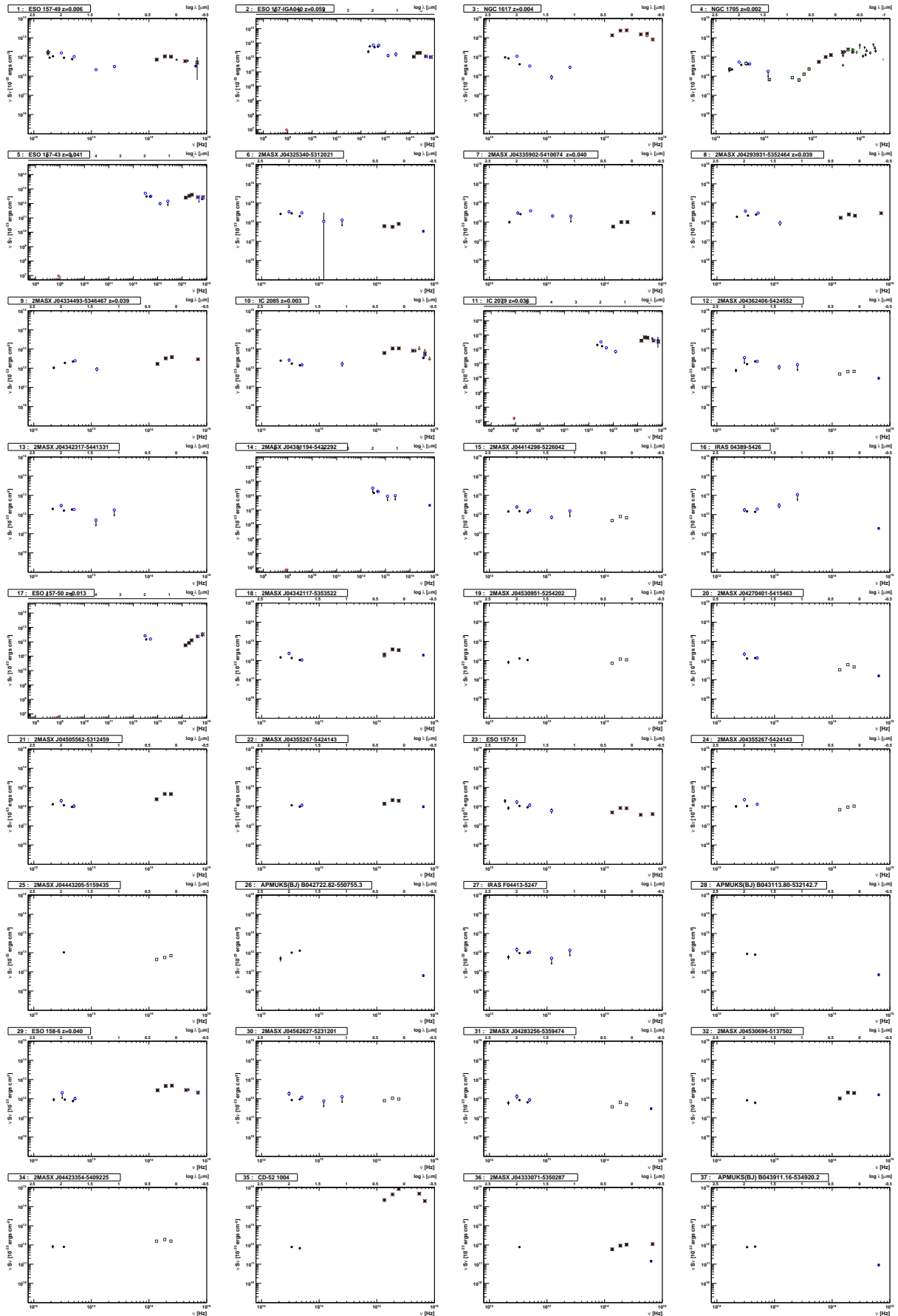


Fig. 1. SEDs for first 36 infrared ADF-S identified sources, using all the information listed in online Tables 3-10. The data points from AKARI Deep Field South (full black circles), 2MASS (open gray squares), SIMBAD database (black eight pointed stars), IRAS (blue open circles), ESO/Uppsala (full blue triangles), APM (full navy blue squares), RC3 (open brown triangles), ISOPHOT (five pointed black stars), Siding Spring Observatory (five pointed gray stars), GALEX (full green triangles), HIPASS catalogue (full green circles), Palomar/Las Campanas Imaging Atlas of Blue Compact Dwarf Galaxies (full magenta squares), IUE (open black diamonds), Spitzer (full red squares), FUSE (upside-down red triangles) and IUV: 1650 2500 3150 nm (full navy blue upside-down

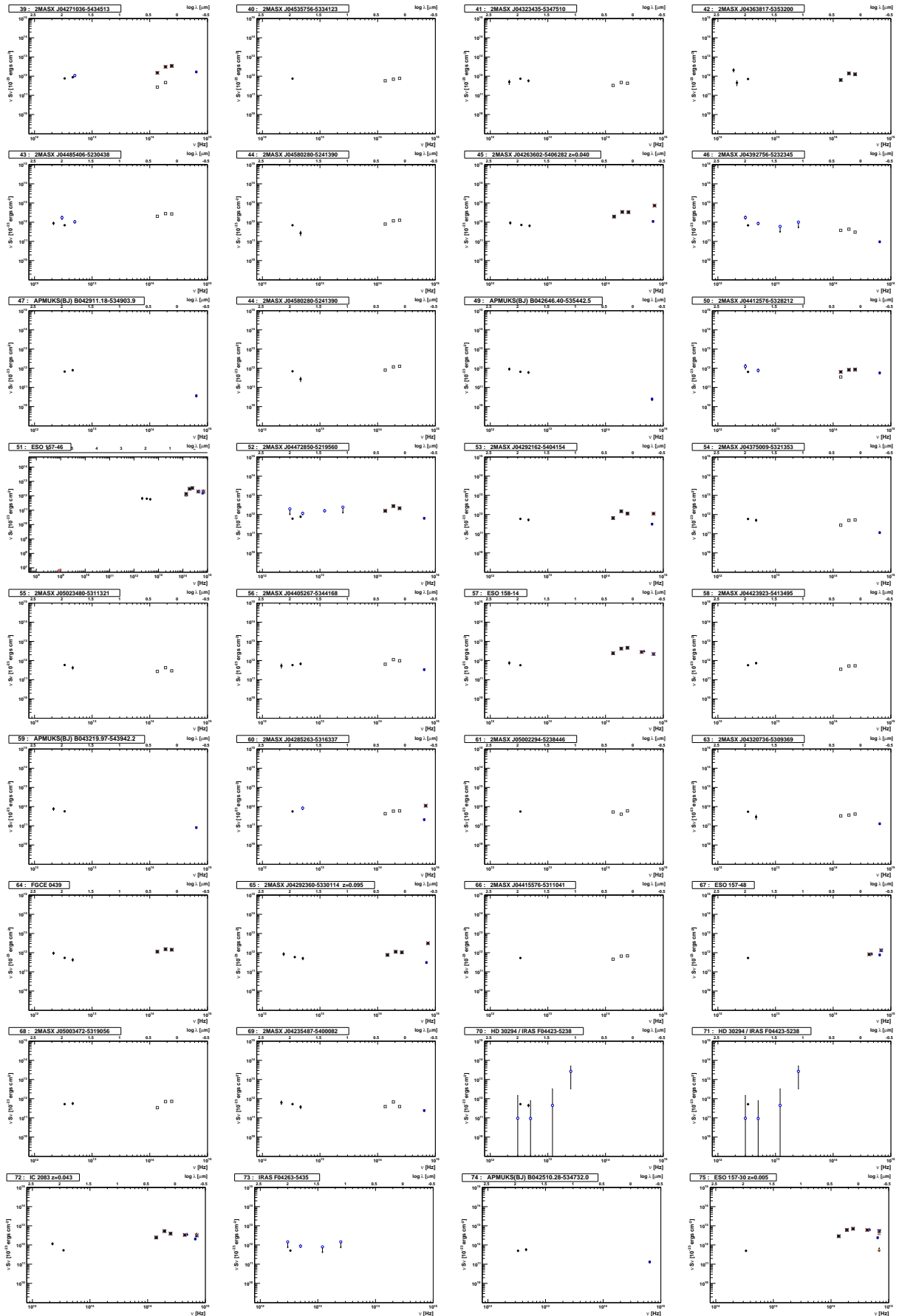


Fig. 2. SEDs for the next 36 ADF-S identified sources, with symbols as in Figure 1.

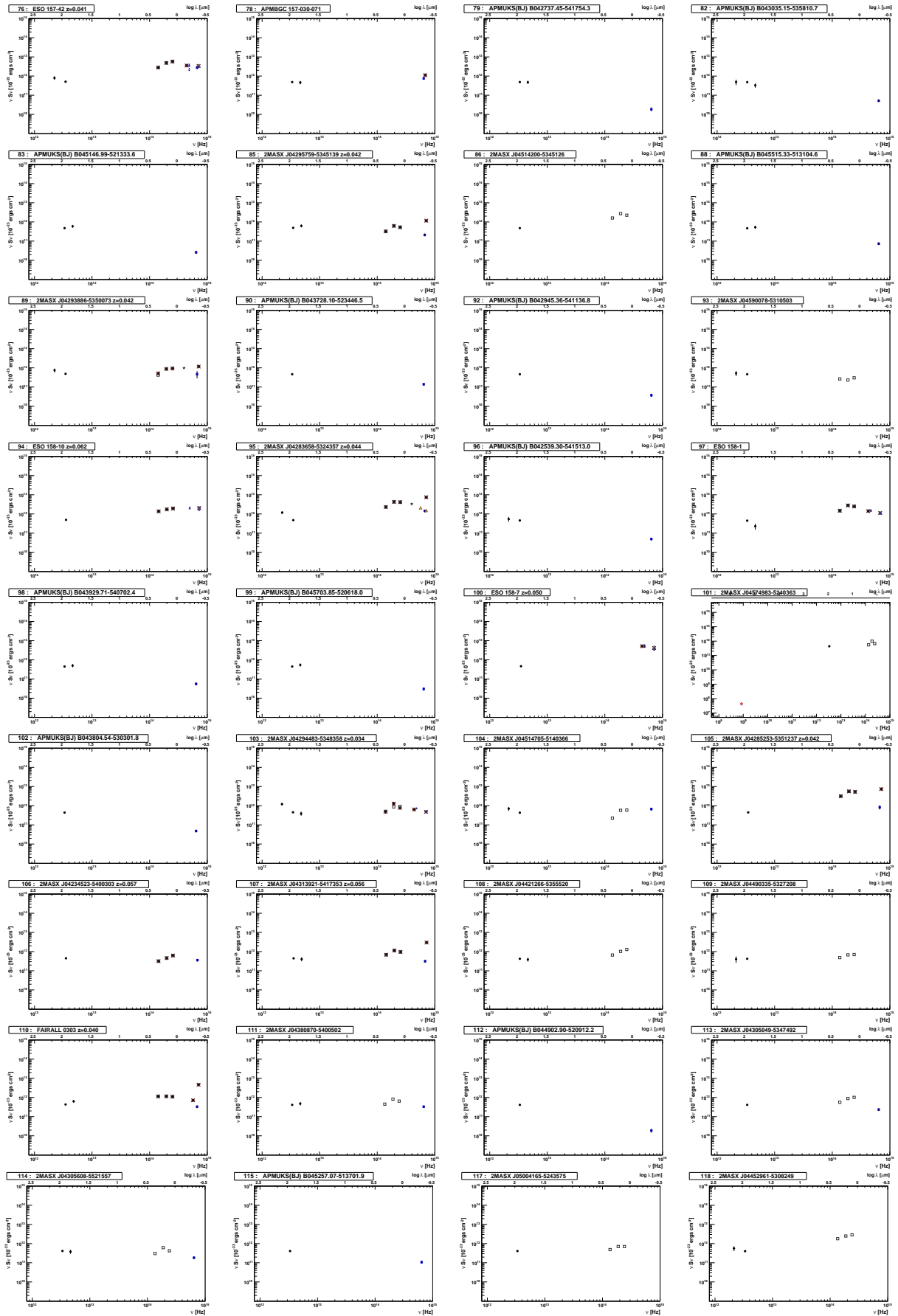


Fig. 3. SEDs for the next 36 ADF-S identified sources, with symbols as in Figure 1.

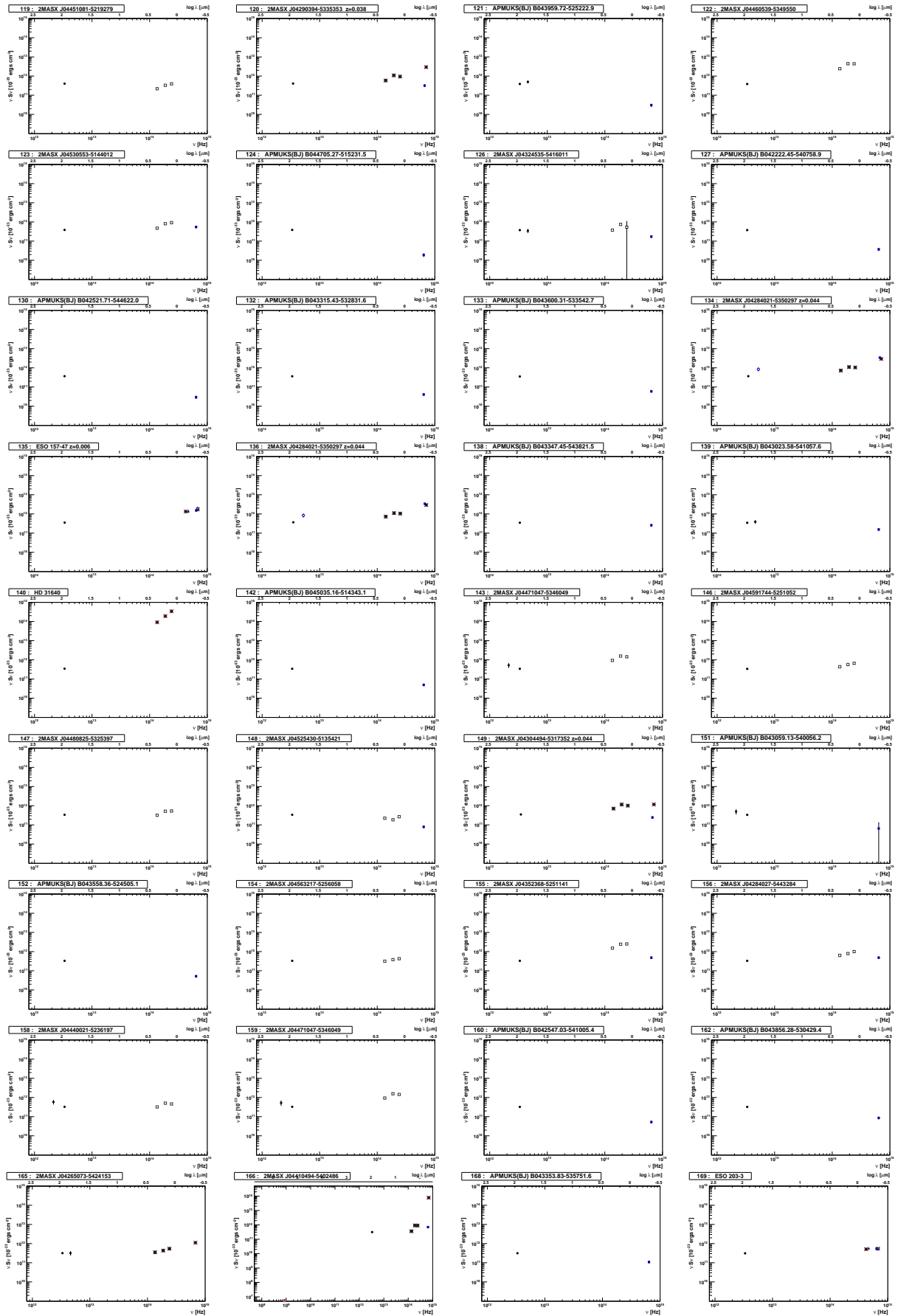


Fig. 4. SEDs for the next 36 ADF-S identified sources, with symbols as in Figure 1.

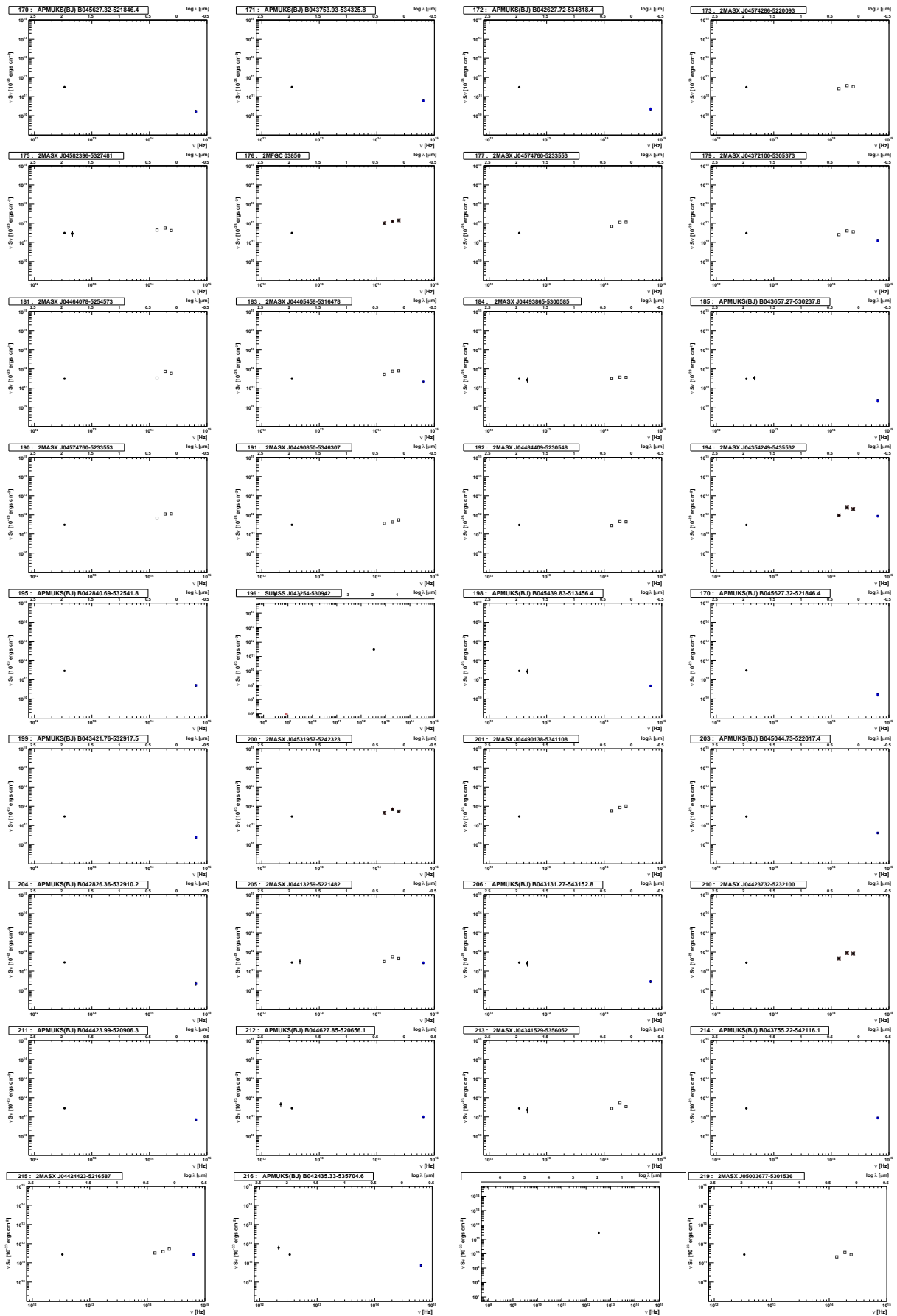


Fig. 5. SEDs for the next 36 ADF-S identified sources, with symbols as in Figure 1.

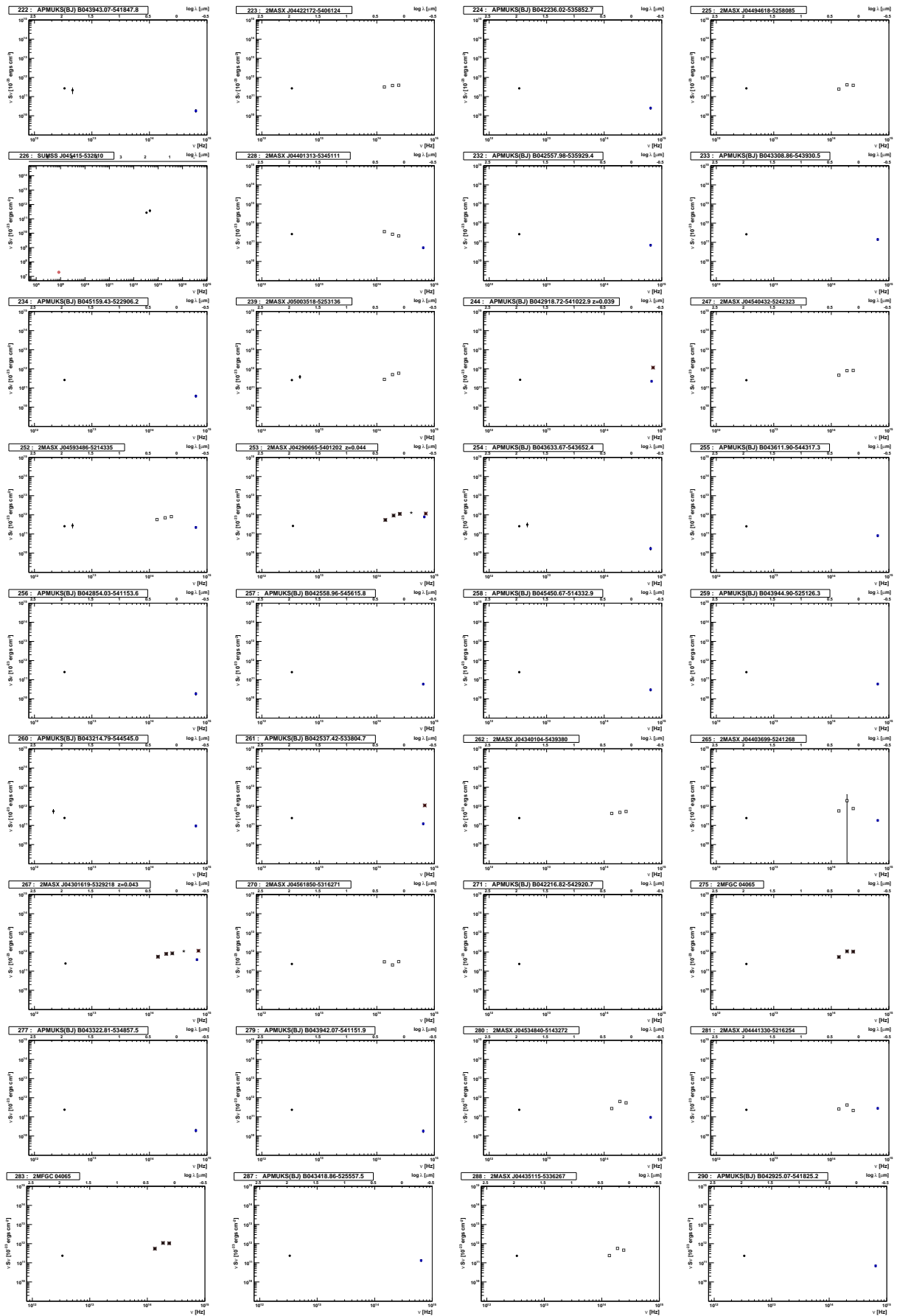


Fig. 6. SEDs for the next 36 ADF-S identified sources, with symbols as in Figure 1.

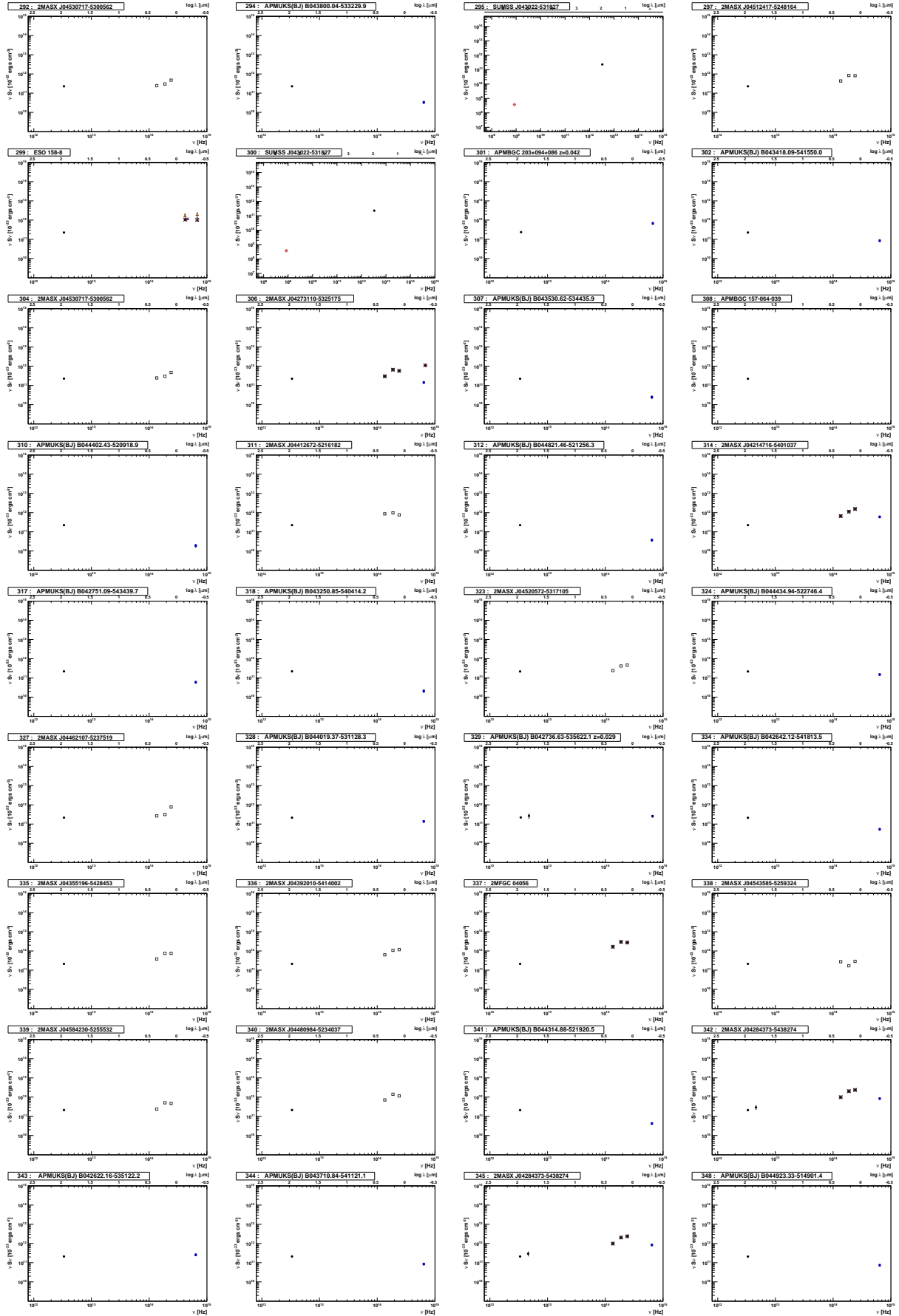


Fig. 7. SEDs for the next 36 ADF-S identified sources, with symbols as in Figure 1.

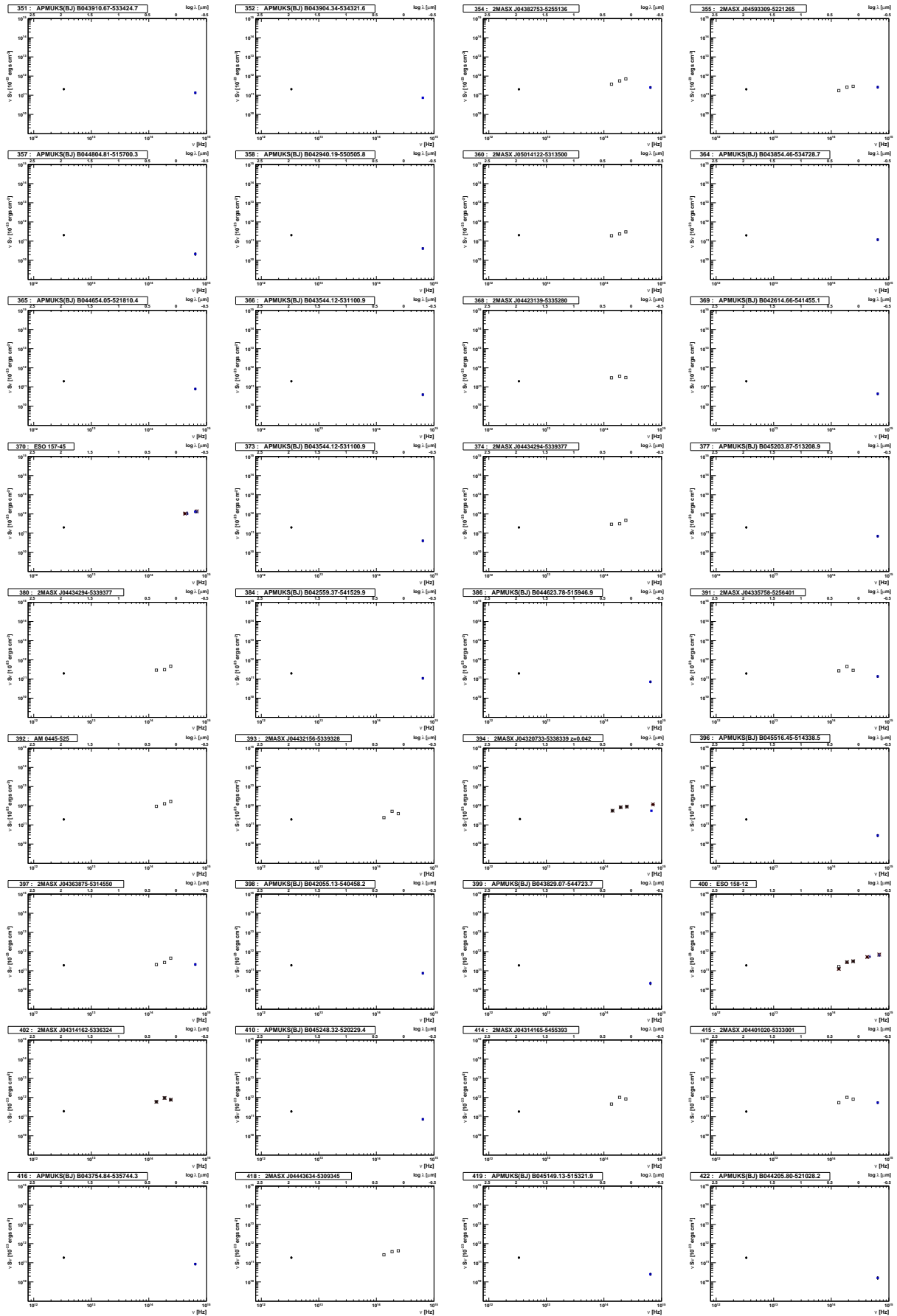


Fig. 8. SEDs for the next 36 ADF-S identified sources, with symbols as in Figure 1.

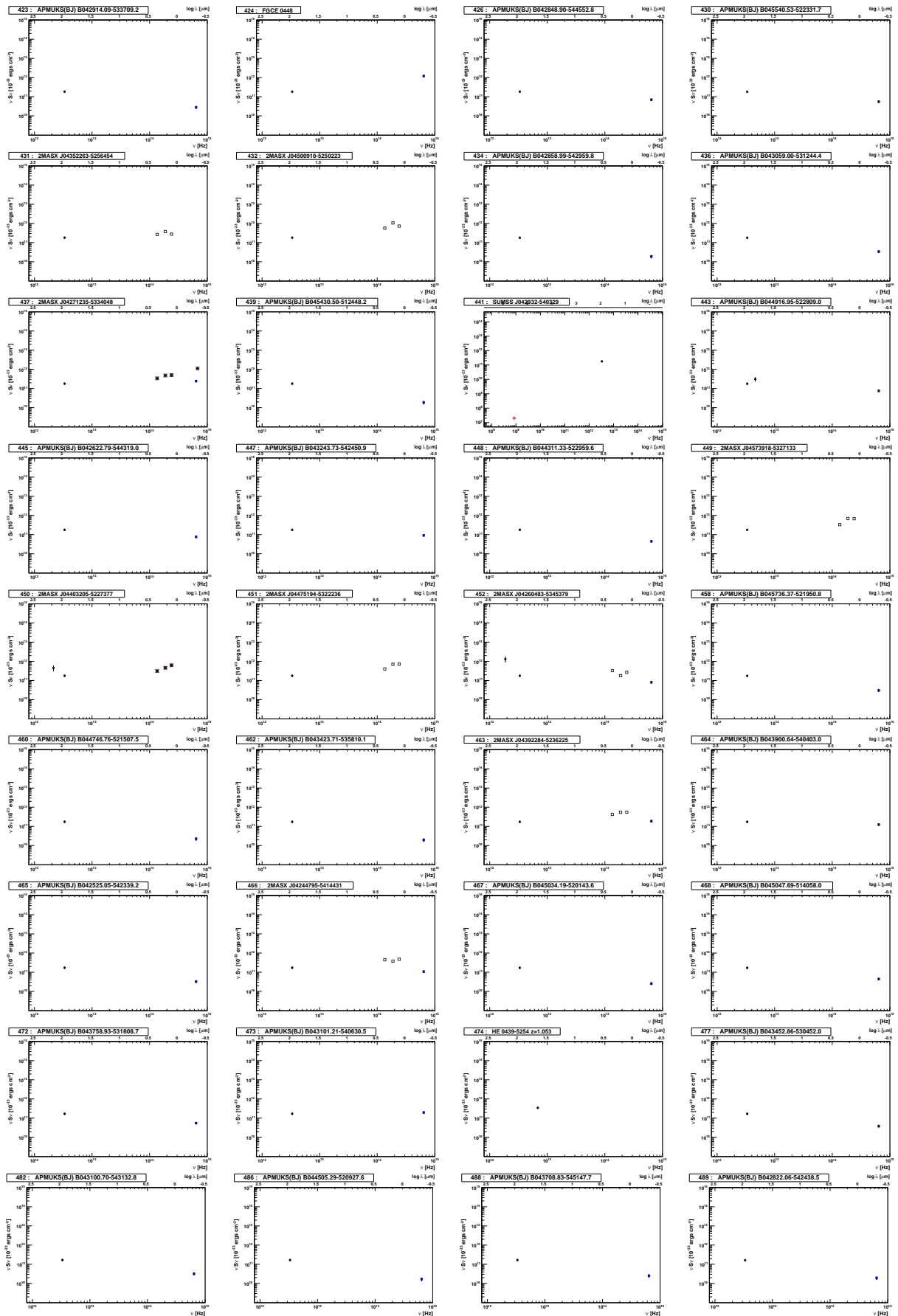


Fig. 9. SEDs for the next 36 ADF-S identified sources, with symbols as in Figure 1.

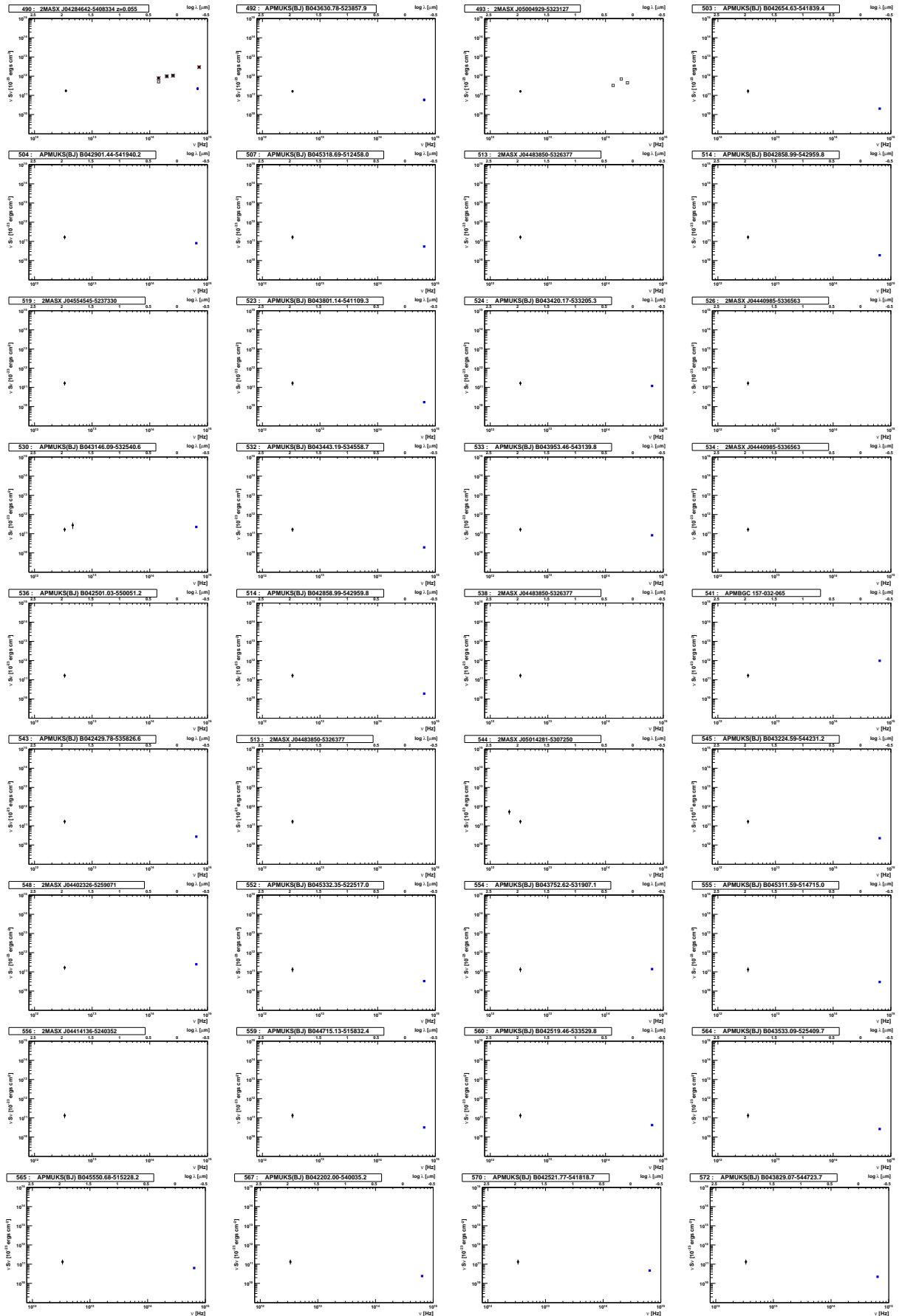


Fig. 10. SEDs for the next 36 ADF-S identified sources, with symbols as in Figure 1.

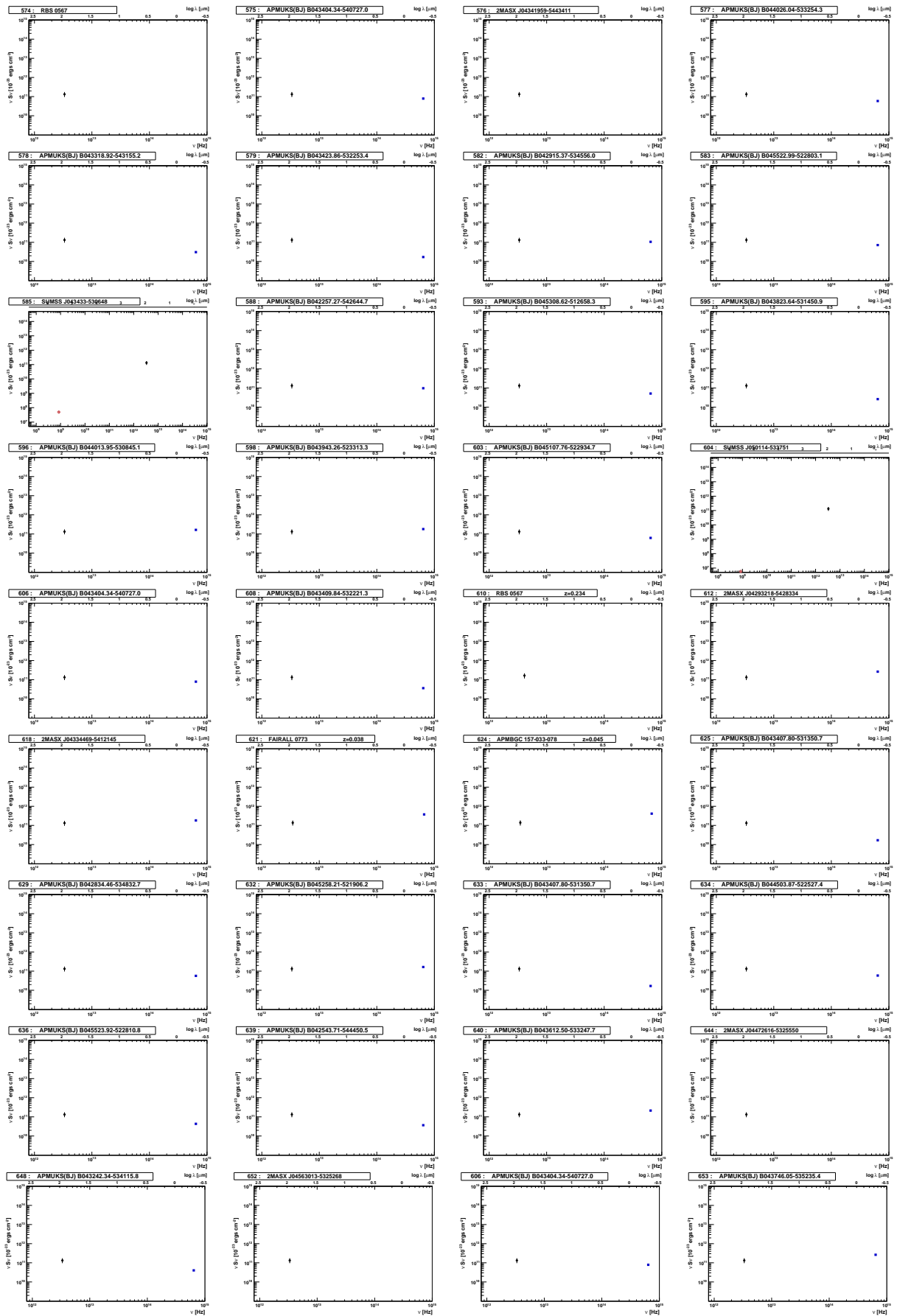


Fig. 11. SEDs for the next 18 ADF-S identified sources, with symbols as in Figure 1.

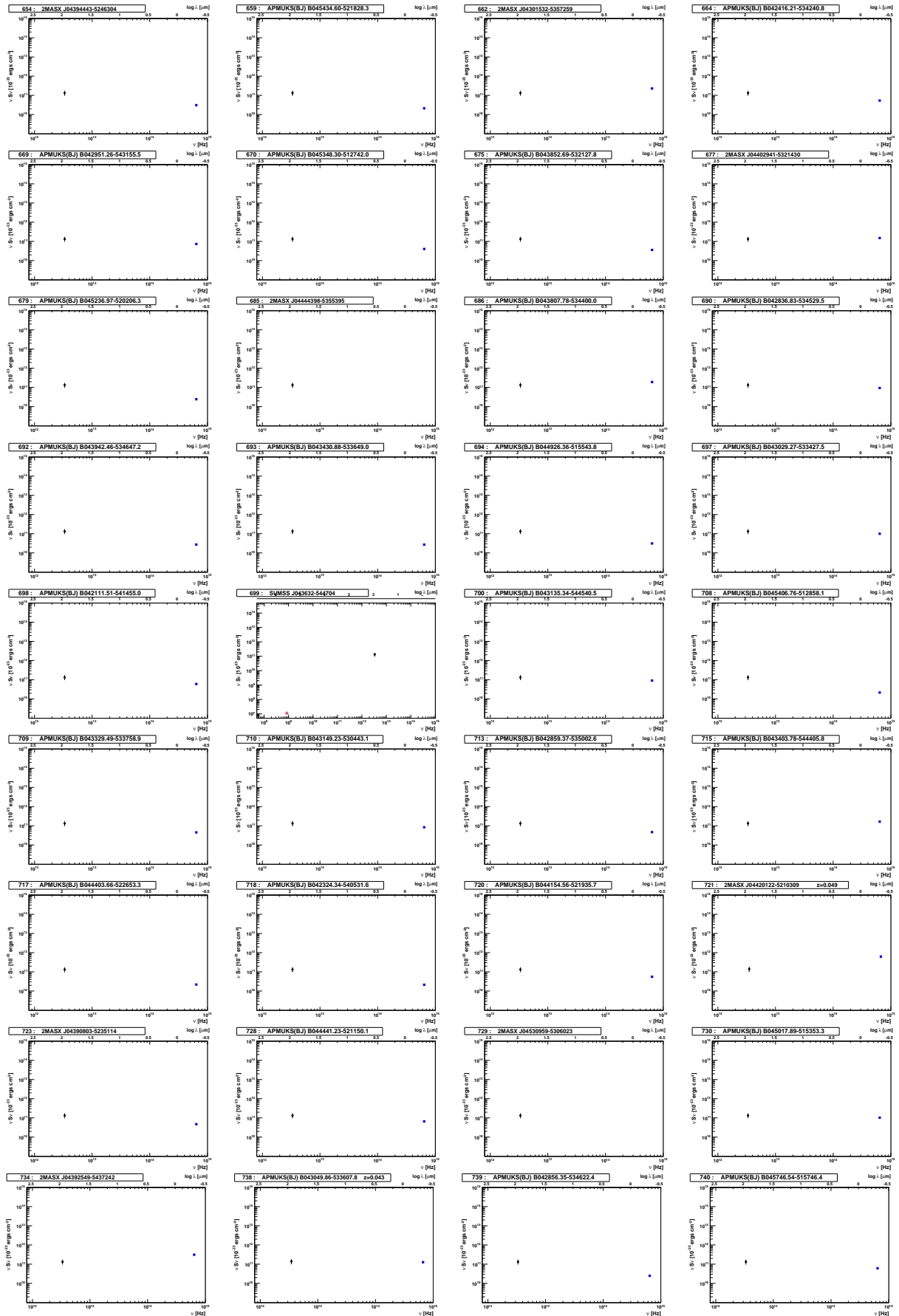


Fig. 12. SEDs for the next 36 ADF-S identified sources, with symbols as in Figure 1.

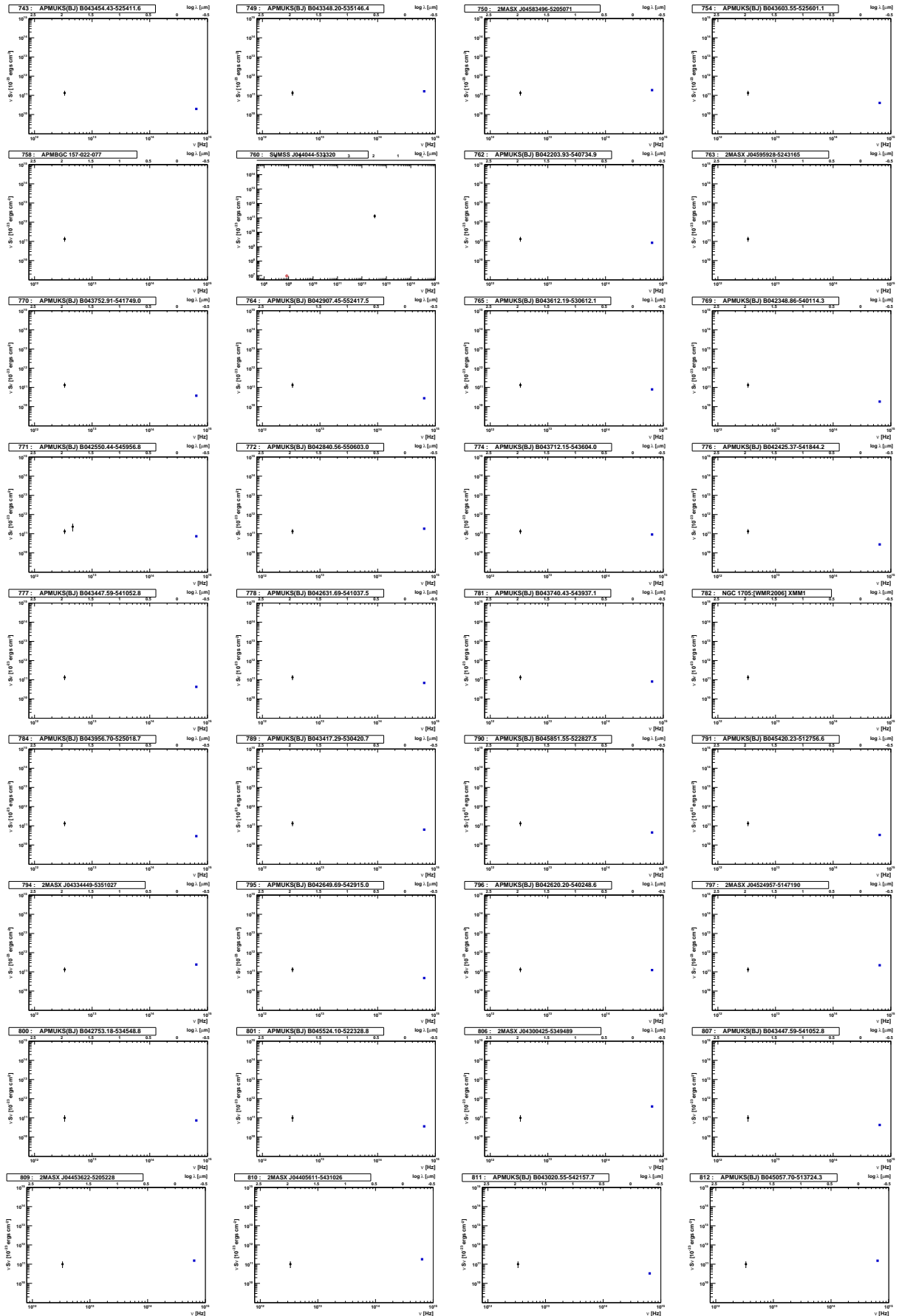


Fig. 13. SEDs for the next 36 ADF-S identified sources, with symbols as in Figure 1.

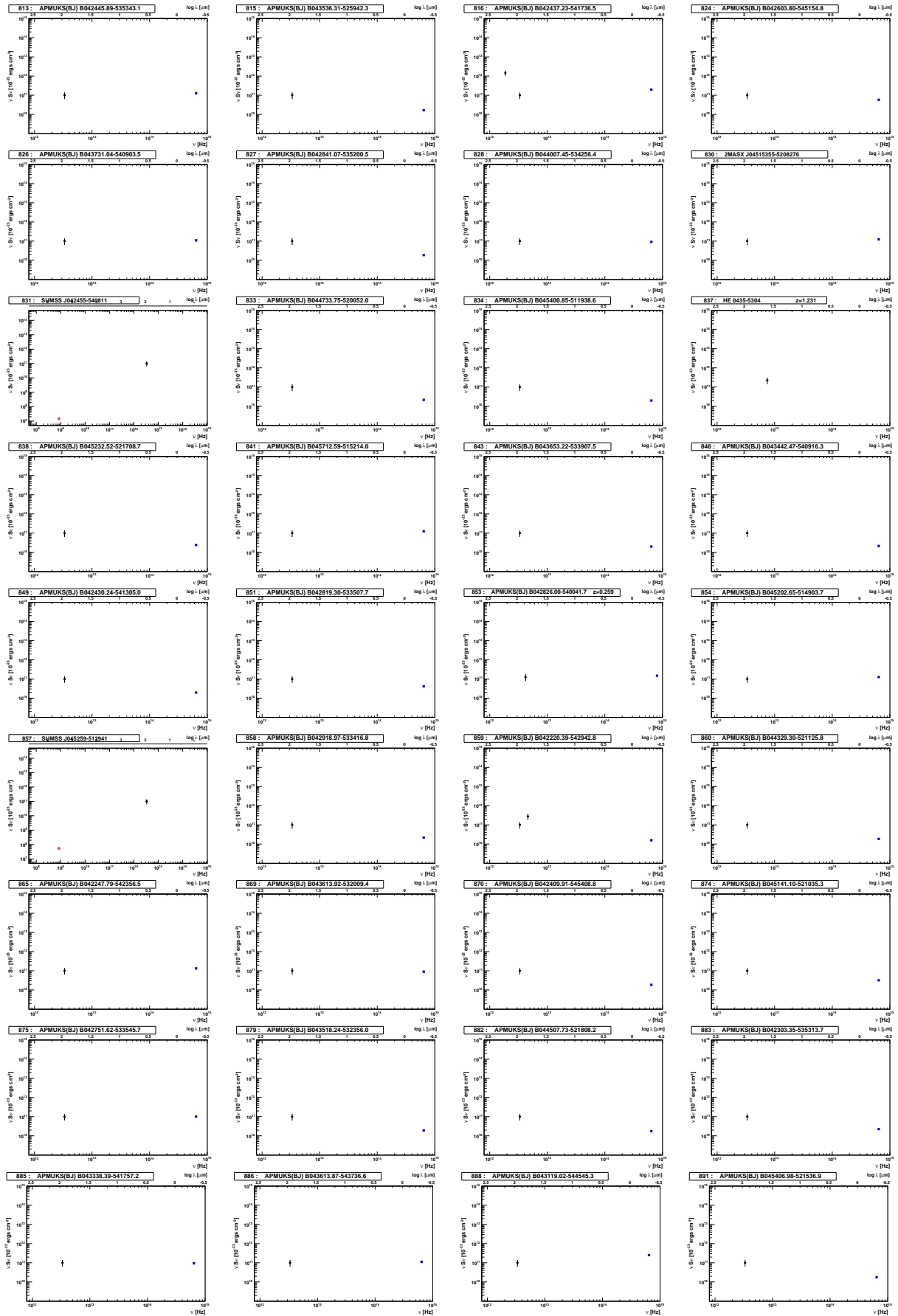


Fig. 14. SEDs for the next 36 ADF-S identified sources, with symbols as in Figure 1.

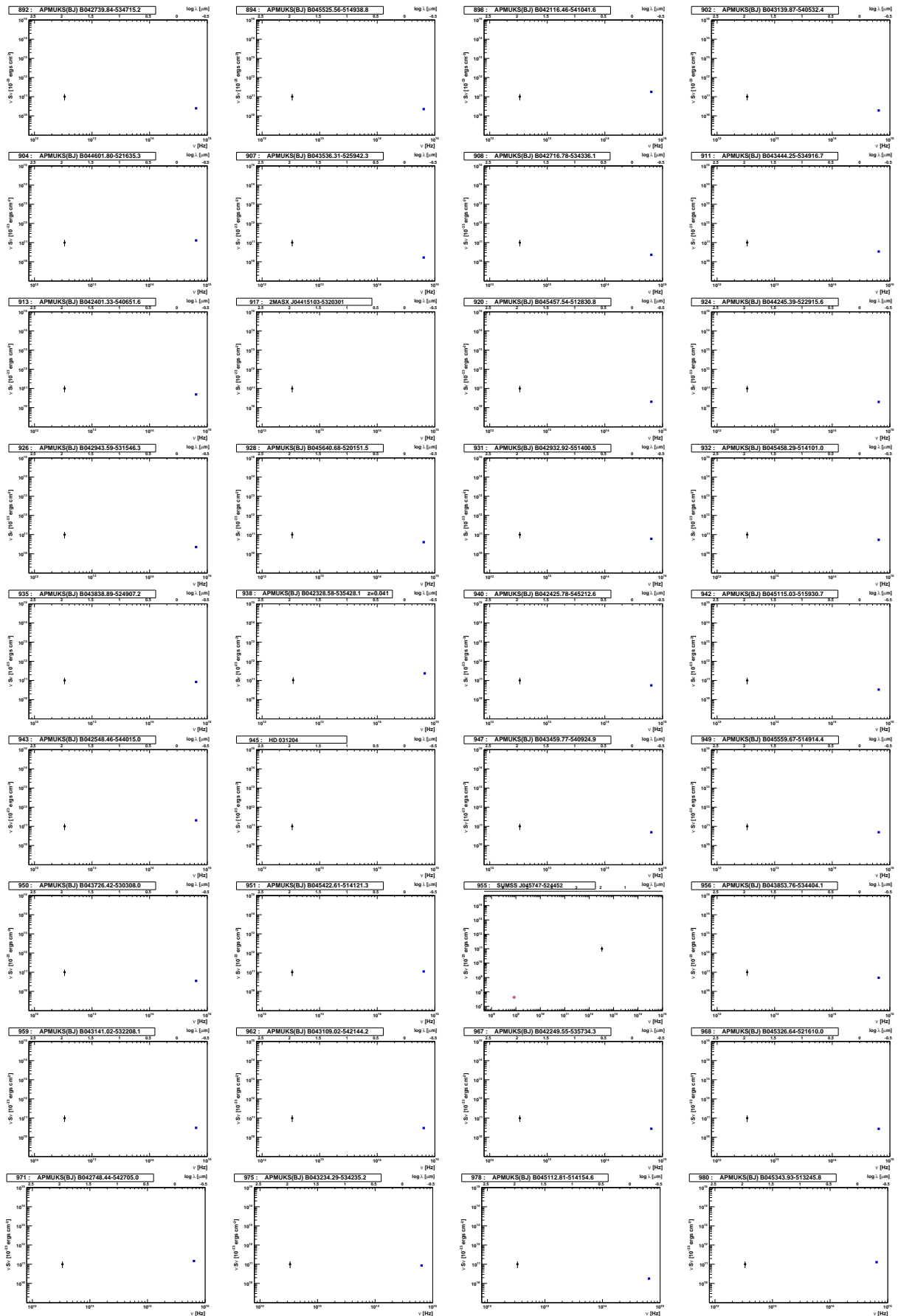


Fig. 15. SEDs for the next 5 ADF-S identified sources, with symbols as in Figure 1.

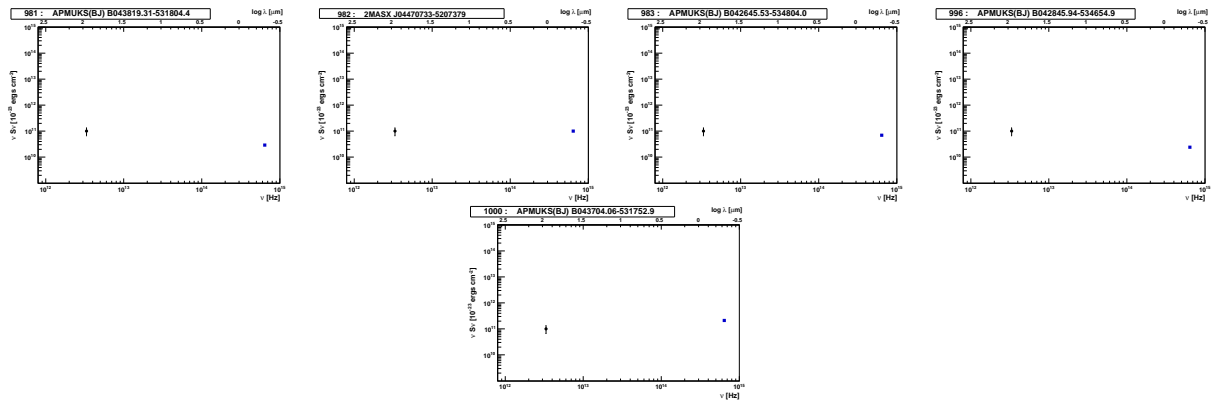


Fig. 16. SEDs for the next 5 ADF-S identified sources, with symbols as in Figure 1.